Kansas Geological Survey

Dynamic Simulation of Saltwater Intrusion at the Siefkes Site, Stafford County, Kansas, and Decision Support for Saltwater Vulnerability Assessment

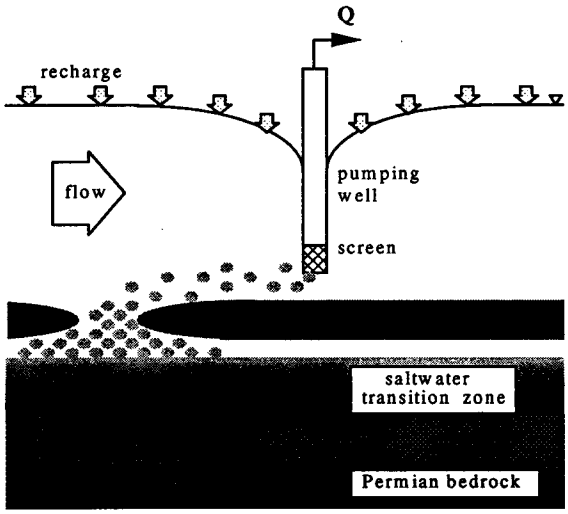

by

Tainshing Ma
Marios Sophocleous

Kansas Geological Survey Open-File Report 96-18
July 1996

GEOHYDROLOGY

The University of Kansas, Lawrence, KS 66047 Tel. (913) 864-3965

Dynamic Simulation of Saltwater Intrusion at the Siefkes Site, Stafford County, Kansas, and Decision Support for Saltwater Vulnerability Assessment

Tainshing Ma
Marios Sophocleous

July, 1996

Kansas Geological Survey
Open-file Report 96-18

ACKNOWLEDGMENTS

This study is based on data collected by Dave Young and Ground-water Management District No. 5 (GMD5) personnel. Discussions and information exchange with them, and with Dr. Yun-Sheng Yu of the Civil Engineering Department, University of Kansas, and Dr. Robert W. Buddemeier, Dr. Donald O. Whittemore, and Glenn Garneau of the Kansas Geological Survey (KGS) are acknowledged. This project is a cooperative effort of KGS and GMD5, and has been financially supported by the Kansas Water Office.

TABLE OF CONTENTS

INTRODUCTION

The major source of freshwater in the Big Bend Groundwater Management District #5 (GMD5) is provided by the Great Bend Prairie aquifer, and most of the ground water used is for irrigation. In the eastern portion of GMD5, the Great Bend Prairie aquifer is in direct hydraulic contact with highly mineralized Permian bedrock, which is the source of brine intrusion into the freshwater aquifer. Records show that the steady increase in ground-water use since 1960 has resulted in significant decline of ground-water levels and deterioration of the water quality due to the upward movement of deeper saline water. In order to sustain a long-term supply of good quality of ground water for the Big Bend Groundwater Management District #5, a sound management strategy must be developed. This strategy must be based on reliable scientific knowledge of the complex subsurface flow and contaminant transport processes. Such knowledge can be acquired through field experiments and mathematical modeling of these processes. Because field experiments are extremely costly and only limited data about the subsurface system are available, a numerical model was used to provide the needed information.

Numerical models also pose problems, however. Limited data about the subsurface leads to uncertainties in model parameters, such as hydraulic conductivities, storativity, dispersion coefficients, and boundary conditions. In GMD5, an additional uncertainty involves the distribution of low-permeability clay lenses observed from scattered gamma-ray logs. These uncertainties raise serious doubts about the reliability of the numerical model for GMD5. For this reason, an area surrounding the Siefkes irrigation well, located in the southeast quarter of section 27, Township 21S, Range 12W was chosen as an intensive study area for field-data collection and numerical modeling since an increasing chloride concentration had been observed during the irrigation season. In addition to the irrigation well at the Siefkes site, two monitoring wells (one screened in the Permian bedrock and the other screened at the base of the aquifer) were also installed by the Kansas Geological Survey for geophysical well-logging and measurement of water

levels. Local stock, domestic, and oil-field water supply wells near the Siefkes site were also used for geophysical well-logging to interpret the stratigraphy of the study area.

The purpose of this study is to determine the effects of the water supply on the mineral intrusion by geostatistical analysis of available data on the ground-water level, saline water interface, elevation of the Permian bedrock, and by mathematical modeling of fluid flow and solute transport processes. A simple ground-water management model was developed to provide technical support for the selection of possible irrigation wells for long-term sustainable ground-water use.

The specific objectives of this research are:

1. To estimate the water table, bedrock elevation, and freshwater-saltwater interface for the study area based on the measured data.

2. To conduct sensitivity analyses to account for the uncertainty of aquifer parameters used in the ground-water mathematical model.

3. To compute the ground-water quantity and quality at the Siefkes site by using a 3-D finite-difference model (SWIFT II).

4. To develop a decision support model for saltwater vulnerability assessment.

GEOHYDROLOGICAL FEATURES AND FIELD DATA

Geohydrological Features of Study Area

The general study area (Fig. 1) covers parts of Barton, Rice, Reno, and Stafford counties with an area of 40 km x 40 km (25 mi x 25 mi). A sub-area of 5.76 km x 4.48 km (3.6 mi x 2.8 mi) near the Siefkes site, as shown in Fig. 1, was chosen for numerical simulation. The Arkansas River and Rattlesnake Creek meander on the north and south sides of the Siefkes site, respectively. According to the 1990 census of population in Kansas, the total population in Barton, Rice, Reno, and Stafford counties was approximately 100,000. Ground water is mainly used for irrigation; urban household, livestock and industry use only a small amount. The study area has a typical continental climate with a wide range of temperatures, high evaporation, and variable precipitation. Most of the precipitation falls during the growing season from April through September. The precipitation records from 1950 to 1995 at the Hudson climatic station (Fig. 1) show that the mean annual precipitation is about 62.81 cm (24.73 in). The annual recharge, mainly from the precipitation, was estimated by Sophocleous (1993) to be approximately 10% of the annual precipitation.

Studies of the geologic formations and the main geologic units in the Great Bend Prairie aquifer were conducted by Latta (1950), Layton and Berry (1973), Fader and Stullken (1978), and Cobb (1980). The geologic formations are shown in Figs. 2A (Latta, 1950) and 2B (Fader & Stullken, 1978). Figure 2A shows that the major geologic units are the Great Bend Prairie aquifer, the Cretaceous formations, the Cedar Hills Sandstone, and the Permian red beds. The Great Bend Prairie aquifer is in the drainage basin of the Arkansas River in south-central Kansas. The aquifer consists of alluvial sand, gravel, silt, and clay that were deposited by the ancestral Arkansas River. It is a relatively shallow alluvial aquifer, with deposits ranging from several meters to over 70 meters. The Cretaceous Dakota formation is generally considered to be a confining or leaky confining layer; it effectively separates the Great Bend Prairie aquifer and the underlying Permian

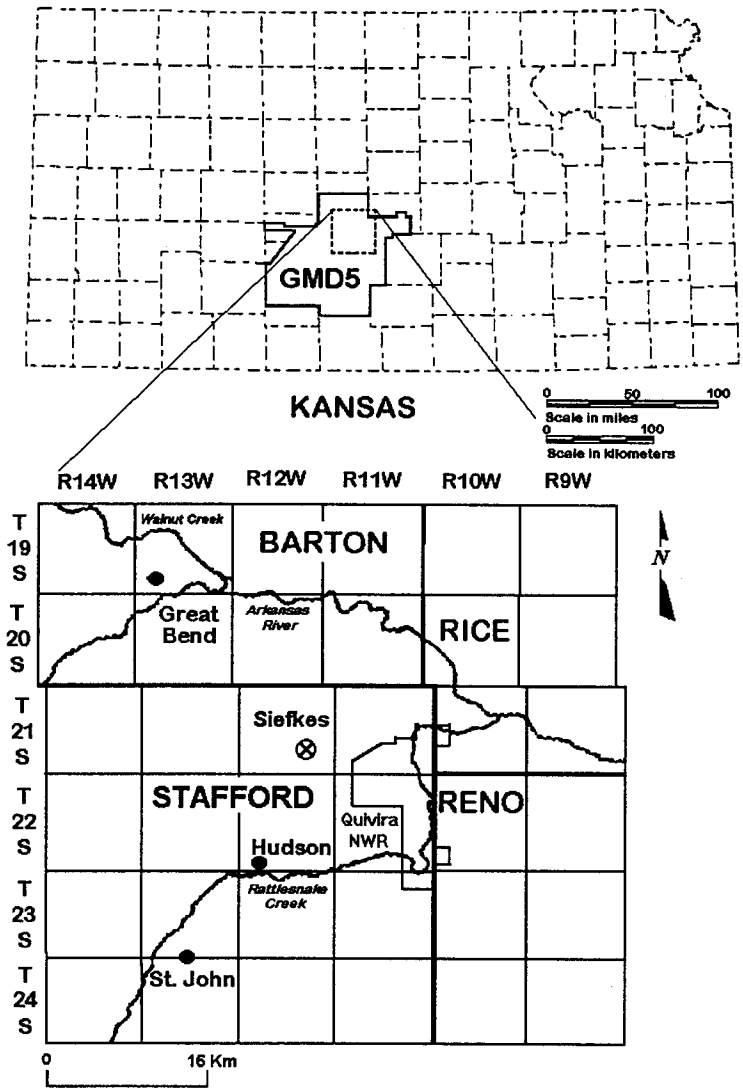

Figure 1. Study area located in the northern part of Groundwater Management District #5 (GMD5).

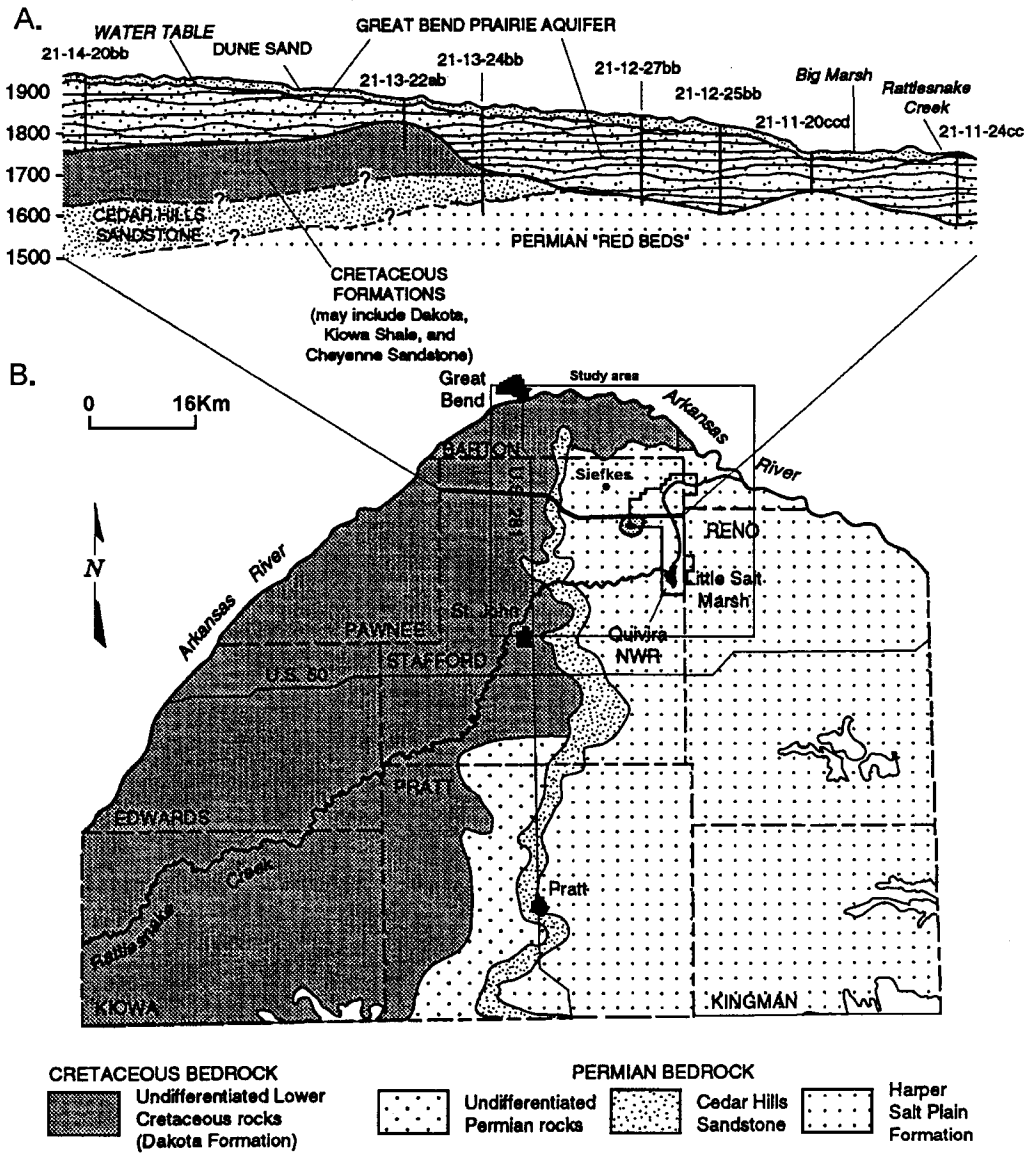

Figure 2. Geological formations of the Great Bend Prairie.

A. Vertical cross section from west to east in Stafford County (Latta, 1950).

B. Configuration of bedrock geology underlying the Big Bend Prairie aquifer (Fader and Stullken, 1978).

water-bearing units. The Permian Cedar Hills Sandstone, which consists mainly of fine-grained sandstone, siltstone, shale, and silty shale, is highly mineralized and may contribute mineralized water to the Great Bend Prairie aquifer. The other Permian formations consist of reddish-brown sandstone, siltstone, shale, salt, gypsum, anhydrite and limestone. These rocks are also known to contain saltwater and are a major source of highly mineralized water.

The study area is mainly located east of US-281 as shown in Fig. 2B. The highly mineralized Permian formations are directly in contact with the base of the alluvial aquifer. The continuous extraction of freshwater mainly for irrigation in this area has accelerated the upward movement of the saltwater, resulting in the deterioration of the water quality. In addition, abandoned oil-field brines, boreholes, and fractures in this area are other sources of salt (Young, 1992); however, the influence from these salt sources is still not clear and is not considered in this study. Fader and Stullken (1978) and Cobb et al. (1982) assumed that the Cedar Hills Sandstone subcrop was the major contributor of saltwater and was used to estimate the amount of upward leakage. However, the Cedar Hills Sandstone subcrop is not the only contributor of saltwater. The relationship between the subsurface formations and their hydraulic properties is uncertain, and therefore a reliable estimation of leakage from the Permian bedrock is still a difficult task.

Figure 3 shows the network of 52 monitoring wells cooperatively constructed by the GMD5 and the KGS and used for geophysical well-logging, hydraulic testing of the aquifer, measurement of water levels, and sampling of ground water. Most of these wells were logged by using an electromagnetic (EM) logging instrument (Buddemeier et al., 1993), and water levels were also measured prior to logging. The gamma-ray response is measured in counts-per-second (cps) and the magnitude of the signal depends on the presence of radioactive elements in the sediment. Since clays contain higher concentrations of radioactive elements than sands, high readings in gamma-ray record imply high clay content. Clay layers were identified when the gamma-ray log reading equaled or exceeded about 100 cps; however, the lateral extent of the clay layers is not

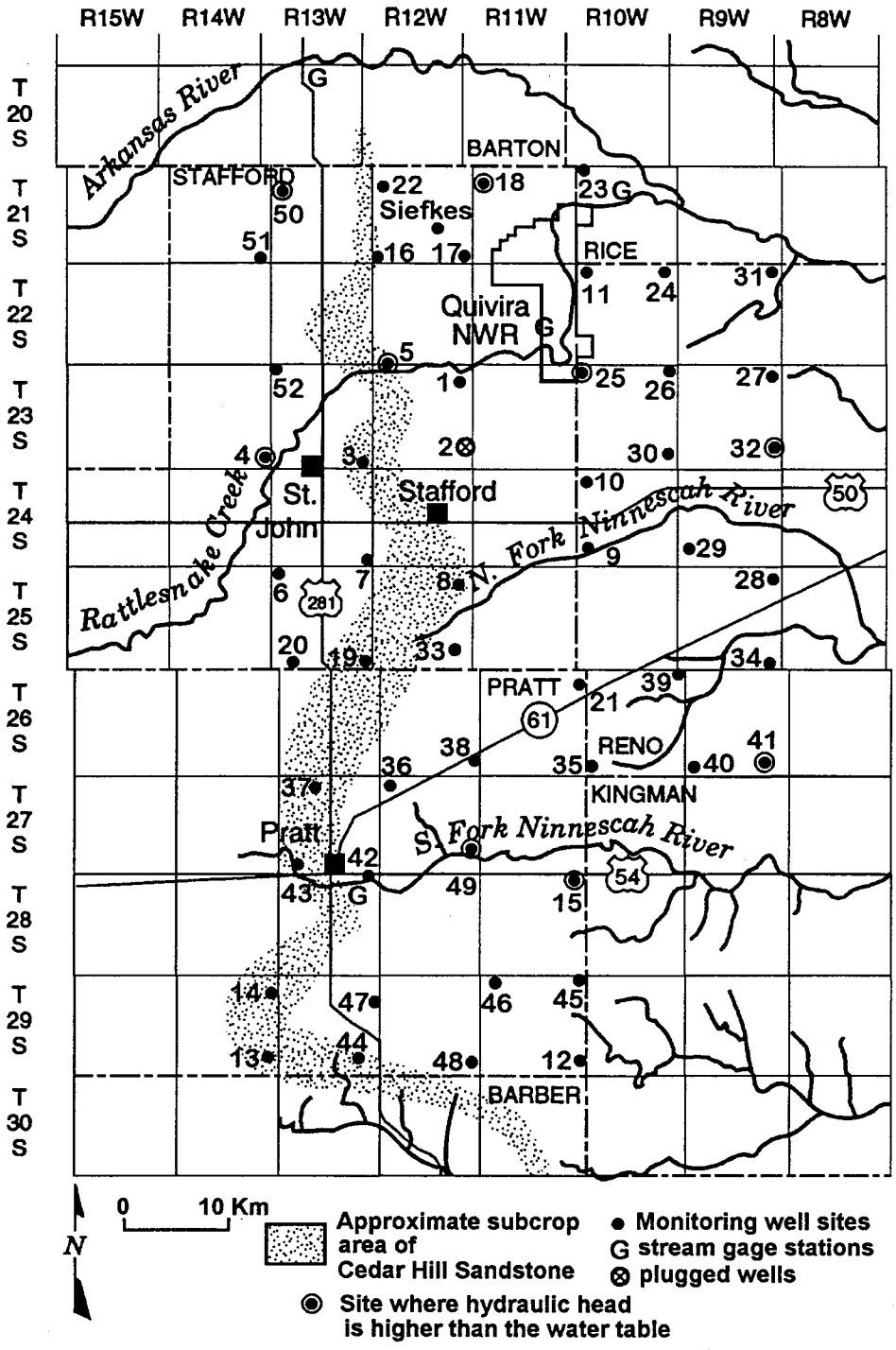

Figure 3. Location of Siefkes site, observation wells, and other physical features in the area of the GMD5/KGS monitoring-well network.

certain. The EM log, measured in millisiemens-per-meter (mS/m), indicates the fluid ionic strength. Because higher cation exchange capacities can be found in clay minerals, the electromagnetic response of clays will be higher. Rosner (1988) used the gamma-ray logs to interpret the stratigraphy of the area. Although the general stratigraphy of the whole GMD5 and the location of major clay layers were roughly identified, detailed descriptions were not given because of the coarse spacing between the monitoring wells, which is approximately 9.6 km (6 miles). However, the determination of the location and size of clay layers in the aquifer is very important in understanding the upward movement of saltwater during the irrigation season.

Tests of the hydraulic conductivity for both the alluvial aquifer and Permian bedrock have been performed by several researchers (Layton & Berry, 1973; Cobb, 1980; Cobb et al., 1982; Butler et al., 1993; Gillespie & Hargadine, 1994) in the GMD5 area. In addition, core samples (Buddemeier et al., 1994) and numerical modeling (Sophocleous and Perkins, 1993) also provide helpful information. The test values indicate that the magnitudes of hydraulic conductivity vary greatly depending on the type of test performed, the location, and the depth of field test. Whittemore (1993) summarized the ground-water geochemistry from samples collected from the monitoring-well network. The report indicates that the salinity of ground water increases with depth and the change in chloride concentration shows a great variation from site to site. The 1991 water-table contours for GMD5 (Sophocleous and Perkins, 1993) indicate that the ground water in the Great Bend aquifer flows generally in eastward direction at an estimated average ground-water velocity of 3.53×10^{-6} m/sec (1 ft/day).

Field Data

The available field data in the study area are very limited and mainly are ground-water level, bedrock elevation, hydraulic conductivity, gamma-ray and EM logs, pumpage and discharged chloride concentration at the Siefkes site, and precipitation data at the Hudson weather station.

Data on ground-water levels for the GMD5 area were collected by GMD5, the Kansas Geological Survey, the Division of Water Resources, and the U.S. Geological Survey. In order to avoid the influence from the irrigation pumping, most of the wells are measured during the nonpumping winter season. The water-level data are published annually by the Kansas Geological Survey. To estimate the 1994 ground-water level that was used in the numerical model as the initial ground-water level, 50 measurements were used in the study area, which were extracted from the KGS ground-water data base compiled by Woods et al. (1994).

Measurements of 564 bedrock elevation points in the study area were extracted from the KGS bedrock data base prepared by Sophocleous, et al. (1990), who compiled data from Fader and Stullken (1978), the water-quality monitoring network established by the GMD5 since 1974, Kansas Geological Survey bulletins, and oil-well and drillers' logs. The measured bedrock-elevations in the study area were used to estimate the topography of bedrock in the mathematical model.

Data on hydraulic conductivity and storativity are very limited and listed in Table 1. The values of hydraulic conductivity in the alluvial aquifer range from 3.3 to 70 m/day. Hydraulic conductivity values in the Permian bedrock are lower, ranging from 0.00006 to 2.9 m/day. Butler et al. (1993) conducted a series of slug tests to determine the hydraulic conductivity for the alluvial aquifer and the Permian bedrock at the Siefkes site and two nearby GMD5 network monitoring wells, site 16 (section 31, Township 21S, Range 12W) and site 17 (section 36, Township 21S, Range 12W). The test values of hydraulic conductivity for the Permian bedrock were 0.0031, 0.0011, and 0.0423 m/day for the two GMD5 monitoring wells and the Siefkes site, respectively. Only the monitoring wells site 16 were tested to determine the hydraulic conductivity for the alluvial aquifer. The hydraulic conductivity values for two alluvial aquifer monitoring wells at site 16 were 9.63 and 17.3 m/day. The tests suggest that the Permian bedrock is approximately three orders of magnitude less than the alluvial aquifer. In addition, the lab tests on core

Table 1. Experimental values of Great Bend Prairie Aquifer parameters.

Methodology	Transmissivity T (m^2 /day)	Hydraulic conductivity, K (m/day)	Storativity, S	Source
5 pumping tests		17 - 39	0.004 - 0.17	Fader & Stullken, 1978
Specific capacities of 235 irrigation wells	230 - 3,250 (ave. = 1,020)			Fader & Stullken, 1978
pumping test near St. John	930	22	0.025	Cobb, 1979,1980
pumping test near Great Bend	1,800 (geom. mean) 1,840 (arith. mean) 460 (std. dev.)	68 70 17	0.00056 0.00074 0.00066	Sophocleous et al., 1987,1988
68 drillers' logs	570 (mean) 295 (std. dev.)	26 12	0.15 0.05	Sophocleous et al., 1993
Slug test		3.3 - 26.8		Butler et al., 1993
Pumping test		47.2 - 70.0	0.1 - 0.15	Layton & Berry, 1973
Permian bedrock				
Slug test		0.0018 - 2.9		Cobb et al., 1982
Slug test		0.001 - 0.04		Butler et al., 1993
Slug test		0.06 - 0.2		Gillespie & Hargadine, 1994
Lab. test on core samples		Hor. 0.0002 - 0.3 Ver. 0.00006 - 0.2		Buddemeier et al., 1994

samples indicate that the vertical hydraulic conductivity is about one order of magnitude less than horizontal conductivity.

According to the United States Department of Health, Education, and Welfare, Public Health Service in 1962, 250 milligrams per liter (mg/L) of chloride concentration is the threshold value for safe drinking water. However, because most of the water in GMD5 is used for irrigation, the minimum chloride concentration considered in this report is higher than 250 mg/L. The main agricultural crops in the study area are wheat, sorghum, corn, and alfalfa, which are crops with a moderate salt tolerance. Experiments conducted by the Kansas Agricultural Experiment Station (Jacobs and Whitney, 1975) indicate that the maximum electrical conductivity, EC, of irrigation water that these type of crops can tolerate in sandy soils is around 3×10^3 μS/cm, and approximately 1.8×10^3 μS/cm in clayey soils. The corresponding chloride concentrations (Whittemore, 1996 personal communication) are approximately 1,100 mg/L for sandy soils and 400mg/L for clayey soils. An approximate ground-water chloride concentration of 500 mg/L is considered to be the target for ground-water suitability for irrigation purposes, and is defined herein as the threshold value for the freshwater-saltwater interface.

The lowest conductivity value that can be reliably read using the KGS EM logging tool is about 100 mS/m because of the noisy conductivity profile from the field measurement. This value corresponds to a chloride concentration of about 3300 mg/L, which is too salty for most uses. Garneau (1995) studied the characteristics of the saltwater-freshwater transition zone of the GMD5 monitoring wells using a statistical approach to minimize the noise on the raw EM logs for the determination of water quality. A curve-fitting technique was employed to produce a smoothly fitted curve, from which the location of the 500 mg/L chloride concentration can be estimated. A sample of the profile of a gamma-ray drilling log, corrected EM log, and converted chloride concentration based on Garneau's approach for the Permian monitoring well at the Siefkes site is shown in Fig. 4. The drop in measured conductivity at bedrock depth is primarily due to the lower bedrock porosity and does not signify less saline conditions at

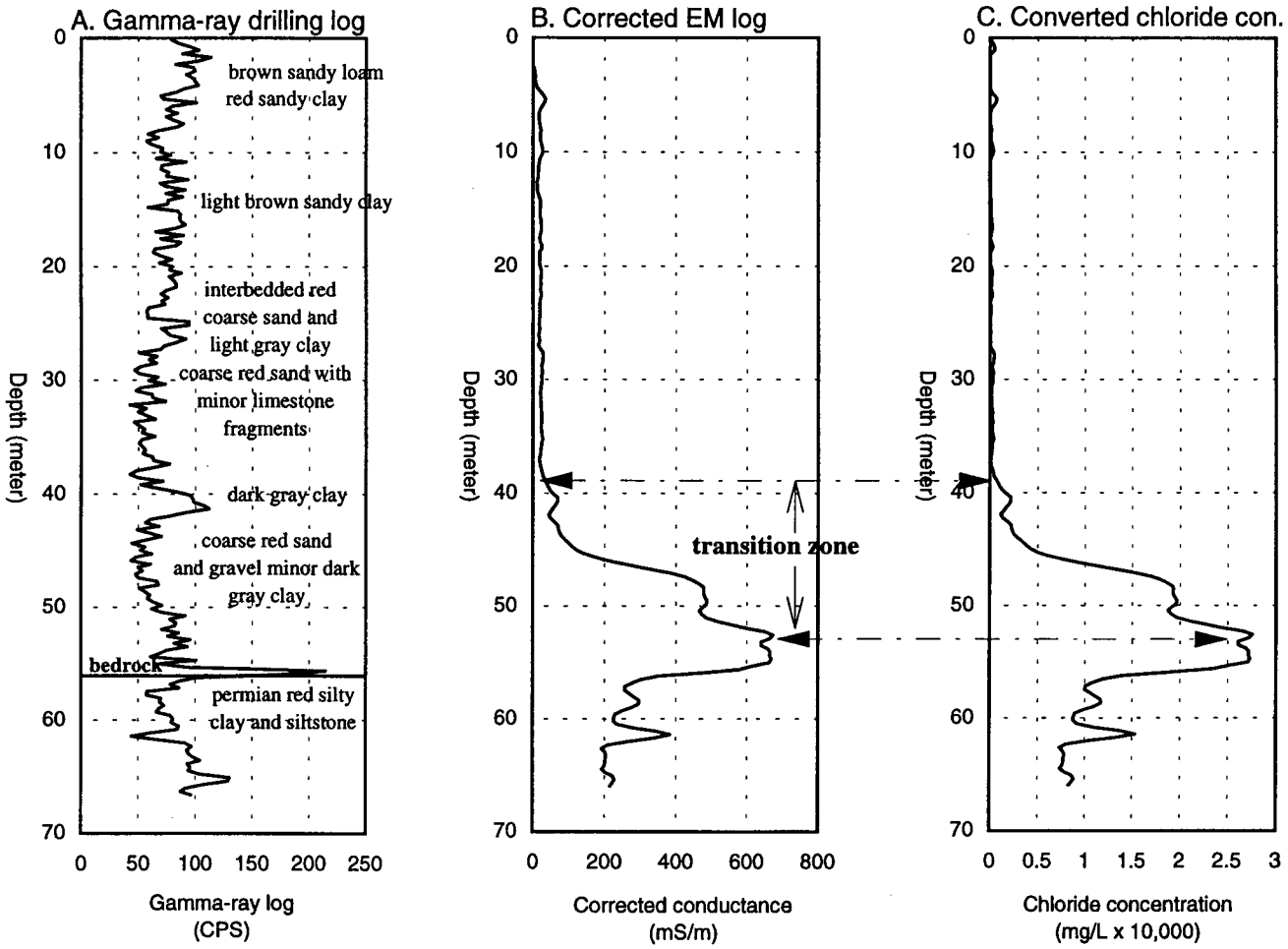

Figure 4. Log profiles: A. gamma-ray drilling log, B. corrected EM log, and C. converted chloride concentration based on Garneau's (1995) statistical approach for the Permian monitoring well at the Siefkes site.

bedrock depths. As can be seen in Fig. 4A, the aquifer at the Siefkes site area is mainly a sand and gravel alluvial deposit with some clay layers interspersed in the aquifer. The thickness of the aquifer from the ground level to the Permian bedrock at the Siefkes site is approximately 57 meters, and the transition zone of saltwater-freshwater interface is approximately 41 meters below the ground level with a layer of dark clay above it. The corrected EM log can be analyzed and converted to its corresponding chloride concentration (mg/L) to indicate the characteristics of the freshwater-saltwater interface and transition zone. The gamma-ray drilling log and corrected EM log at four existing shallow wells, (the stock (S), east oil-field supply (EOS), north oil-field supply (NOS), and north-east oil-field supply (NEOS) wells), and four GMD5 monitoring network wells around the Siefkes site are shown in Appendix A (Buddemeier et al., 1993). The logs from the shallow wells and GMD5 monitoring wells are used to interpret the stratigraphy at the Siefkes site area. Garneau (1995) indicated that the changes of saltwater-freshwater interface at the four GMD5 monitoring wells around the Siefkes site were very small from 1993 to 1994.

The logging of the Siefkes site monitoring wells and monitoring efforts to determine the effects of irrigation pumping on the freshwater-saltwater interface began in early 1993. Figure 5 shows the measured water level at the Siefkes deep-aquifer monitoring well, discharged chloride concentration at the Siefkes irrigation well, water use at the irrigation well, and the corresponding monthly precipitation at the Hudson weather station. As can be seen, the measured water level in spring 1994 was greater than spring 1993 due to the unusually high precipitation (high recharge) in 1993. Water levels increased approximate 2 meters between April and October 1993, and the measured water levels in March-April 1994 were still approximately 1 meter higher than the March-April 1993 levels. Because of the more normal weather conditions in 1994, irrigation was more active in 1994 than in 1993 and water levels showed a net drop of approximate 1.5 meters from March through November, 1994. In addition, subsurface recharge was not

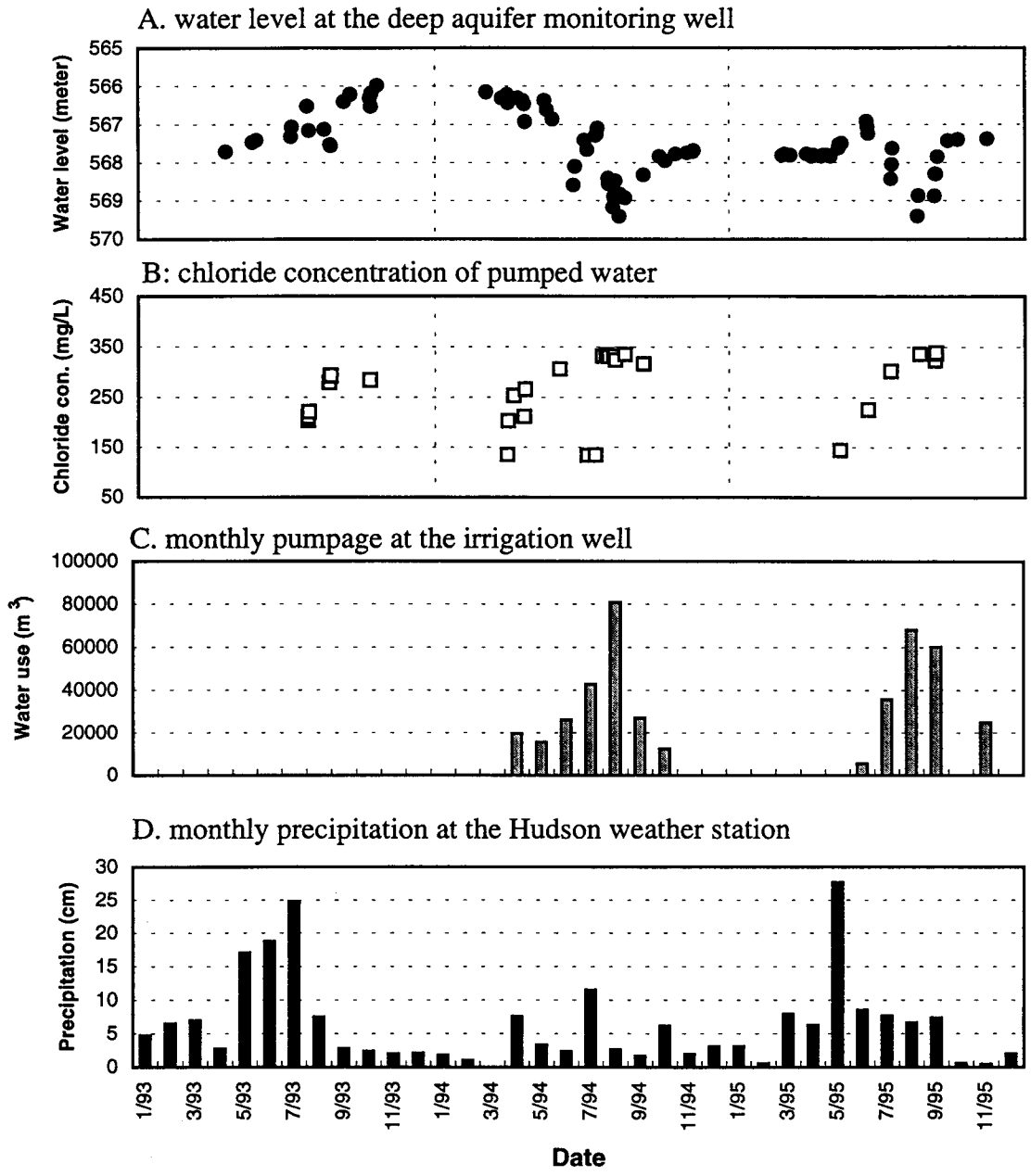

Figure 5. Plots of measurements: A. measured water level at the Siefkes site deep aquifer monitoring well; B. discharged chloride concentration at the Siefkes site irrigation well; C. monthly pumpage at the Siefkes site irrigation well; and D. monthly precipitation at the Hudson weather station.

significant during the 1994 winter nonirrigation season; the measured water level in spring 1995 was about the same as in winter 1994.

Although ground-water heads fluctuated significantly from 1993 to 1995, the amount of salt and the characteristics of transition zone at the Siefkes site remained rather stable. Because of recovery during the nonirrigation season, the lowest chloride concentration was usually measured in early irrigation season. The highest chloride concentration was observed later in the irrigation season since the pumping was heaviest during that period. As Fig. 5B shows, chloride concentration ranges from the early irrigation season value of 135 mg/L to the late irrigation season value of 339 mg/L which shows an increasing trend during each irrigation season. The low chloride concentrations on March 31, 1994 (135 mg/L) and May 17, 1995 (145 mg/L) were due to the previous non-irrigation season. Other low chloride concentrations observed on July 8 (134 mg/L) and 21(139 mg/L), 1994 were due to rain storms in early and mid July.

In 1994, a water meter was installed on the Siefkes irrigation well to track water use. Figure 5C shows the approximate monthly water use on the irrigation well from 1994 to 1995. Figure 5D is the monthly precipitation at the Hudson weather station. As can be seem from Figures 5A to 5D, water use is inversely proportional to rainfall and water level is proportional to the amount of water use. The discharged chloride concentration is also proportional to the water level. Usually, the most pumping activity occurs during July, August, and September and water levels are lowest and chloride concentrations are highest during this period.

GEOSTATISTICAL ANALYSIS OF FIELD DATA

Geostatistics initially stood for estimation problems in two- or three-dimensional fields using probabilistic tools (Matheron, 1963). More recently, the term has been used more generally to describe all applications of statistics in hydrogeology and geology. For ground-water flow, the heterogeneity of the subsurface often cannot be adequately characterized for use in deterministic models. Geostatistical simulations must be used to generate realizations of the random model parameters involved in the mathematical model. The mineral intrusion problem is solved numerically by two coupled partial differential equations, the fluid flow equation and solute transport equation. Since no closed-form solution is obtainable, these two coupled equations are solved numerically by using the finite-difference technique. The numerical technique divides the aquifer model into a finite number of grid cells, and the aquifer geometry and properties for each discrete cell have to be estimated. The ordinary kriging technique is used to estimate the 1994 ground-water levels and bedrock elevations at the nodes of a grid system. The kriged values of the 1994 ground-water levels are used as the initial condition for the three-dimensional numerical model in the next chapter; the kriged bedrock elevations provide the topography of the Permian bedrock in the model. The theory of geostatistics was briefly discussed in a previous report (Ma and Sophocleous, 1994) and computations were performed by using the GSLIB (Deutsch and Journel, 1992) software.

Estimation of Ground-water Levels

The study area shown in Fig. 6 is bounded by the Arkansas River and Rattlesnake Creek, with a total area of approximately 40 x 40 km^2 (25 x 25 mi^2). The area was extended to 59.2 x 59.2 km^2 (37 x 37 mi^2) to take the advantage of available measurements outside the study area. For the extended area, there are 50 monitoring wells for ground-water levels in 1994. These measured values at sampled sites are used to obtain the optimal estimates of the values at unsampled locations by kriging.

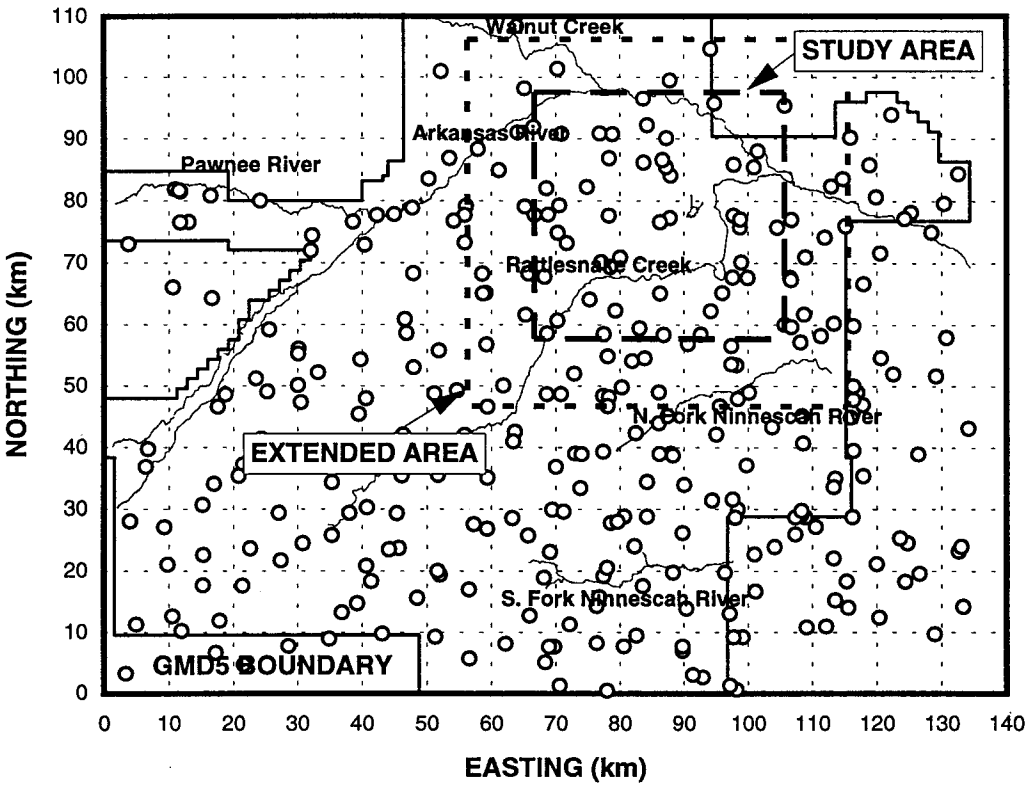

Figure 6. Locations (open circles) of measured piezometric heads in 1994 (Woods, 1994).

The estimation procedure starts by finding the semivariogram that characterizes the spatial variability of the ground-water levels. A semivariogram model is chosen, followed by cross-validation (Davis, 1987). In the cross-validation, the model is used to determine the kriged values at sampled sites. If the mean and variance of the estimation error based on the semivariogram model are close to zero and one, respectively, the model is judged to be acceptable. The results of cross-validation can be presented as a scatter plot of the estimated values versus the measured values, and the plotted points should lie close to the 45-degree line if the model is valid. The validated semivariogram model is then employed to estimate the values at unsampled locations.

Previous analysis of the measured ground-water levels indicates that the ground-water level generally dips from the west to the east (Mitchell, et al., 1993), which implies that a significant spatial trend exists in the ground-water level data. Thus the calculated semivariogram is expected not to reach a constant sill as the distance increases because of the nonstationarity of the data. Consequently, the trend must be estimated and be removed from the original data so that the residuals required for kriging satisfy the stationarity condition, from which a semivariogram model can be found. To accomplish this, a nonlinear trend is fitted with first-degree and second-degree polynomials as follows:

$$\textit{Water level elevation} = -1.354\,X - 0.037\,Y + 0.0003\,XY - 0.005\,X^2 - 0.0059\,Y^2 + 583.25 \qquad (1)$$

where X and Y are the coordinate along the east and the north direction, respectively.

The coefficient of determination, r^2, used to determine the goodness-of-fit of Eq. 1, had a value of 0.98, indicating a good fit; therefore, the fitted trend (Eq. 1) was removed from the measured data.

After the nonlinear trend was removed from the original data set, the cumulative probability distribution and histogram for the data were established. (Fig. 7). The points

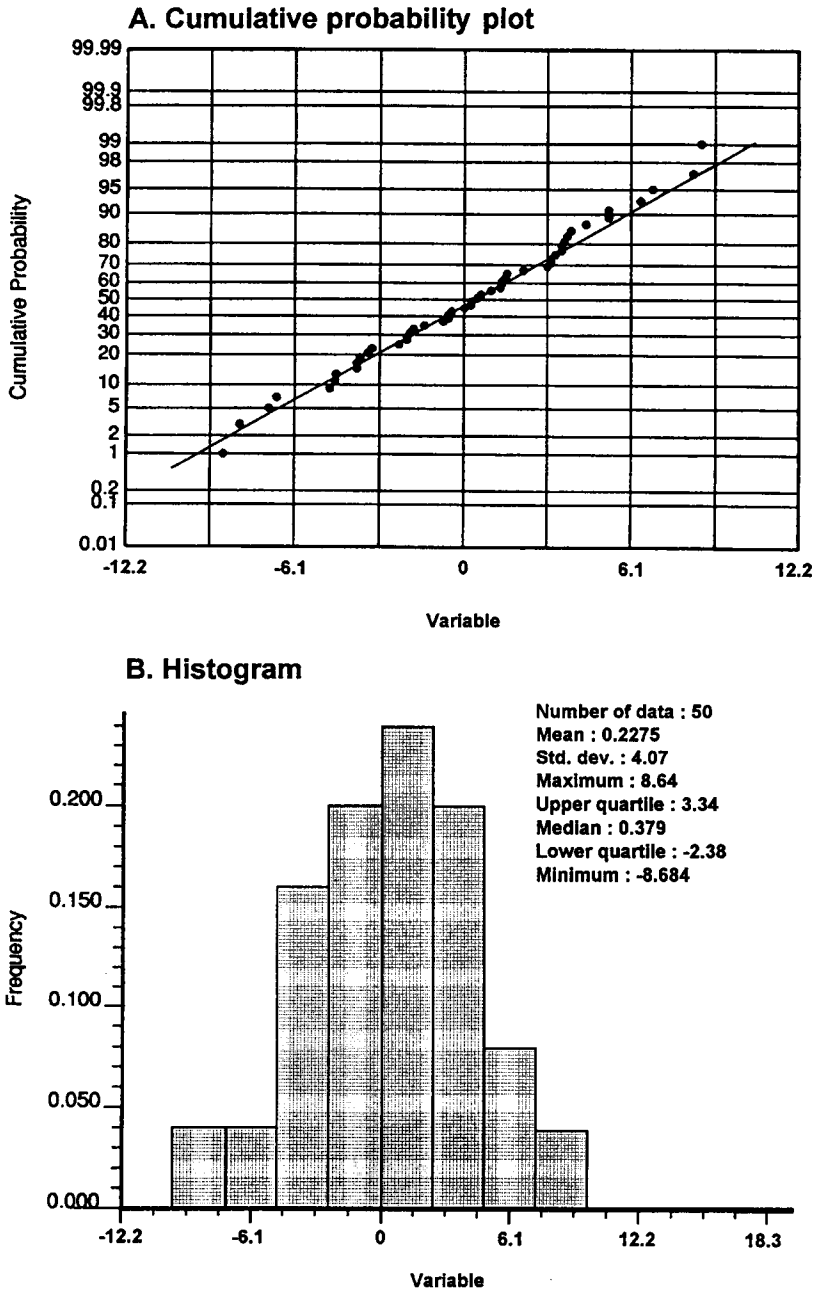

Figure 7. Cumulative probability and histogram for measurements at 50 observation wells in 1994.

plotted on a normal probability paper shown in Fig. 7A indicate that the residuals are normally distributed except for a few high and low values.

Omnidirectional search is conducted for semivariograms of residuals with a lag of 2.88 km and a tolerance of ± 1.44 km. The accuracy of kriged values depends mostly on the semivariograms at small lags; therefore, the best fitted semivariogram model is determined based on the first few semivariogram points. Selection of the best-fitted model is performed by using the semivariogram model-fitting software developed by Jian, Olea, and Yu (1996). Fitting of the model is based on the weighted least-squares method and the Akaike information criterion, AIC (Akaike, 1979) for selecting the best model. The AIC is:

$$A\hat{I}C = n\ln\left(\frac{R_m}{n}\right) + 2p, \tag{2}$$

where n is the number of points in the experimental semivariogram, p is the number of parameters in the model, and R_m is the sum of the squares of the weighted differences.

Table 2 shows the calculated AIC values for Spherical, Exponential, and Gaussian models and their corresponding nugget effect, sill, and range. Figure 8 shows the calculated semivariograms and the best-fitted model, which is the spherical model of the following form:

$$\gamma(h) = \begin{cases} C_0 + C_1\left(1.5\,\frac{h}{a} - 0.5\left(\frac{h}{a}\right)^3\right), & h \le a, \\ C_1 & , \; h > a \end{cases} \tag{3}$$

where the nugget effect C_0 is 0; the sill $C_0 + C_1$ is 16.21; h is the lag distance; and the range a is 14.53 km.

Table 2. Akaike Information Criterion (AIC), nugget, sill, and range for spherical, exopnential, and Gaussian models for piezomeric head.

Model	AIC	Nugget	Sill	Range
Spherical	25.92	0.00	16.39	14.53
Exponential	27.35	0.00	17.37	19.99
Gaussian	26.79	0.85	16.22	11.01

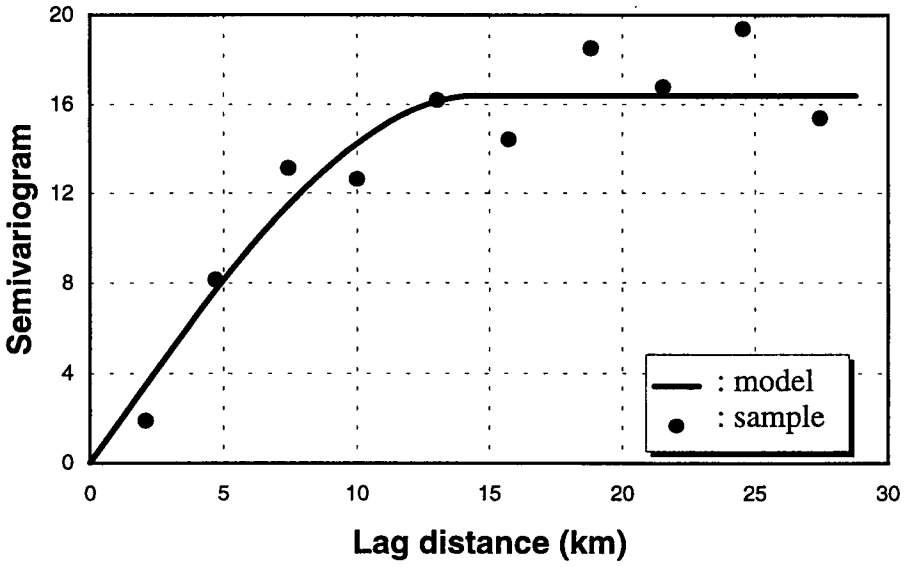

Figure 8. A plot of sample semivariograms based on the measured values of piezometric head in 1994 and the spherical model.

Cross-validation is carried out based on the best-fitted model, and the resulting scatter plot is shown in Fig. 9. The plotted points generally cluster around the 45-degree line; therefore, the spherical model is chosen for kriging.

The final results are obtained by adding the removed trend back to the kriged residuals. The 1994 ground-water elevation contours are shown in Fig. 10. The highest water level is 580 meters, and the lowest elevation is 520 meters. The piezometric heads are very smooth, with higher heads at the southwestern corner gradually decreasing as they move eastward.

Estimation of Bedrock Elevations

A similar analysis was carried out for the bedrock-elevation data at 564 locations shown in Fig. 11. The cumulative probability distribution and histogram for the data are shown in Fig. 12. The points plotted in Fig. 12A indicate that the bedrock elevations data are normally distributed except for a few very low and very high values.

The measured bedrock elevations generally decrease from west to east. All semivariograms were calculated with lag 2.24 km and a tolerance ± 1.12 km, and for directional semivariograms an angular tolerance of ± 22.5 degrees was used. Figure 13 shows the calculated omnidirectional and directional semivariograms. All semivariogram plots show an increasing trend except in the north-south direction, which is perpendicular to the main trend of bedrock. The continuous rise of the semivariance in Figs. 13A, C, D, and E indicate that no limited range can be specified. Therefore, the sampled semivariogram along the N-S direction is used for fitting a model because of its good continuity at the origin and nearly constant semivariance. Table 3 shows the calculated AIC values for Spherical, Exponential, and Gaussian models and their corresponding nugget effect, sill, and range. Figure 14 shows the calculated semivariograms and the best-fitted model. The best-fitted semivariogram model selected for kriging is the following spherical model:

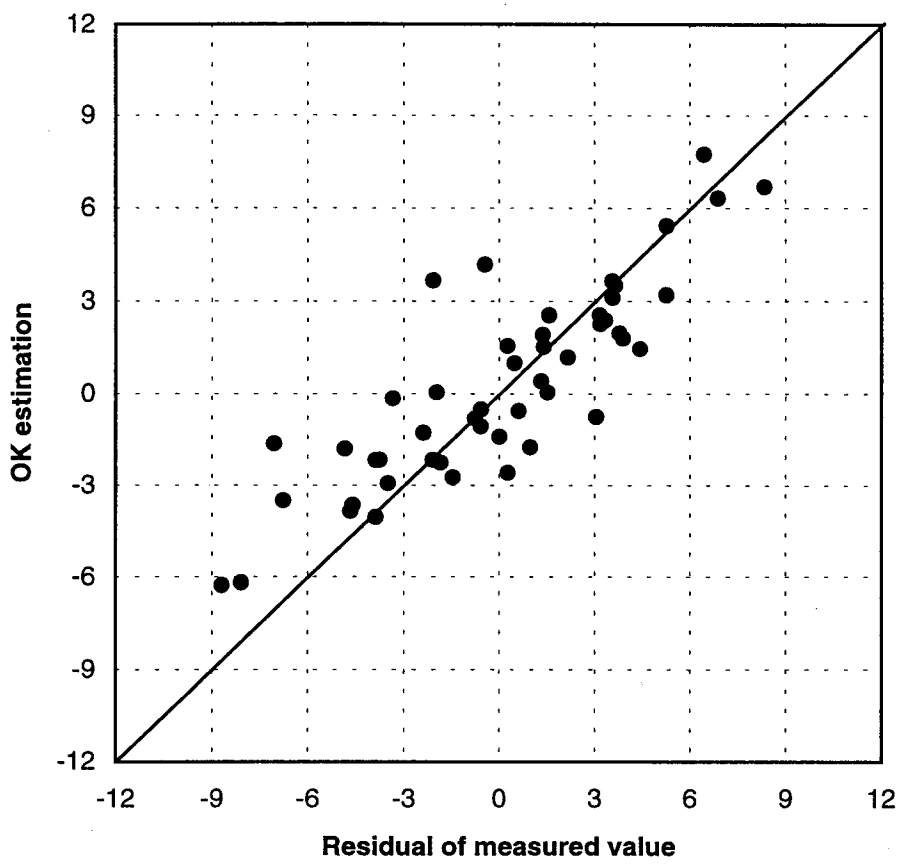

Figure 9. Scatter plot of residuals of measured 1994 water levels versus kriged residuals at sampled sites.

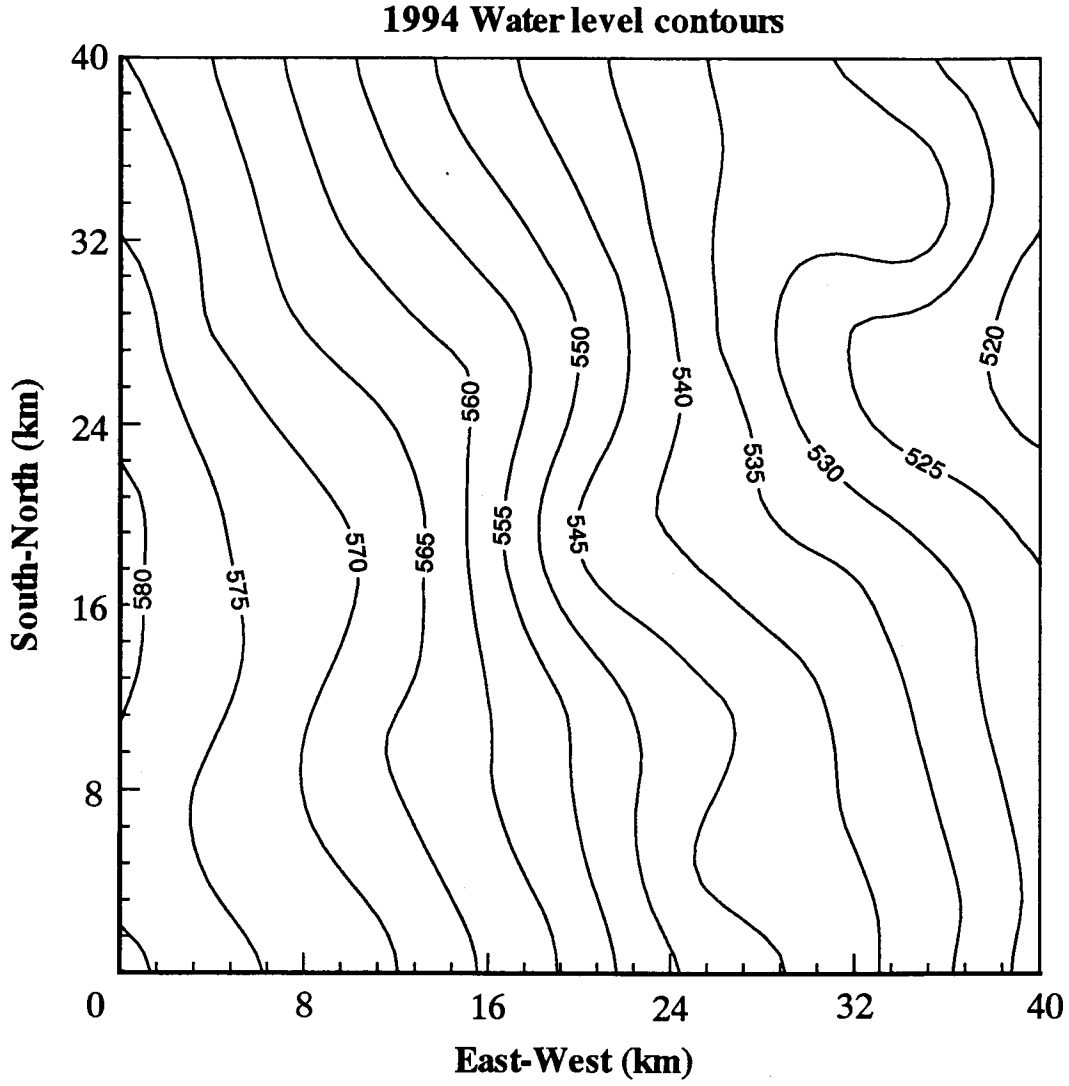

Figure 10. Contours of the kriged piezometric heads based on the measured 1994 water levels.

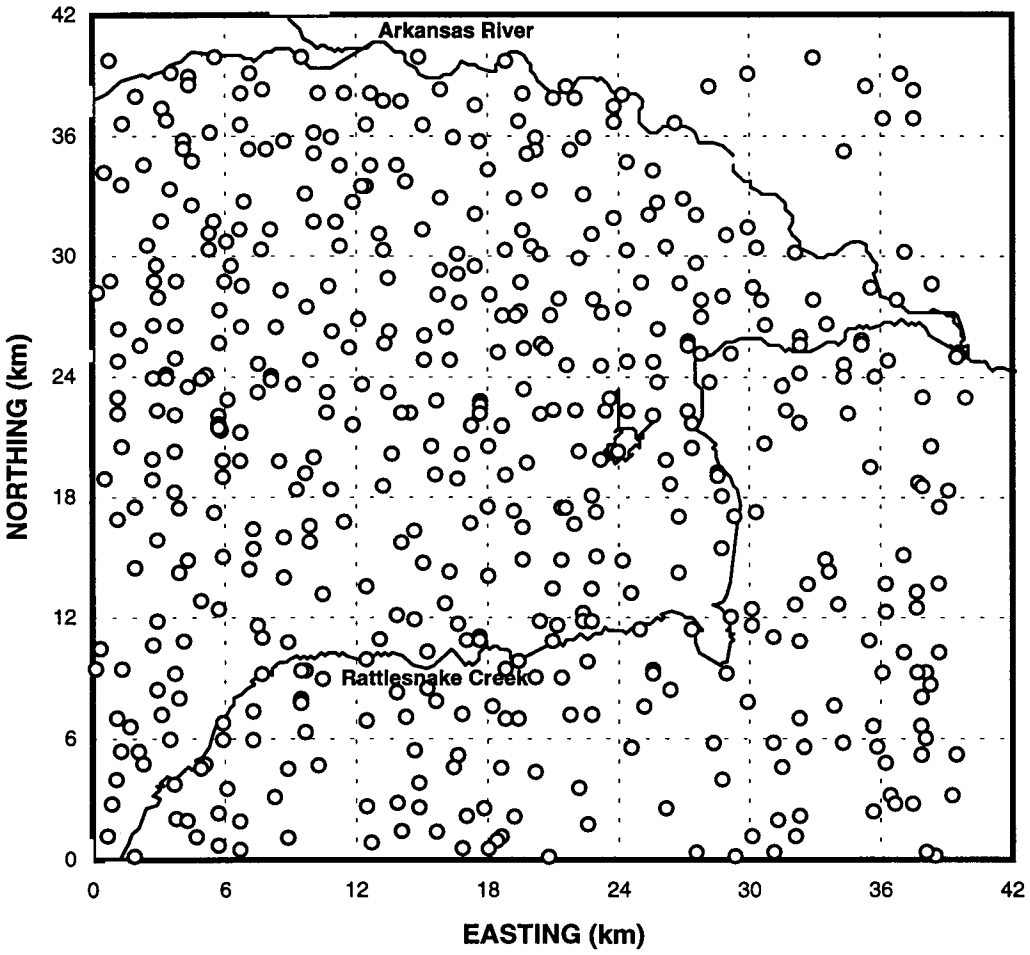

Figure 11. Locations (open circles) of measured bedrock elevations (Sophocleous et al, 1990).

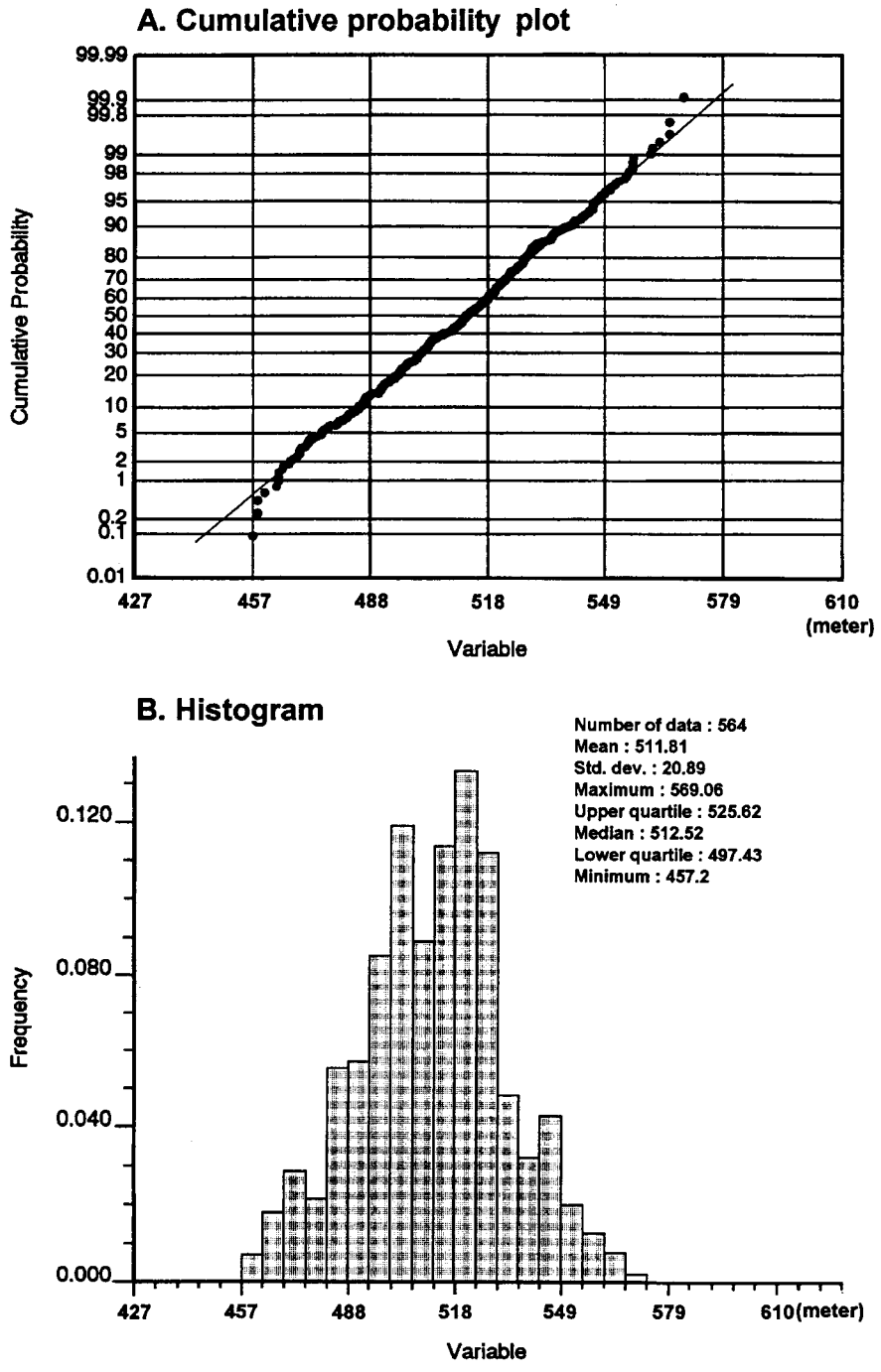

Figure 12. Cumulative probability and histogram for 564 measurements of bedrock elevation in the study area.

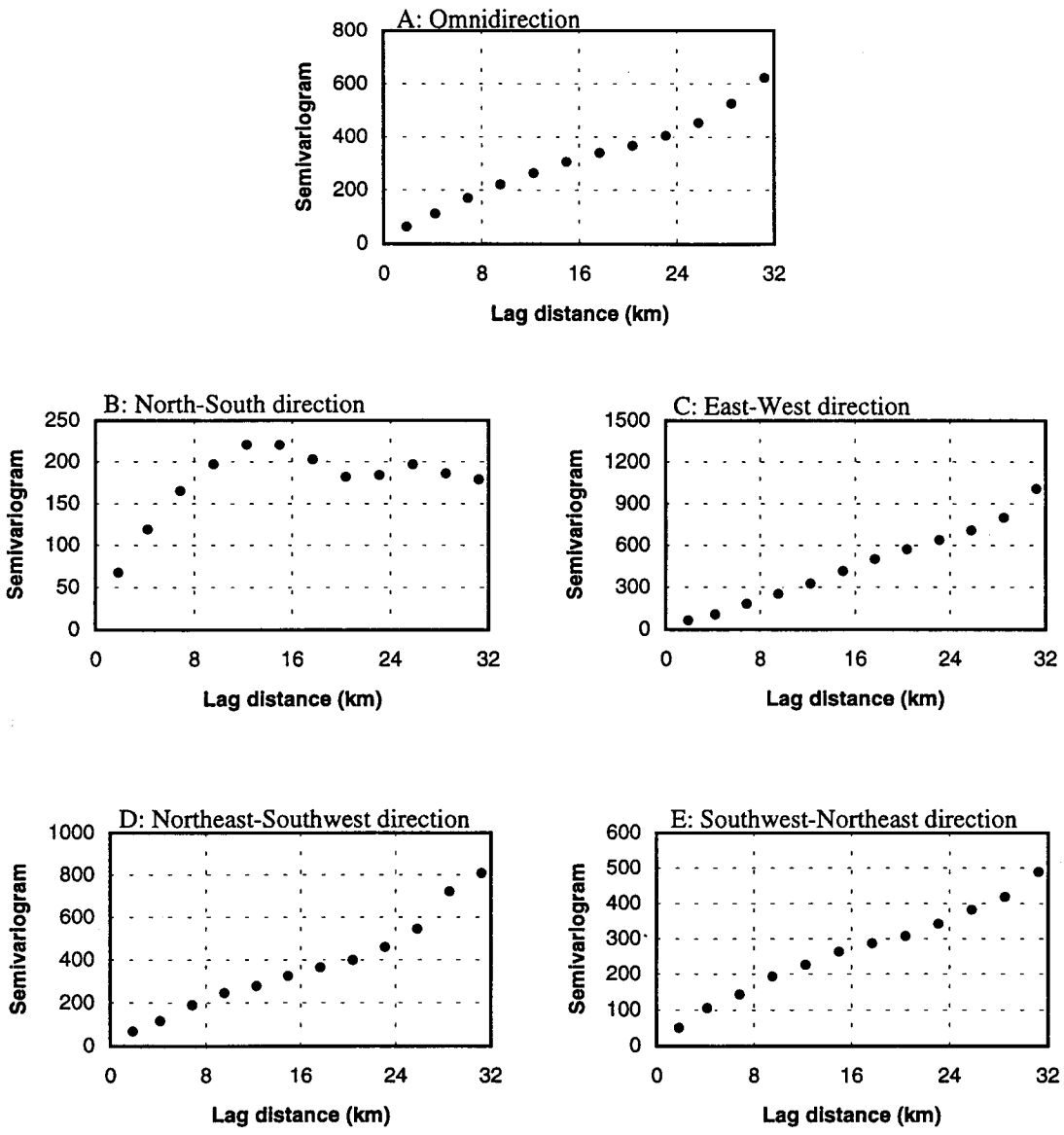

Figure 13. Plots of semivariograms for the measured bedrock elevations.

Table 3. Akaike Information Criterion (AIC), nugget, sill, and range for spherical, exponential, and Gaussian models for bedrock elevation.

Model	AIC	Nugget	Sill	Range
Spherical	66.39	9.81	201.31	10.34
Exponential	71.34	0.00	197.70	11.38
Gaussian	67.73	49.10	196.39	9.16

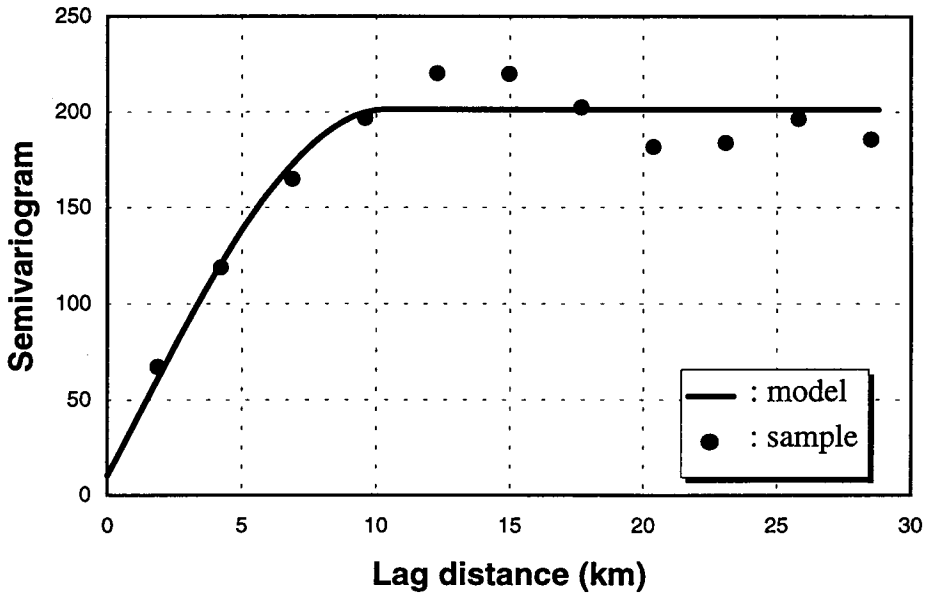

Figure 14. Sample semivariograms for bedrock elevation and the spherical model.

$$\gamma(h) = \begin{cases} C_0 + C_1\left(1.5\,\frac{h}{a} - 0.5\left(\frac{h}{a}\right)^3\right), & h \le a, \\ C_1 \qquad\qquad\qquad\quad , & h > a \end{cases} \tag{4}$$

where the nugget effect C_0 is 9.81; the sill $C_0 + C_1$ is 201.31; h is the lag distance; and the range a is 10.34 km.

Again, cross validation was performed for the best-fitted model (Eq. 4). The kriged values at sampling locations are plotted versus the sampled values in Fig. 15. The clustering of the plotted points around 45-degree line indicates that the spherical model is adequate for estimating the bedrock elevations at unsampled sites to provide a detailed pattern of the bedrock topography.

A plot of contours of bedrock elevation obtained from the kriged values is shown in Fig. 16. The highest elevation is 558 meters and the lowest is 468 meters. Figure 16 shows the ragged features of the bedrock with high elevations in the southwest corner and low elevations in the east. The variability of the bedrock elevation will be included in developing a three-dimensional numerical model and will be used for interpretation of saltwater intrusion.

Cokriging for Saltwater-Freshwater Interface

Since 1993, field measurements of the saltwater-freshwater interface, piezometric heads, and bedrock elevations have been obtained at a limited number of sampling locations. The measured values in 1993 and the sampling locations are listed in Table 4 and shown in Fig. 17. The correlation coefficients and the rank correlation of water table versus interface and bedrock elevation versus interface are also presented in Fig. 18. It is seen that a better correlation exists between the bedrock elevation and interface with a value of about 0.79 for both correlation and rank correlation coefficients. Instead of using both bedrock and ground-water levels, two secondary variables to estimate the location of

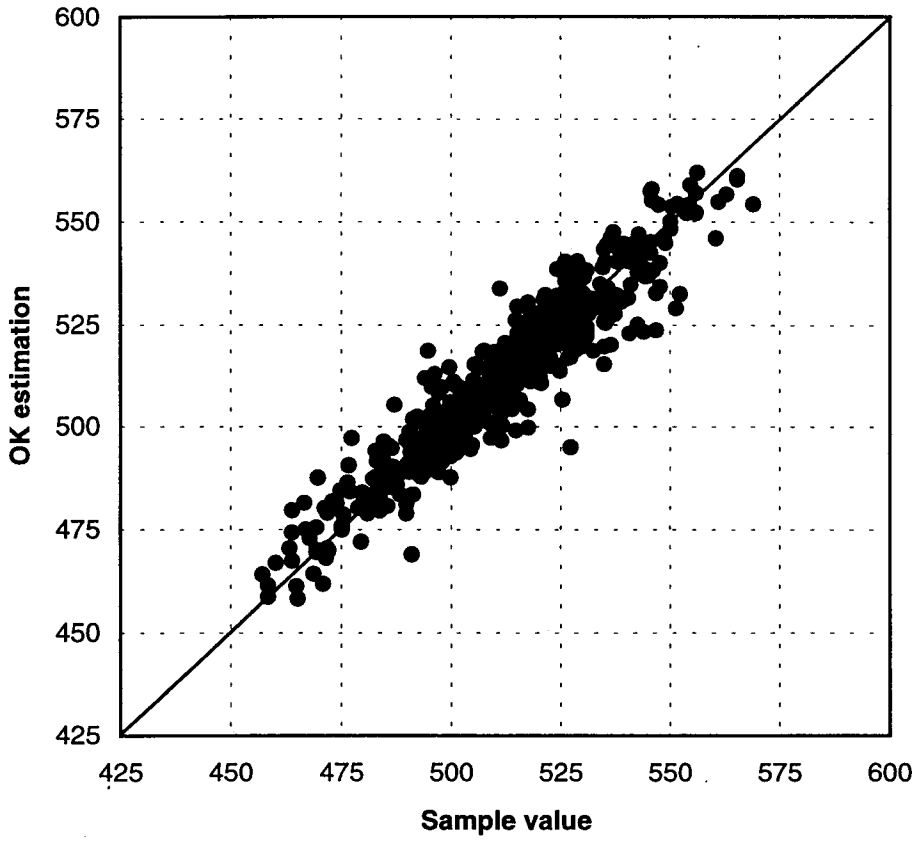

Figure 15. Scatter plot of measured bedrock elevations versus kriged values at sampled sites.

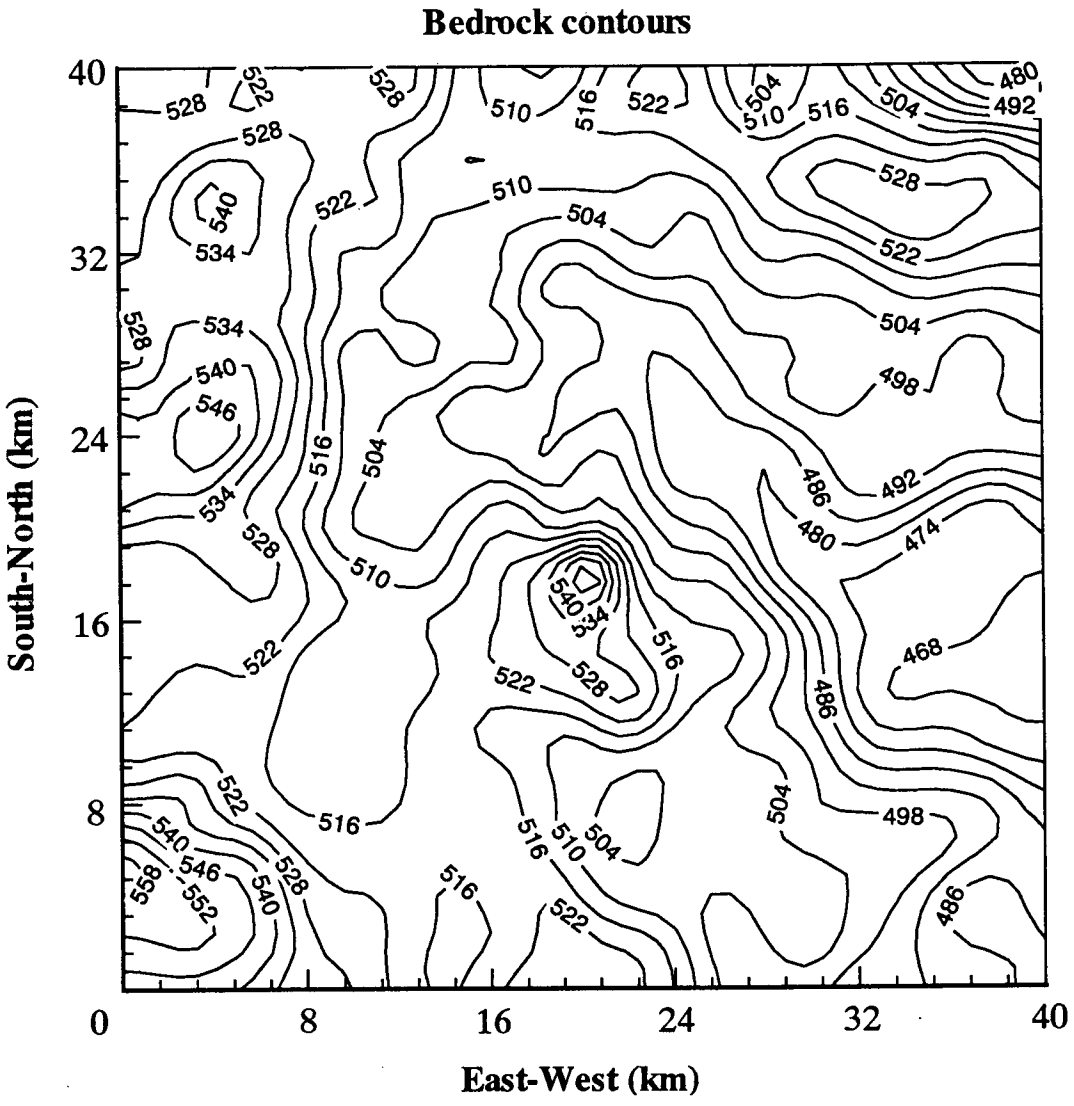

Figure 16. Contours of the kriged bedrock elevation.

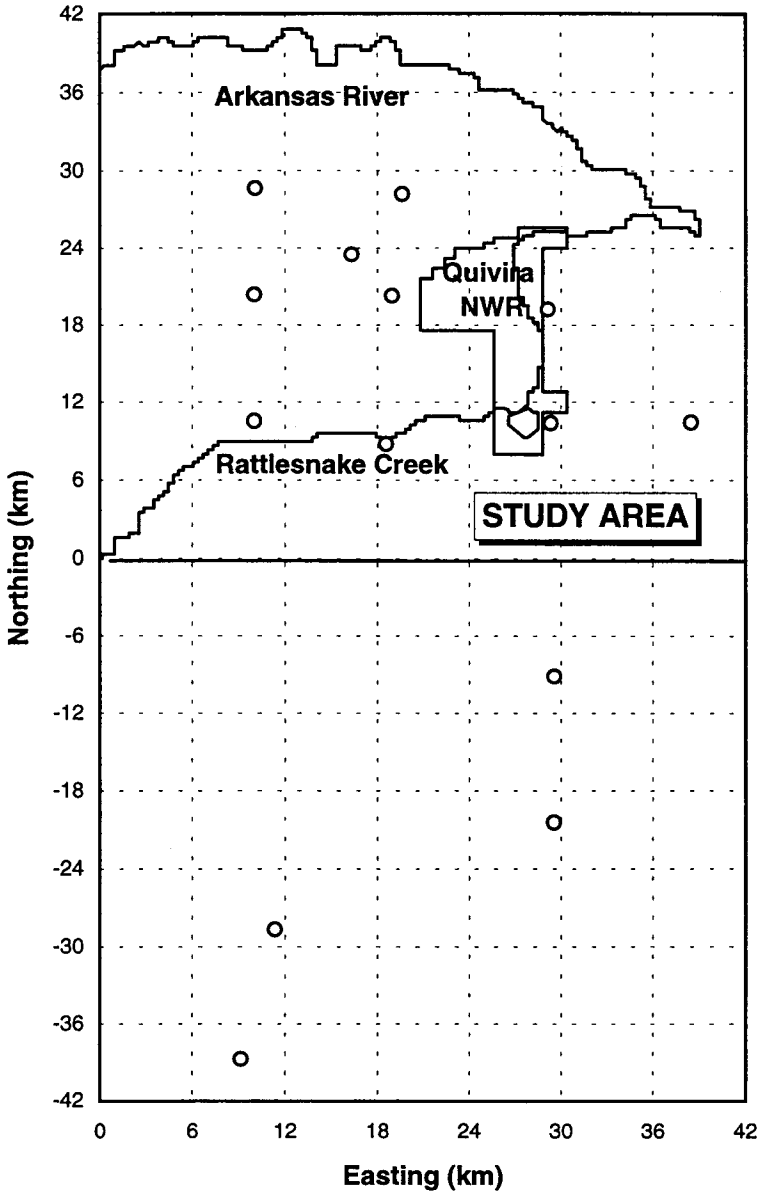

Figure 17. Locations (open circles) of saltwater-freshwater interface measurements.

Table 4. Measured water level, bedrock elevation, and elevation of 100* mS/m at 14 sites.

Site	Location	(See Fig. 17 for X, Y origin)		Water level elevation (meter)	Bedrock (ft) elevation (meter)	100 mS/m elevation (meter)
		X dir. (km)	Y dir. (km)			
1	23-12-12BAA	19.38	8.74	555.25	512.37	522.82
5	23-12-06BBB	10.82	10.50	564.86	510.24	541.11
9	24-10-31CBC	30.35	-9.12	532.18	508.41	511.58
11	22-10-06CBB	29.94	19.20	533.25	473.96	492.77
16	21-12-31CCC	10.82	20.34	566.93	503.53	525.84
17	21-12-36DDC	19.76	20.26	546.32	515.11	524.23
18	21-11-07BBB	20.43	28.16	545.90	486.46	507.80
21	26-11-01DDD	30.34	-20.46	542.36	507.19	514.50
22	21-12-06CCB	10.88	28.59	560.50	499.87	511.88
25	23-10-06BBA	30.13	10.35	540.62	512.67	534.86
26	23-10-01AAA	39.28	10.38	527.67	475.79	505.08
36	27-12-06BAA	12.16	-28.67	568.15	517.25	526.63
42	28-13-01CBA	9.95	-38.78	553.49	508.71	514.84
Siefkes	21-12-27DADD	16.34	23.47	558.09	504.14	515.93

* Approximate detection limit of EM instrument employed; it corresponds to a chloride concentration of about 3,300 mg/L.

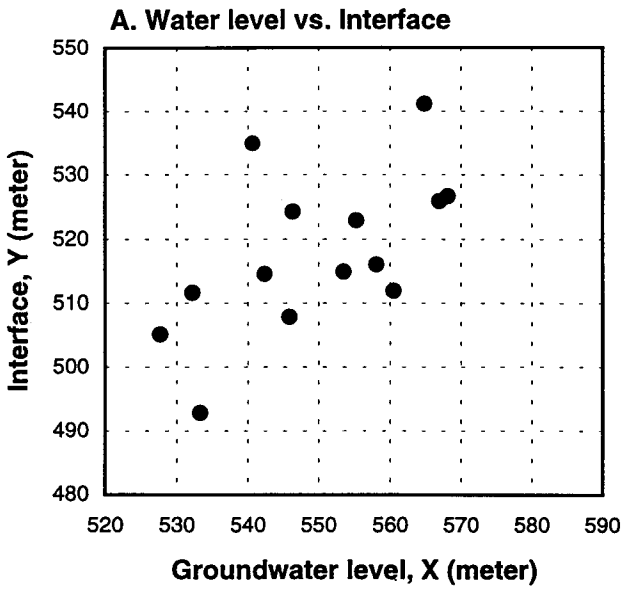

Number of samples : 14
Variable X : Mean : 549.68
Std. dev. : 12.88
Variable Y : Mean : 517.85
Std. dev. : 12.04
Correlation : 0.589
Rank correlation : 0.644

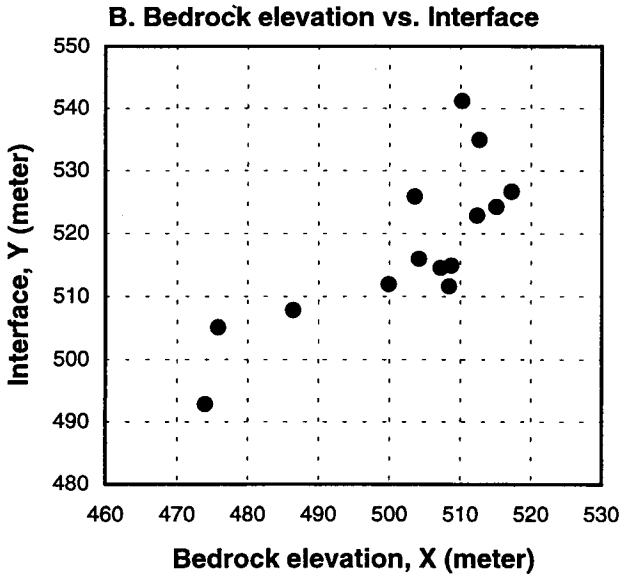

Number of samples : 14
Variable X : Mean : 502.55
Std. dev. : 13.44
Variable Y : Mean : 517.55
Std. dev. : 12.04
Correlation : 0.786
Rank correlation : 0.789

Figure 18. Correlations between the measured interface and hydraulic head, and between the interface and bedrock elevation.

saltwater-freshwater interface, only the bedrock elevation is used in the cokriging technique to estimate the elevation of the saltwater-freshwater interface.

In cokriging, in addition to the semivariogram model for the bedrock elevation (Eq. 3), the semivariogram model for the interface and the cross-variogram model between the bedrock and the interface are also needed. Table 5 shows the calculated AIC values for Spherical, Exponential, and Gaussian models and their corresponding nugget effect, range, and sill for both cases. Figure 19 shows the calculated semivariograms and the best-fitted semivariogram models for the saltwater-freshwater interface and the cross-variogram model between the bedrock and the saltwater-freshwater interface. The best fitted models for both cases are determined as the spherical model.

The semivariogram model for the saltwater-freshwater interface was estimated using a distance lag of 8.8 km, and a tolerance ± 4.4 km. The fitted omnidirectional spherical model is:

$$\gamma(h) = \begin{cases} C_0 + C_1\left(1.5\,\frac{h}{a} - 0.5\left(\frac{h}{a}\right)^3\right), & h \le a, \\ C_1 \qquad\qquad\qquad\qquad , & h > a \end{cases} \tag{5}$$

where the nugget effect C_0 is 0, the sill $C_0 + C_1$ is 204.63, h is the lag distance, and the range a is 17.4 km.

Because of the limited number of measured values, the fitted model does not match well the sample variograms for distance lags beyond 20 km. For lags less than 16 km, the semivariograms compared well with the sample. Therefore, Eq. 5 is still considered as an acceptable semivariogram model.

The cross-variogram for the interface and the bedrock was calculated with lag 8.8 km, tolerance ± 4.4 km. The following spherical model (with nugget effect 38.27, sill 128.27, and range 24.9 km) was selected as the fitted cross-variogram model. The fitted omnidirectional spherical model is:

Table 5. Akaike Information Criterion (AIC), nugget, sill, and range for spherical, exponential, and Gaussion models for A. Interface semivariogram. B. Interface-bedrock cross-variogram.

A. Interface semivariogram model

Model	AIC	Nugget	Sill	Range
Spherical	25.22	0.00	204.63	17.36
Exponential	26.69	0.00	209.15	19.44
Gaussian	27.14	0.00	211.43	15.17

B. Interface-bedrock cross-variogram model

Model	AIC	Nugget	Sill	Range
Spherical	21.31	38.27	128.27	24.94
Exponential	22.83	9.02	126.70	23.70
Gaussian	21.84	2.99	126.70	15.60

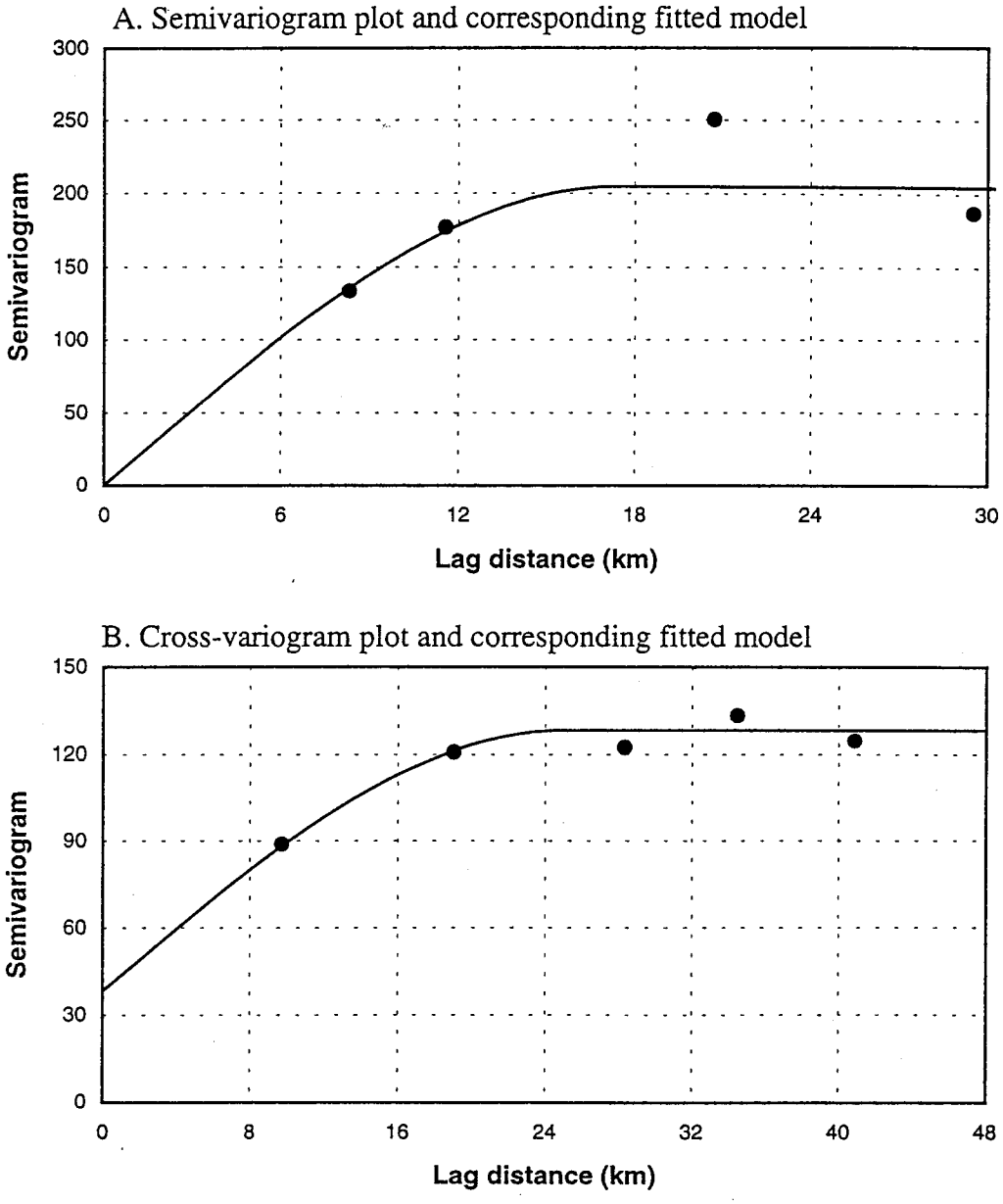

Figure 19. Sample semivariograms and cross-variograms and their corresponding fitted models.

$$\gamma(h) = \begin{cases} C_0 + C_1\left(1.5\,\frac{h}{a} - 0.5\left(\frac{h}{a}\right)^3\right), & h \le a. \\ C_1 \qquad\qquad\qquad\qquad , & h > a \end{cases} \tag{6}$$

Based on the linear combination of the above fitted models (Eqs. 4, 5, and 6), cokriging was performed and the estimated elevations of the saltwater-freshwater interface is shown in Fig. 20. The corresponding standard deviation is also estimated and the contour of the estimated standard deviation is shown in Fig. 21.

As can be seen in Fig. 20, the highest elevation is 550 m in the west and the lowest is 485 meters in the east. Because the high correlation between the bedrock and the interface, the contours of the interface are similar in pattern to the contours of the bedrock elevation shown in Fig. 16. The contours of estimation error (Fig. 21) shows that in an approximately square area defined by four measured wells, the error increases sharply from the location of the well to a maximum located around the center of the square area. A reasonable solution would be to place an additional observation well near the center of each square (highest estimation error).

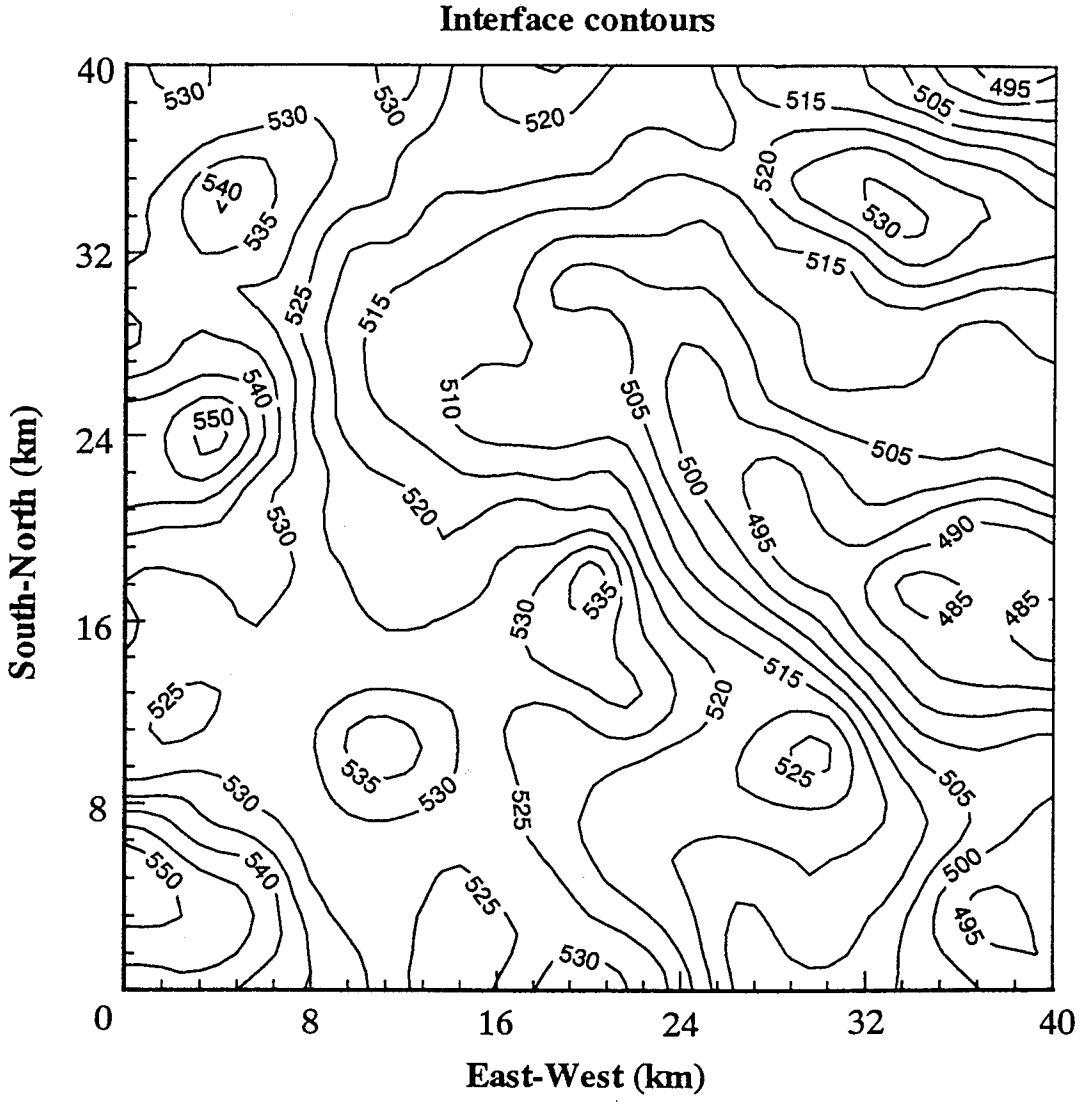

Figure 20. Contours of the cokriged saltwater-freshwater interface elevation based on the measured interface and bedrock data.

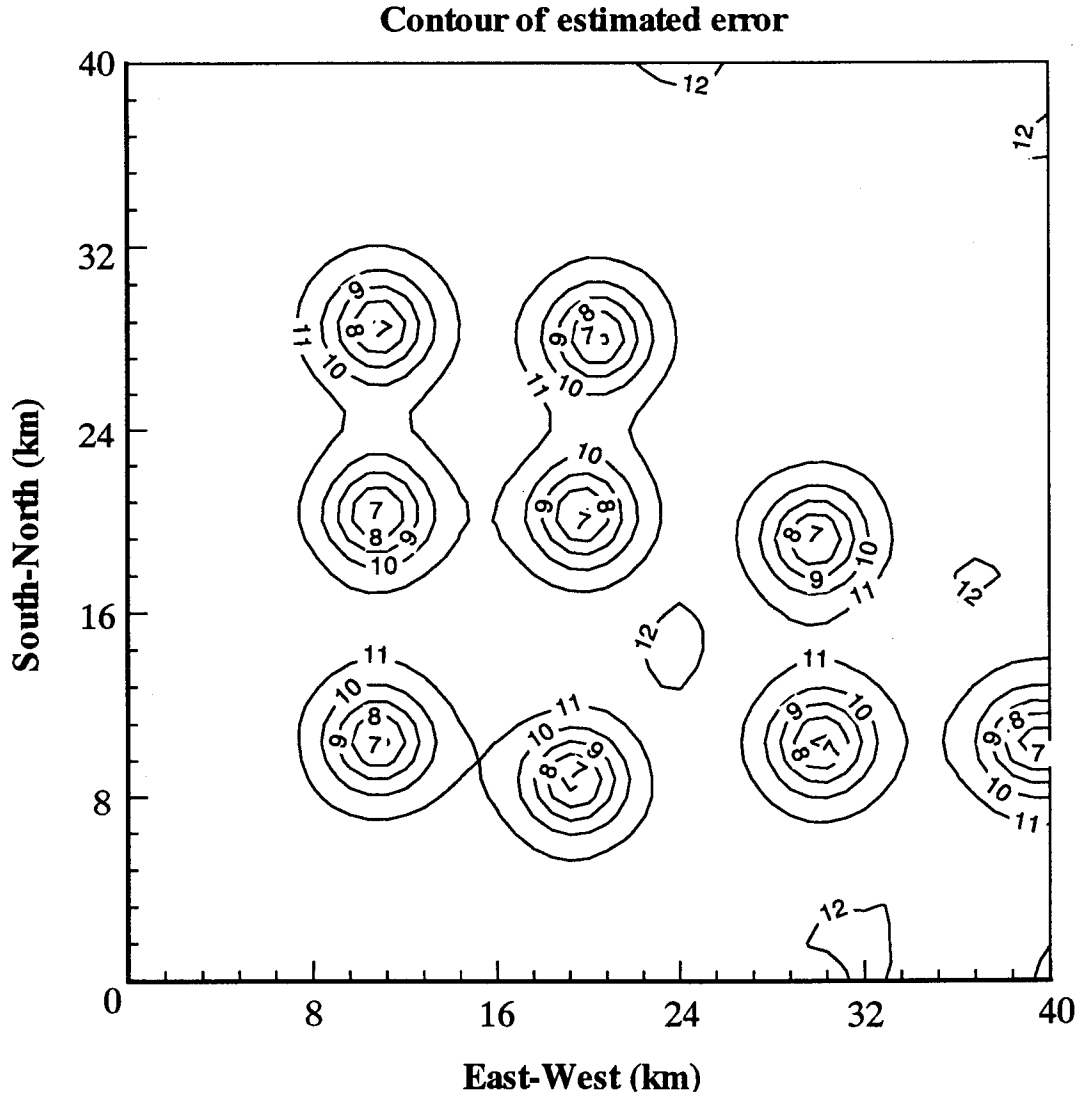

Figure 21. Contours of the estimated standard deviations for the cokriged interface elevation.

NUMERICAL MODEL FOR SALTWATER INTRUSION

The ground-water flow at the Siefkes site, which is located in the northern GMD5 (Fig. 1), is stratified with freshwater in the upper portion of the aquifer and saltwater in the lower portion of the aquifer. The source of the saltwater is the highly mineralized water of the Permian bedrock. The discharged water from an irrigation well at the Siefkes site becomes increasingly saline during the pumping season. In this study, an analysis of the basic characteristics of saltwater upconing in response to model input parameters, regional flow, and multi-well pumping are conducted using three-dimensional numerical models. The density-dependent solute-transport approach was employed, and two nonlinear partial differential equations (the ground-water flow equation and the advection-diffusion equation) are solved simultaneously by using a block-iterative, two-line, successive overrelaxation method (Varga, 1962). The finite difference model, SWIFT-II (Reeves, et al., 1986), is employed to solve these two governing equations. Two governing differential equations, the ground-water flow equation and the transport equation, and the initial and boundary conditions used to describe the saltwater intrusion in aquifers with a freshwater-saltwater transition zone are briefly discussed herein.

Conservation of Mass Balance of Fluid

The conservation of mass expresses the balance of water and solute mass in a solid matrix. The ground-water equation is based on the conservation of mass coupled with Darcy's law for flow in a porous medium. The general equations are:

$$-\nabla \cdot (\rho \underline{u}) - Qw + Rc' = \frac{\partial}{\partial t}(\phi \rho) \qquad \text{and} \qquad (7)$$

$$\nabla = \left(\frac{\partial}{\partial x}\right) i + \left(\frac{\partial}{\partial y}\right) j + \left(\frac{\partial}{\partial z}\right) k \,, \qquad (8)$$

where ρ is fluid density (ML^{-3}); $\underline{u}$ is fluid velocity vector (LT^{-1}); Qw is sink or source [$(M(L^3T)^{-1}$]; a positive sign denotes a sink, a negative sign denotes a source; ϕ is the effective porosity; Rc′ is the salt dissolution [$(M(L^3T)^{-1}$]; and *i*, *j*, and *k* are unit vectors in Cartesian coordinates.

The flow equation is Darcy's law:

$$\underline{u} = \left(\frac{k}{m}\right) \cdot (\nabla p - rg\nabla z) \tag{9}$$

where κ is the solid matrix permeability (L^2), a vector quantity; μ is the fluid viscosity [$M(LT)^{-1}$]; g is the gravitational acceleration (L/T^2); and z is the potential head (L).

Fluid density is assumed to be a function of salt concentration and pressure and effective porosity ϕ is a function of pressure p. The fluid viscosity μ depends on the salinity concentration and the temperature of the fluid.

Conservation of Solute Mass Balance

The solute mass balance is expressed as:

$$-\nabla\cdot\left(\rho\,\hat{C}\,\underline{u}\right) + \nabla\cdot\left[\rho\left(D_{i,j} + D_m I\right)\cdot\nabla\hat{C}\right] - Q_w\hat{C}_l = \frac{\partial}{\partial t}\left(\phi\,\rho\,\hat{C}\right) \tag{10}$$

where D_m is the molecular diffusivity (L^2T^{-1}); $D_{i,j}$ is the dispersion tensor (L^2T^{-1}); and I is the identity tensor.

Equation 10 describes the rate of change of solute in the fluid phase in terms of the net dispersive and diffusive flux, the net advective flux, and the solute source or injection rate.

The dispersion coefficient is originally from Bear (1961) and Scheidegger (1961). For an isotropic porous medium, the dispersion tensor $D_{i,j}$ is a function of velocity of ground-water flow, and can be expressed by the longitudinal dispersivity α_L (m) and the transverse dispersivity α_T (m):

$$D_{ij} = (\alpha_L - \alpha_T)\frac{u_i u_j}{u} + \alpha_T u \delta_{ij}, \tag{11}$$

$$u = \left(u_1^2 + u_2^2 + u_3^2\right)^{1/2}, \tag{12}$$

where u_i(x,y,t) is the velocity in the i the direction; δ_{ij} is the Kronecker delta function; and i and j are unit vectors in the Cartesian coordinates.

Initial and Boundary Conditions

For the problem of interest, supplementary information (initial and boundary conditions) has to be provided for the solutions of the above equations. The hydrostatic equilibrium is assumed for the initial pressure distribution. The boundary condition is to specify that the dependent variables are known functions of space and time in the simulated domain. The boundary conditions can be generally classified into three types, Dirichlet, Neumann, and Cauchy.

The initial and boundary conditions and the above two partial different equations (Eqs. 7 and 10) are solved by the finite-difference scheme to determine the piezometric heads and the concentrations at nodes inside the aquifer boundary. Numerical procedures for solving the governing equations require an appropriate mesh and time steps. The set of linear equations generated by spatial discretization have to be solved repeatedly as the simulation time advances. To solve the partial differential equations (Eqs. 7 and 10) by using the finite-difference technique, the two-line, successive overrelaxation method (Varga, 1962) is employed. It is a block-iterative method, the optimal overrelaxation

factor is first estimated to increase convergence; then two neighboring lines of nodes are oriented and solved together by direct elimination. Once the optimal relaxation parameters and the optimal directions are determined at the time step for each transport equation, a convergent solution can be achieved. Although this matrix solver is efficient, numerical dispersions and oscillations will occur and accumulate at each time step due to the truncation of the high order derivatives of the Taylor series. The finite difference equations are considered to be stable if the numerical dispersion and oscillations are less than a certain tolerance. The numerical instability is mainly from the diffusion-convection equation (Price et al., 1966); therefore, stability analysis is preferable. A general guide to avoid numerical problems is to check the Courant number (*Co*), which controls numerical oscillation from the discrete approximation of the time derivative, and the Peclet number (*Pe*), which controls oscillations from spatial discretization. These two constraints provide a general guide for the selection of the local grid spacing in x, y, and z directions and for the time step, Δt (Frind, 1982). The two criteria corresponding to the x coordinate direction are:

$$Co_x = \frac{v_x \Delta t}{\Delta x} \leq 1 \qquad \text{and} \qquad (13)$$

$$Pe_x = \frac{v_x \Delta x}{D_{xx}} \leq 2 \ . \qquad (14)$$

The same criteria also apply to y and z coordinate directions. For multi-dimensional transport, stability criteria are functions of variables in all directions.

The flow equation (Eq. 7) does not involve the convective diffusion term; therefore, the numerical instability is not significant and usually can be ignored.

Sensitivity Analysis of Saltwater Upconing under pumping stress

The conceptual model employed in this study is largely based on the actual field conditions at the Siefkes site. The saltwater transition zone is shown in the corrected EM log (Fig. 4B). The thickness of the aquifer from the ground level to the Permian bedrock is approximately 60 m. The saltwater-freshwater interface is defined as a zone approximately 40 m below the surface with a clay lens above it and a chloride concentration exceeding 500 mg/L. An irrigation well exists at the Siefkes site with the pumping rate of 50 x 10^{-3} m^3/s (800 gpm), and the well is screened from 18 to 24 m and 27 to 37 m below ground level.

The physical system of the simulated area in the X-Z and Y-Z planes and boundary conditions are shown in Fig. 22. The alluvial aquifer extends from 0 to 39 m in the Z direction and the Permian bedrock from 39 to 45 m. To evaluate the impact of clay-layer stratigraphy on saltwater intrusion, a continuous clay layer, a discontinuous clay layer, and a partial clay layer were simulated, and the physical systems for each of these are shown in Fig. 23. In the discontinuous clay layer case, a 300-m-wide discontinuity is assumed to be located 9 m below the pumping well (Fig. 23B). In the partial clay layer, a 900 m continuous clay layer is assumed to be located 9 m below the pumping well (Fig. 23C). The entire simulated area is 6000 m by 3300 m by 45 m, and this simulated area is meshed by a 20 x 11 x15 grid with uniform spacing of 300 m in the X and Y directions and uniform spacing of 3 m in the Z direction. The pumping well is screened from 21 to 24 m below the initial water table.

Although the physical set up of the model is not exactly the same as the Siefkes site, it is similar enough that the mechanism of saltwater migration is also expected to be similar. The major source of the salt comes from the Permian bedrock. Brine concentration is calculated by dividing the total mass of discharged salt during each time step by the total mass of pumpage during the same period. The porewater chloride concentration in the upper portion of the Permian bedrock is approximately 28,000 mg/L (Garneau, 1995) (average seawater chloride concentration = 19,400 mg/L), which was

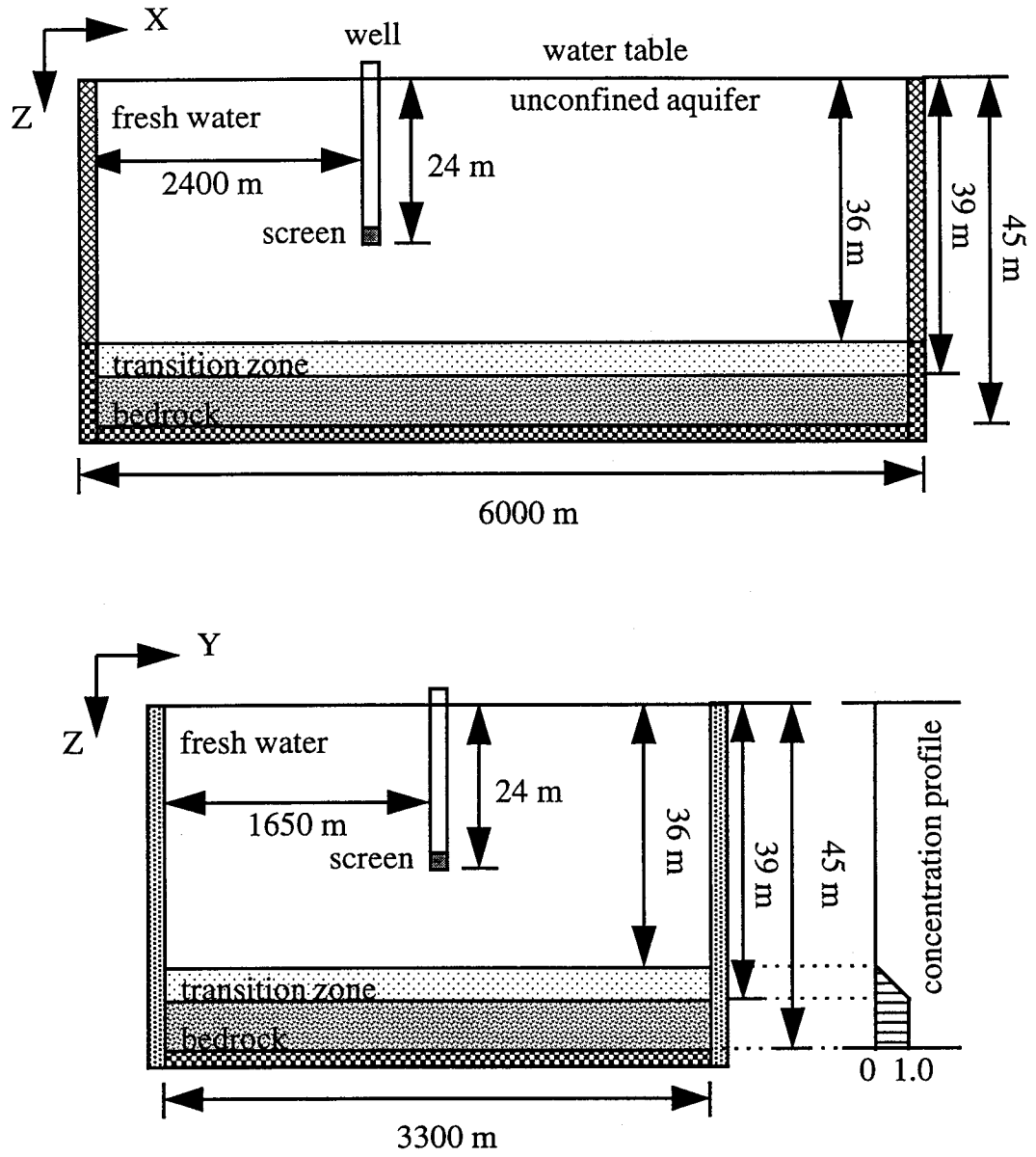

Figure 22. Physical system and boundary conditions for the conceptual model.

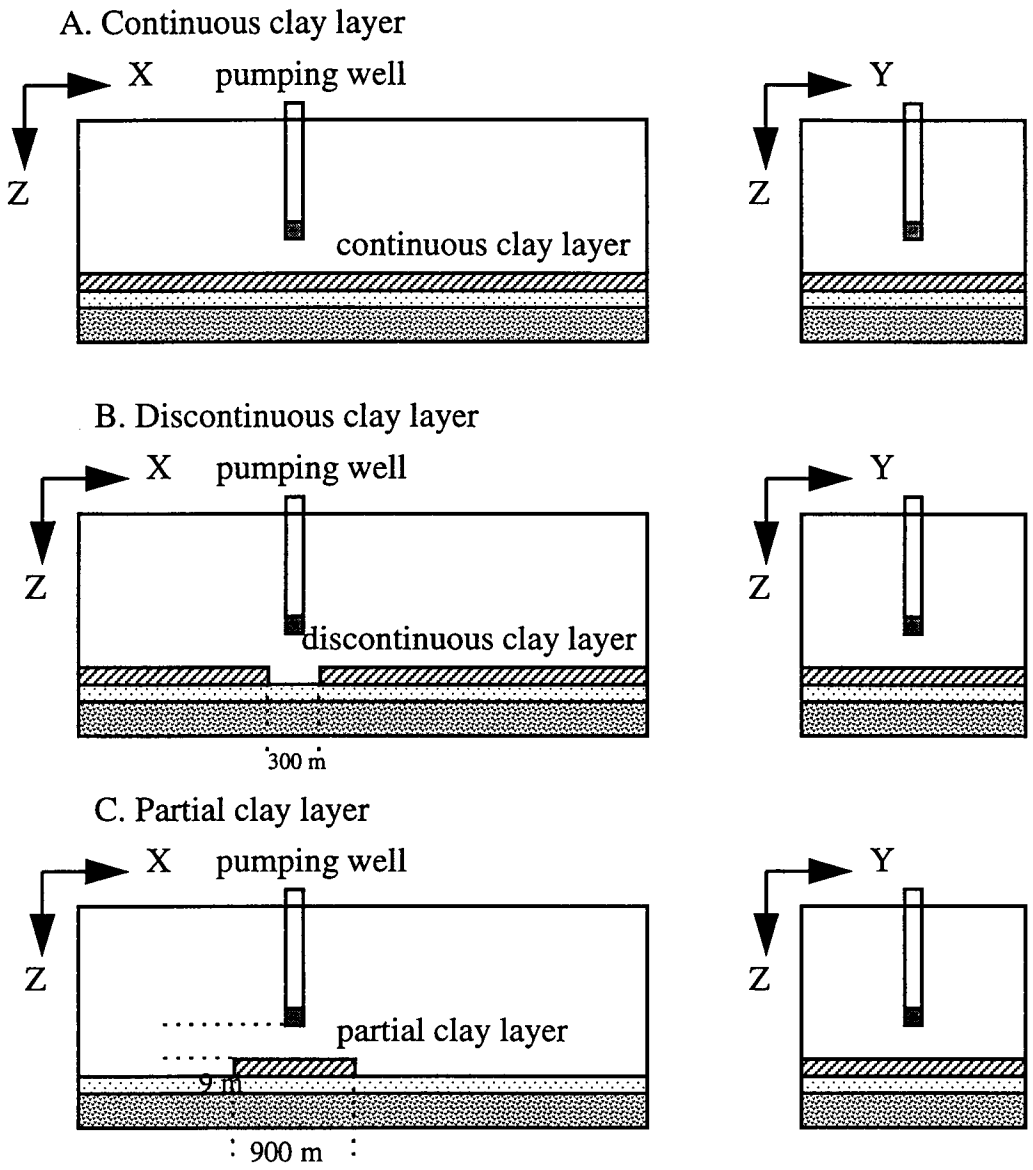

Figure 23. Configurations of the clay layer.
A. continuous clay layer
B. discontinuous clay layer
C. partial clay layer

normalized as dimensionless brine concentration of 1.00 and used in the numerical model.

Thirteen simulation cases were considered in this study. These are summarized in Table 6. In the basic model (Case #1), the initial water table condition was assumed to be horizontal and the initial saltwater thickness starts at 36 meters below the initial water table with brine concentration varying with depth from 0.0 to 1.00. The initial saltwater-freshwater transition zone was assumed to extend from 36 m to 39 m in depth, with brine concentration equal to 0.50, whereas the brine concentration of the bedrock is assumed to be 1.00. At a fixed pumping rate of 0.05 m^3/sec (800 gpm), the computation is carried out with one-day time increments for 365 days to determine the temporal variation of salinity of discharged water. The values of model variables, parameters, and the properties of clay layer and bedrock are summarized in Table 7.

In simulation case #2, the effect of horizontal conductivity was investigated. The values of horizontal conductivity were changed from 2.3 m/d to 230 m/d. Similarly, to investigate the effect of vertical conductivity (Case #3), the values of vertical conductivity were changed from 0.23 m/d to 23 m/d. Hydraulic conductivity can vary several orders of magnitude and is usually considered to be a highly uncertain parameter in simulations. The mixing of freshwater and saltwater is dominated by the horizontal conductivity; this process will dilute the brine concentration and render the upconing of saltwater less significant. Increasing the vertical hydraulic conductivity will increase the vertical velocity, thereby increasing the velocity of saltwater upconing. If K is defined as the ratio of horizontal hydraulic conductivity, Kx, divided by the vertical conductivity, Kz, dimensionless ratios of K = 1, 10, and 100 are used in both above-mentioned cases (cases #2 and #3). The computed temporal variations of the dimensionless salinity of pumped water are shown in Fig. 24. Increasing the ratio of horizontal to vertical hydraulic conductivity decreases the upward motion of saline water and lowers the salinity discharged water. For K = 100, the year-end salinity of pumped-out water is about 5% of the maximum dimensionless salinity, whereas for K = 1, the year-end value is 17.4%,

Table 6. Simulation cases in the three-dimensional numerical model for saltwater upconing simulation.

Case No.	Descriptions
1.	Single pumping well (basic case). The input parameters, variables, and boundary conditions are described in Table 7 and Fig. 22, respectively.
2.	Investigation of the effect of horizontal conductivity, *Kx* and *Ky*, by changing the *Kx* and *Ky* from 2.3 m/day to 230 m/day (7.5 ft/day to 750 ft/day).
3.	Investigation of the effect of the vertical conductivity, *Kz*, by changing the *Kz* from 0.23 m/day to 23 m/day (0.75 ft/day to 75 ft/day).
4.	Investigation of the effect of the longitudinal dispersivity, α_L, by changing the α_L from 0.1 m to 10 m (0.33 ft to 33 ft).
5.	Investigation of the effect of the transverse dispersivity, α_T, by changing the α_T from 0.01 m to 1 m (0.033 ft to 3.3 ft).
6.	Investigation of the effect of well-screen location by moving the well screen 9 m up and 9 m down from the reference model.
7.	Investigation of the effect of the porosity, ϕ, by changing the ϕ from 0.1 to 0.4.
8.	Investigation of the effect of various recharge amounts by uniformly imposing 0.05, 0.127, and 0.254 m/year (2, 5, and 10 in./yr) recharge to the aquifer.
9.	Investigation of the effect of preferential recharge by imposing 10, 30, and 50% of total pumpage as irrigation return recharge to the aquifer.
10.	Investigation of the effect of the pumpage by changing the pumpage from 0.01 m^3/s to 0.09 m^3/s (160 gpm to 1440 gpm).
11.	Investigation of the effect of the spatial distribution of clay layers. A continuous clay layer, a discontinuous clay layer, and a partial clay layer are considered.
12.	Investigation of the effect of water-table gradient by changing the slope of water table from 0 to 0.015.
13.	A second pumping is considered and located 300 and 900 meters on both up and down stream. The water-table gradient is 0.0025.

Table 7. Values of parameters used in the basic model.

(a) The basic model

Aquifer Parameters

Horizontal hydraulic conductivity	K_X & K_Y = 23 m/d (75 ft/d)
Vertical hydraulic conductivity	K_Z = 2.3 m/d (7.5 ft/d)
Porosity	ϕ = 0.2
Bulk porous matrix compressibility	$\alpha = 2.58 \times 10^{-7}[kg/(m\ s^2)]^{-1}$
Longitudinal dispersivity	α_L = 1 m
Transverse dispersivity	α_T = 0.1 m

Properties of water and brine

Density of water	$\rho_o = 1{,}000\ kg/m^3$
Density of brine	$\rho = 1{,}036\ kg/m^3$
Coefficient of viscosity of water	$\mu = 1.0 \times 10^{-3}\ kg/(m\ s)$
Solute molecular diffusivity	$D_m = 1.0 \times 10^{-10}\ m^2/s$

Bedrock Properties

Location (m)	Thickness (m)	K_X & K_Y (m/d)	K_Z (m/d)	Porosity
39-45	6	0.023	0.0023	0.05

(b) The modified model (basic model plus a clay layer)

Clay Layer Properties

Location (m)	Thickness (m)	K_X & K_Y (m/d)	K_Z (m/d)	Porosity
33-36	3	0.023	0.0023	0.4

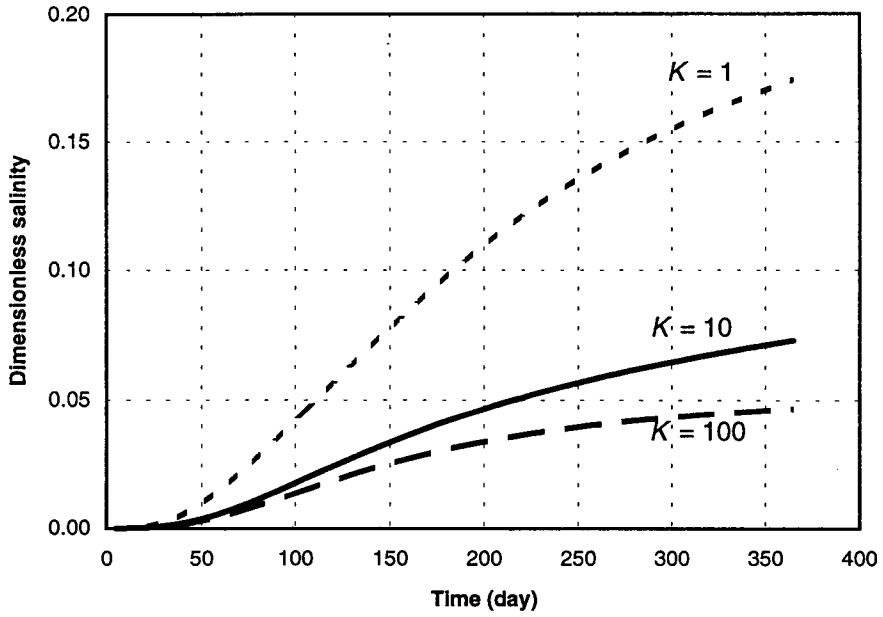

Figure 24. Effects of different values of horizontal to vertical hydraulic conductivity ratio, K (= Kx/Kz) on salinity of discharged water.

which represents a chloride concentration of 4,882 mg/L. Such concentration exceeds the maximum recommended value of 500 mg/L for irrigation water.

In case #4 the effect of longitudinal dispersivity, α_L, was evaluated. The values of α_L were changed from 0.1 m to 10 m. The effect of transverse dispersivity, α_T, was investigated in case #5: values of α_T were changed from 0.01 m to 1 m. Figure 25 summarizes the results for cases #4 and #5. Saltwater migration is generally controlled by the combination of advection, dispersion, and diffusion. Dispersion and diffusion are not critical in the saltwater-upconing simulation since the dominant factor is advection. The dispersion tensor, D (Eq. 11), is a function of flow velocity and is used to represent the mixing of saltwater and freshwater. Higher values of α_L or α_T will result in more significant mixing of freshwater and saltwater; however, the impact of longitudinal and transverse dispersivities is not as significant as the hydraulic conductivity.

The effect of well-screen location was investigated in case #6. The location of the well screen was shifted 9 meters up and down, thus changing the distance from the well screen to the saltwater-freshwater interface. Flow velocity is inversely proportional to the distance to the pumping well. Therefore, as Fig. 26 shows, the upward movement of saltwater becomes less significant when the distance between the well screen and the saltwater-freshwater interface increases.

In case #7 the effect of porosity, ϕ, was evaluated by changing the values of ϕ from 0.1 to 0.4 (Fig. 27). The average velocity, V, is given by the specific discharge obtained from Darcy's law (Eq. 9) divided by the effective porosity; in other words, V is inversely proportional to the porosity. The brine is mainly transported by advection; therefore, the saltwater upconing was less significant when porosity is high (and vice versa).

To investigate the effect of recharge (case #8), values of 0.05, 0.127, and 0.254 m/year (2, 5, and 10 in./year) of recharge were imposed. This recharge was uniformly distributed into the aquifer. Under these circumstances, a recharge value of 0.05 m/year only contributes 1.43×10^{-4} m^3/s (2.3 gpm) to each cell in the simulation model, which is

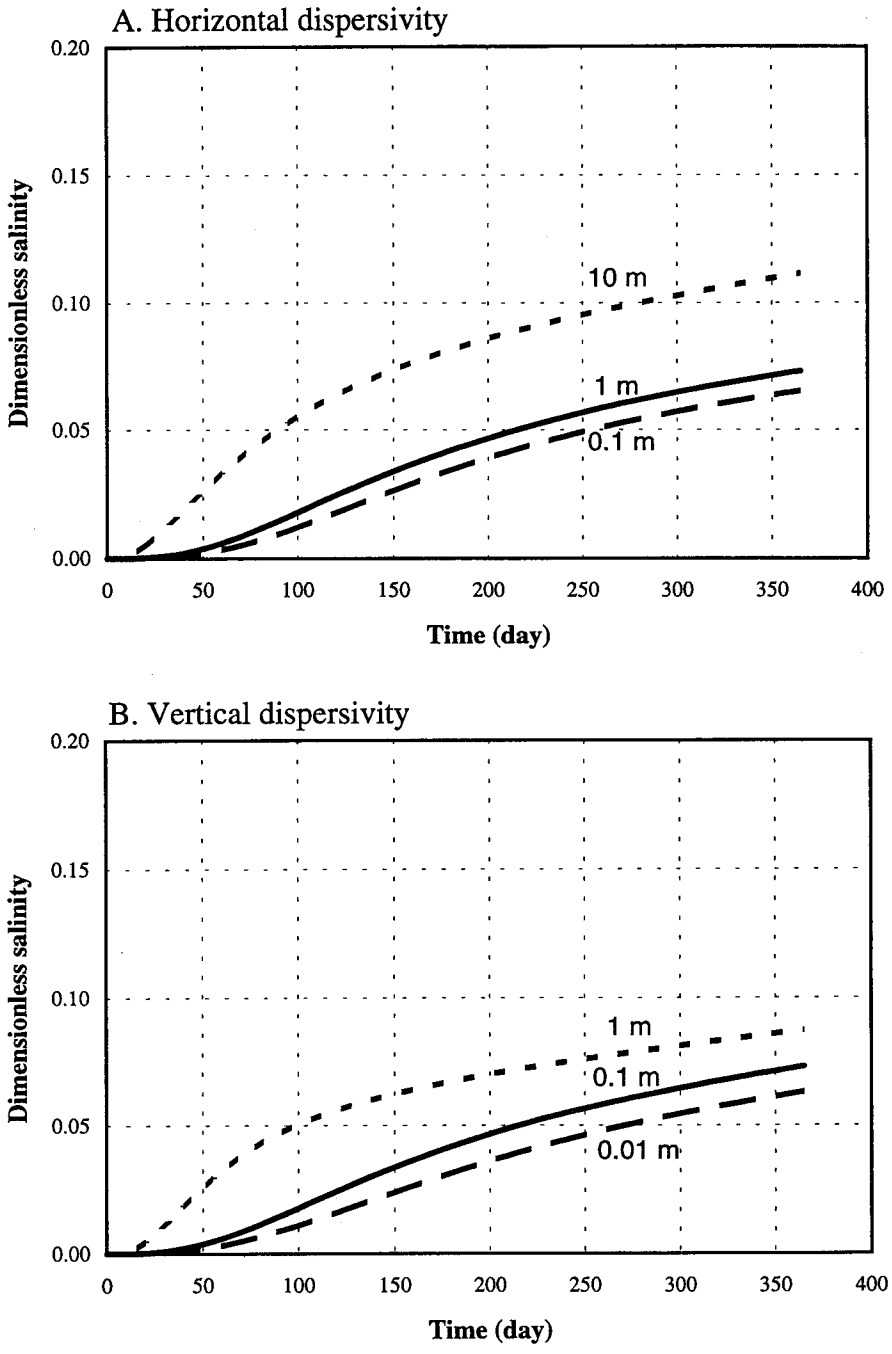

Figure 25. Effects of dispersivities on salinity of discharged water:
A. horizontal dispersivity.
B. vertical dispersivity.

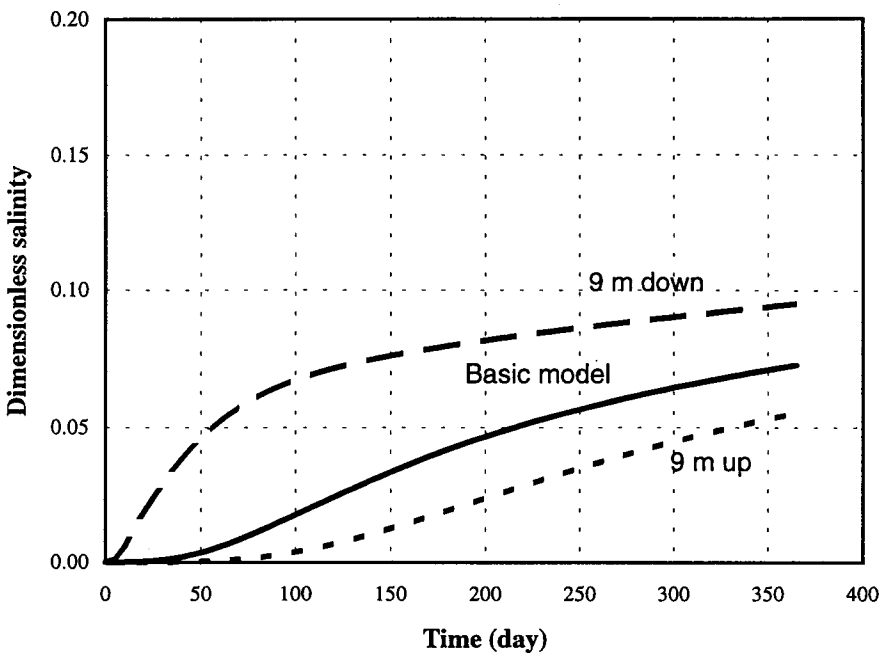

Figure 26. Effects of screen location on discharged water salinity.

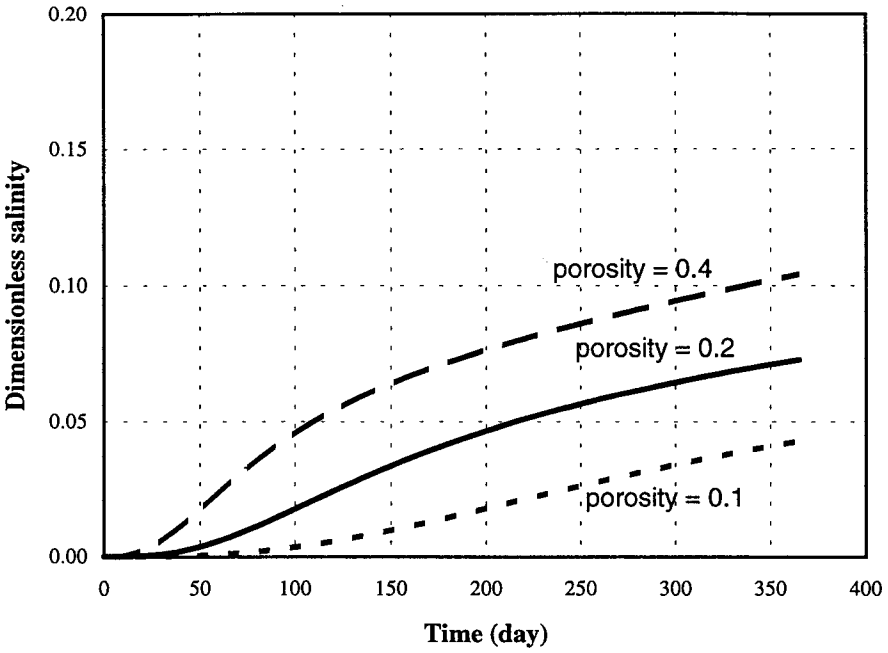

Figure 27. Effects of effective porosity on discharged water salinity.

much lower than the local pumping rate (800 gpm). Increasing recharge will alleviate the saltwater upconing problem; however, the average annual recharge in south-central Kansas is about 0.05 m (Sophocleous, 1992, 1993). Therefore, the surface recharge considered in case #8 will not significantly relax the saltwater upconing. These results are shown in Fig. 28.

The effect of focused recharge was investigated in case #9. The 1994 water samples collected from the Siefkes site irrigation well (Young, 1995) showed a great fluctuation in chloride concentration (from 135 mg/L to 335 mg/L). Lower concentrations were observed when pumping stopped for a while or when thunderstorms occurred before pumping; this may imply that the upconing of saltwater is significantly diluted by local recharge during the nonpumping period. Sophocleous (1981) used 10%, and Luckey et al. (1986) used 30 to 55% of total pumpage as irrigation return water to ground water in their studies; therefore, in this simulation (case #9) 10, 30, and 50 percent of the discharged ground water was returned to the aquifer through the pumping cell area. The effects of this preferential recharge are illustrated in Fig. 29 and demonstrate the importance of localized recharge on the upconing of saltwater.

It was initially surprisingly to find that uniform surface recharge did not significantly alleviate the saltwater-upconing problem. The relatively low recharge rate and the fact that recharge and pumping were activated at the same time may be the main reasons for the insignificant impact; however, as case #9 shows, irrigation return as additional recharge had considerable impact.

In case #10 the pumping rate was changed from 0.01 m^3/s to 0.5 m^3/s (160 gpm to 8000 gpm). The large increase in salinity as the pumping rate increases was expected. The daily variations in the salinity of discharged water during 365 days of continuous pumping at 0.01, 0.1, and 0.5 m^3/s are shown in Fig. 30. At a rate of 0.01 m^3/s (160 gpm), the year-end increase in salinity is relatively insignificant. This pumping rate would probably be safe over the long term without causing severe deterioration of the water

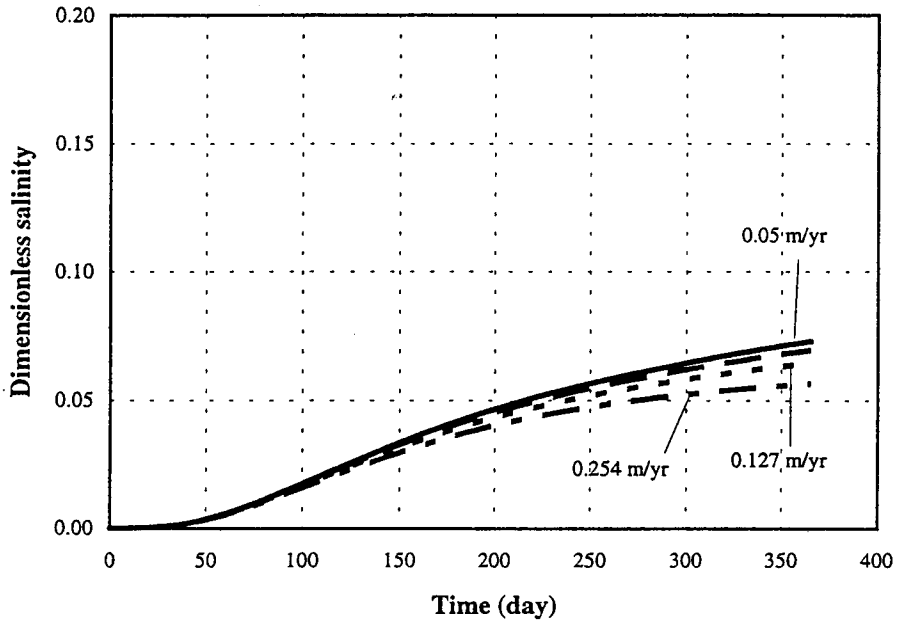

Figure 28. Effects of uniform recharge on discharged water salinity.

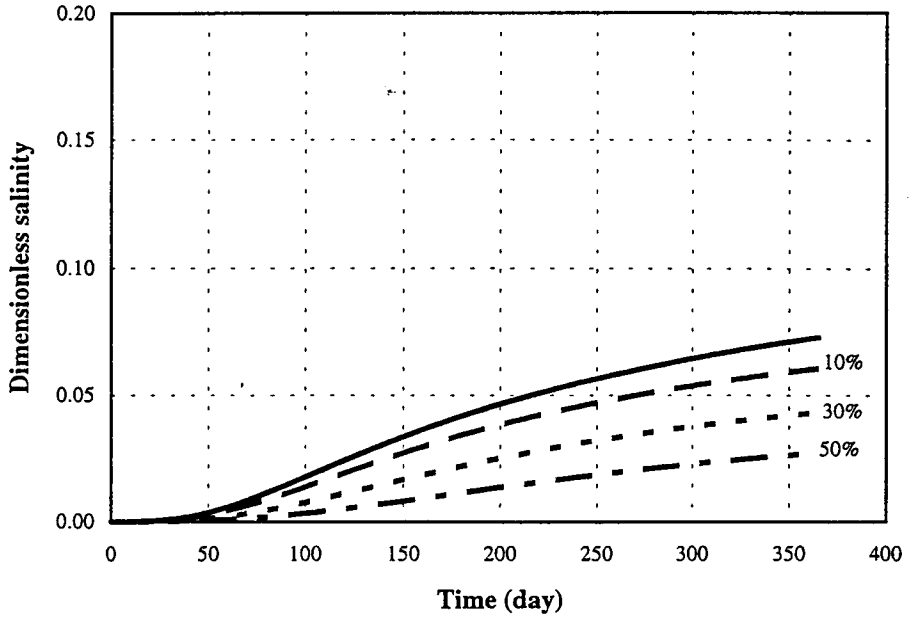

Figure 29. Effects of preferential recharge on discharged water salinity.

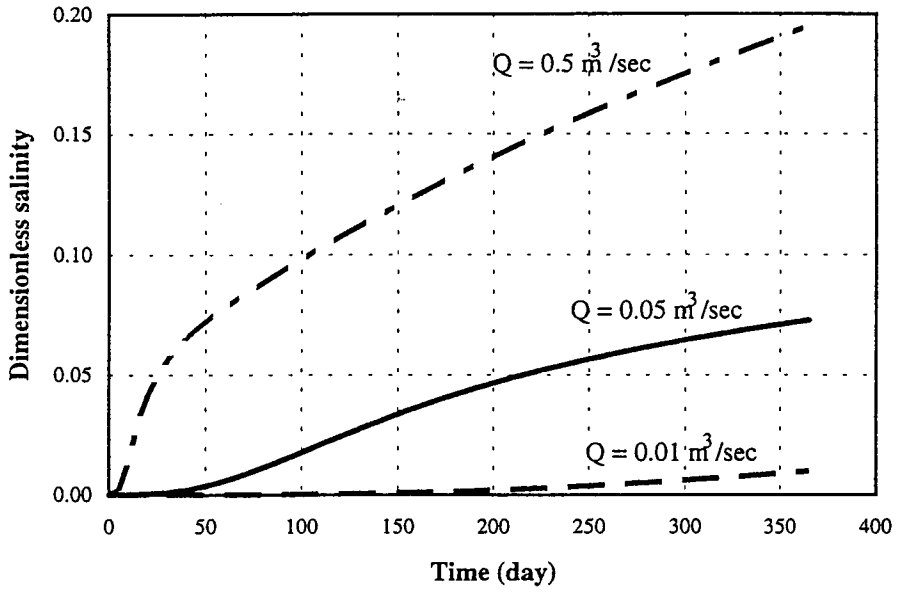

Figure 30. Effects of different pumping rates on discharged water salinity.

quality. Obviously, a pumping rate of 0.5 m^3/s (8,000 gpm), which causes the salinity to increase from zero to 0.20 in a year, is unacceptable.

The effect of the spatial distribution of clay layers was studied in case #11. A continuous clay layer (Fig. 23A), a discontinuous clay layer (Fig. 23B), and partial clay layer (Fig. 23C) were considered and compared with the basic case (case #1). As can be seen from the simulation results (Fig. 31), the clay layer is the most important factor controlling the migration of saltwater. Saltwater upconing can barely be seen with the protection of a continuous and partial clay layer; however, a discontinuous clay does not offer much protection.

In case #12 the effect of regional flow was investigated by changing the slope of water table from 0 to 0.0015 with flat bedrock. The physical system of investigation of the effect of regional flow is shown in Fig. 32. Because of the resistance of the aquifer media, ground-water flow is a slow process. The influence of regional flow on the migration of saltwater is much less significant than the local pumping activity. Figure 33 shows that regional flow has little effect on salinity and can practically be ignored.

The effect of locating an additional pumping well upstream and downstream was investigated in case #13. The physical system of multi-well cases is shown in Fig. 34, and the separation distances, *d*, considered in this simulation are 300 meters and 900 meters upstream and downstream. The results of the above three cases are shown in Fig. 35. This simulation demonstrates the importance of nearby pumping activity; the influence of an additional pumping well is inversely proportional to the separation distance. However, wells closer together than 300 meters were not considered due to the model grid-spacing.

As shown above, saltwater intrusion is affected by numerous parameters. We ranked all the parameters considered in this study according to their impact on water quality in the alluvial aquifer. To assess this, we used the following formula based on the results of discharged brine concentration at the end of the simulation period (the 365th simulation day):

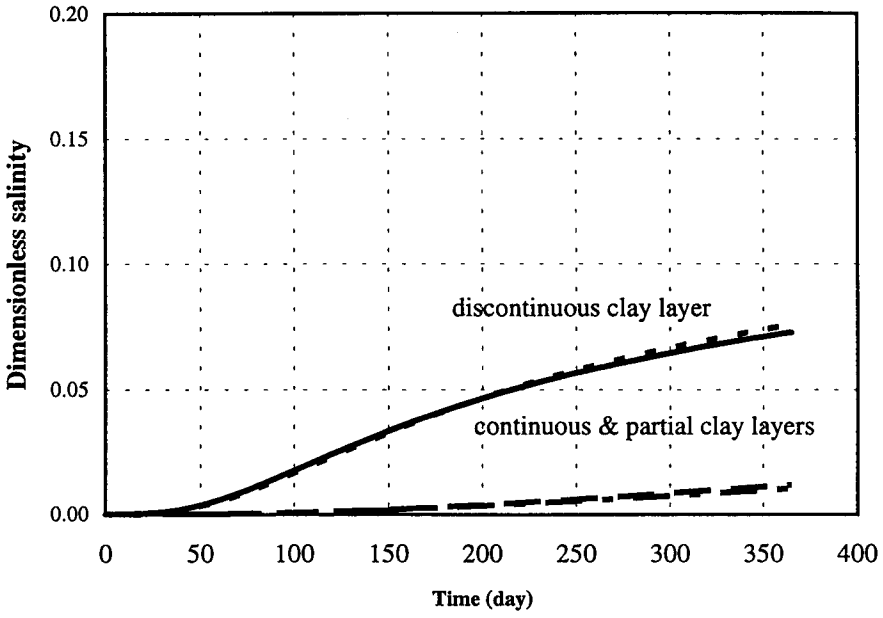

Figure 31. Effects of spatial distribution of clay layers on salinity of discharged water salinity.

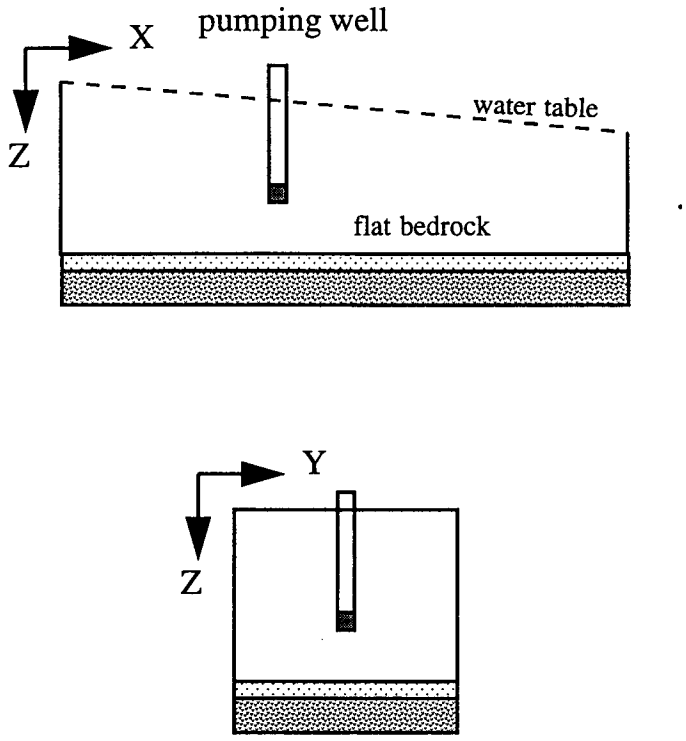

Figure 32. Physical system of numerical model considered in case #12. The water table gradient ranges from 0 to 0.0015.

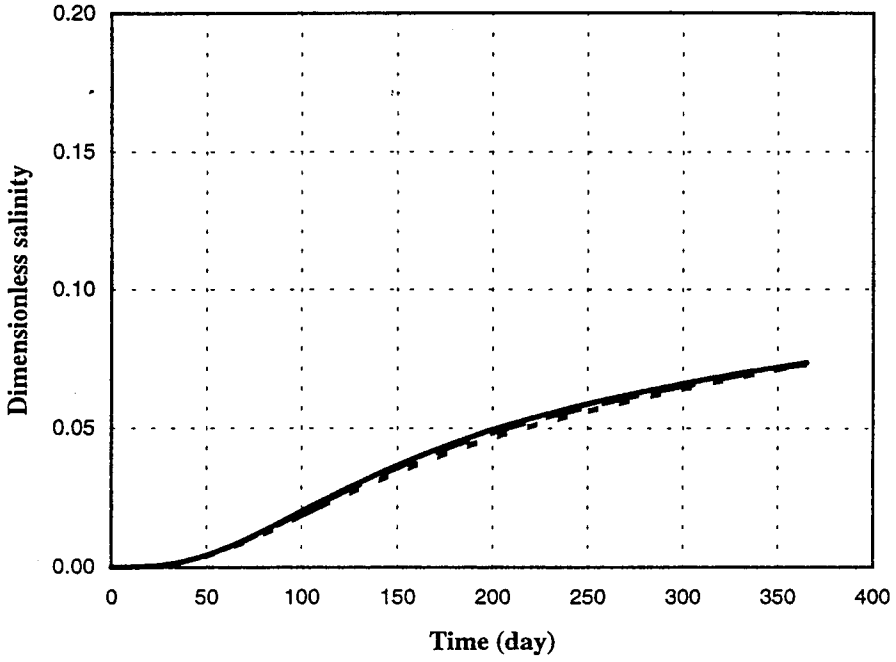

Figure 33. Effects of water table slope on discharged water salinity.

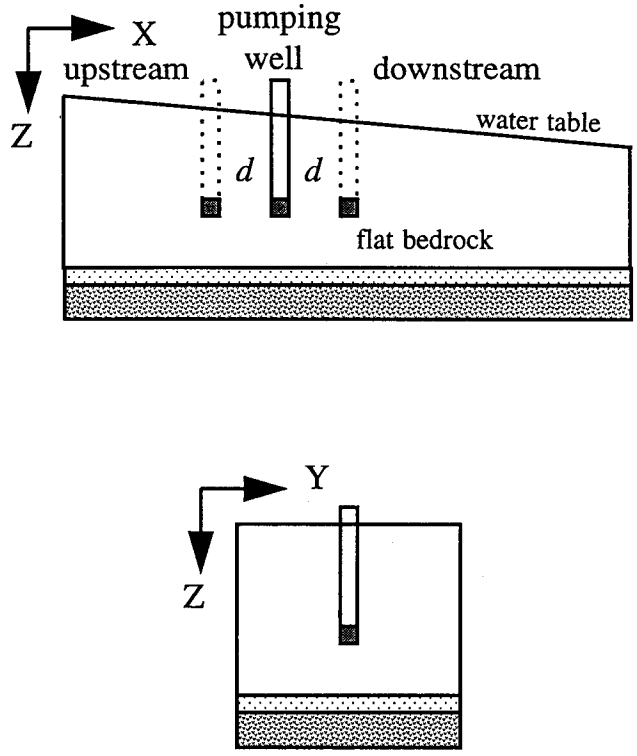

Figure 34. Plot of two-well system (case #13). The initial water table gradient is zero and the separation distances between the wells are 300 and 900 meters, in both upstream and downstream.

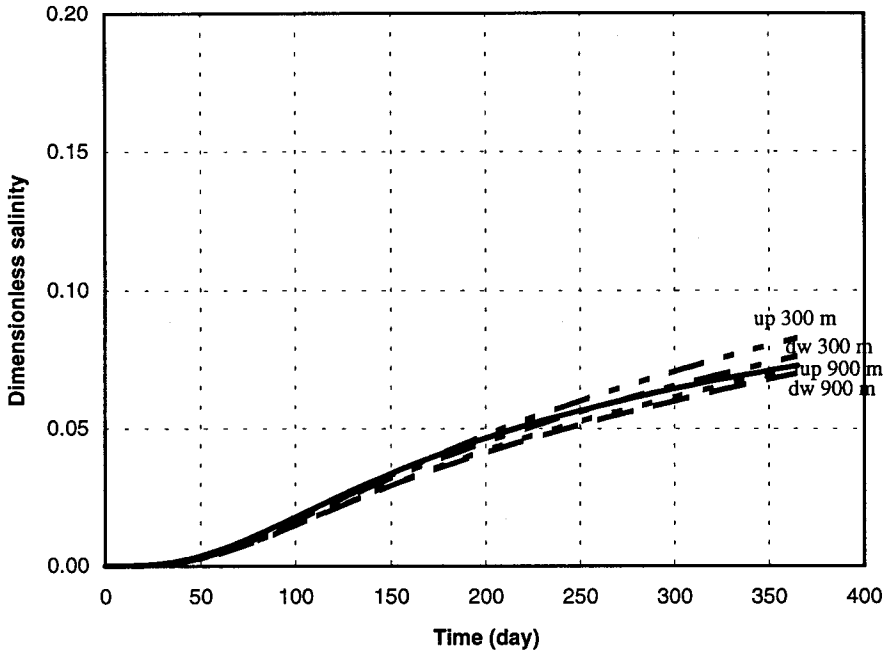

Figure 35. Effects of second well on discharged water salinity; water table has a gradient of 0.0025.

$$\text{brine - concentration change (\%)} = \frac{\text{model output} - \text{basic model output}}{\text{basic model output}} \times 100 \quad (15)$$

In Eq. 15, a negative percentage in brine concentration change indicates a decrease in brine concentration, whereas a positive percentage indicates an increase in brine concentration. Table 8 lists the percentage change in the brine concentration for the thirteen test cases. The variable that decreased the brine concentration the most is considered to have the most significant impact on the saltwater intrusion. As mentioned above, the existence of a clay layer has the greatest impact on brine concentration. It provides an effective barrier to saltwater intrusion even, in an aquifer which is otherwise favorable to saltwater upconing. Pumping rate and hydraulic conductivity also significantly affect the chloride concentration of the discharged water, in some instances, these factors are of even greater importance than the existence of clay layers. For example, a pumping rate of 0.01 m^3/sec causes a total percentage change of -86.6%, which is somewhat greater than that for the case with continuous and partial clay layers. However, this pumping rate is much lower than the actual pumping rate (0.05 m^3/sec) at the Siefkes site and is considered as an extreme case.

From the above investigation, saltwater upconing is influenced by the following factors (in descending order of significance): (1) existence of clay layers, (2) pumping rate, (3) ratio, *K*, of horizontal to vertical hydraulic conductivity, (4) localized recharge (irrigation return flow), (5) location of the well screen, (6) effective porosity, (7) longitudinal and transverse dispersivities, (8) uniformly-distributed recharge, and (9) regional flow.

Because of the grid spacing adopted in the numerical model, the impact of saltwater intrusion caused by nearby pumping activities (case #13) was not considered in the ranking. A significant impact from the nearby pumping well is expected if the separation distance between wells is less than 300 meters. In addition, the regional flow

Table 8. Percentage change of pumped water brine concentration relative to the basic model.

Parameters	Percentage change (%)
continuous clay layer	-83.8
discontinuous clay layer	4.2
partial clay layer	-85.9
Q_p = 0.01 m^3/sec (160 gpm)	-86.6
Q_p = 0.09 m^3/sec (1440 gpm)	28.6
Q_p = 0.50 m^3/sec (8000 gpm)	167.6
K = 1	139.4
K = 100	-36.0
localized recharge	
recharge = 10 % (of total pumpage)	-16.7
recharge = 30 % (of total pumpage)	-40.7
recharge = 50 % (of total pumpage)	-62.9
screen area 9 meters up	-24.1
screen area 9 meters down	30.6
ϕ = 0.1	43.0
ϕ = 0.4	-41.2
α_L = 0.1 m	-10.8
α_L = 10 m	52.9
α_T = 0.01 m	-13.5
α_T = 1 m	19.4
uniform recharge	
recharge = 0.05 m/yr (2 in./yr)	- 4.6
recharge = 0.127 m/yr (5 in./yr)	-11.3
recharge = 0.254 m/yr (10 in./yr)	-22.3
2nd well 300 m upstream	13.7
2nd well 300 m downstream	4.7
2nd well 900 m upstream	-1.7
2nd well 900 m downstream	-3.7

gradient (0 to 0.0015) had the least impact on the upconing of saltwater in the simulated cases, probably because of the relatively small slopes observed in the study area.

Simulation of the Study Area

The simulation was not intended to simulate a large area because of uncertainties in aquifer parameters, boundary conditions, distribution of low permeability clay layers, and limited field data in the Great Bend Prairie. The simulation area employed in this study is focused on the actual field conditions at the Siefkes site. As mentioned previously, the drilling log of the Siefkes site (Fig. 4A) indicates that the aquifer is mainly an alluvial deposit of sand and gravel interspersed with clay layers or clay lenses. A layer of dark clay exists around 42 m from the ground surface; however, the lateral extent of the clay layer is not certain. The thickness of the aquifer from the ground level to the Permian bedrock is approximately 57 m at the Siefkes site, and the chloride concentration increases from a depth of about 39 m to 54 m where the bedrock is located (Figs 4B & 4C).

Samples of profiles of the measured EM logs and gamma-ray drilling logs for the monitoring wells around the Siefkes site (Appendix A) were analyzed by Olea (personal communication, 1996) using automated correlation procedures (Olea, 1988) to determine the spatial distribution of the low-permeability clay layers in the simulation area. The results suggest that the distribution of clay layers is extensive except for the southeastern part of the simulation area. However, the position and existence of the clay layers is uncertain based on the available drilling logs and other criteria since the spacing between the drilling logs of the GMD5 monitoring wells is approximately 9.6 km, and the drilling logs around the Siefkes site are of shallow depth only.

Salt comes mainly from the highly mineralized Permian bedrock, the upper part of which has a chloride concentration of 28,000 mg/L (Garneau, 1995). This chloride concentration is normalized as the dimensionless brine concentration 1.00 used in the numerical model. A linear salinity profile is assumed as the initial condition in modeling.

Because of the uncertainty of the distribution of clay layers, two hypothetical (but plausible) distributions of clay layers around the Siefkes site were assumed (Figs. 36 and 37). The distribution of clay layer based on Fig. 36 assumes that the source of salt is from downstream saline water. The continuity of the upstream clay layer prevents the upper freshwater aquifer from being intruded; however, the discontinuity of the downstream clay layer allows downstream saline water to move upstream and be discharged during the pumping season. Incoming upstream ground water will dilute the high-salinity ground water and carry the saline water downstream during the nonpumping season. The distribution of clay layers based on Fig. 37 assumes that the clay layer is extensive; however, a discontinuity of upstream clay layer, located 150 meters away from the Siefkes site irrigation well, allows upstream saline water to move downstream and be discharged during the pumping season. Surface recharge from both the precipitation and return irrigation water is the main factor to dilute the saline water around the irrigation area during the nonpumping period.

Because two types of clay-layer distributions were considered in this study, the assumptions and size of the simulation area used for their numerical simulation were slightly different. To accommodate the distribution of the clay layer used in the numerical simulation, the size of simulation area used for handling the case of Fig. 36 is 5.5×4.1 km^2, and is meshed in the X-Y plane by a 18 x 14 grid with variable spacing ranging from 25 m to 400 m in both X and Y directions (Fig. 38). The Z direction is meshed by a grid of 20 rows with variable spacing of 2 m in the top 5 grids, 3 and 4 m in the 6th and 7th grid, and 5 m for the remaining grids. Figure 38 also shows the location of seven existing irrigation wells in the simulation area. The annual ground-water pumpage for the seven wells from 1979 to 1995 is listed in Table 9. Because water meters were not installed until 1994, the pre-1994 figures are based on estimated provided by users and must be viewed with some caution. The size of simulation area used for handling the case of Fig. 37 is 5.8×4.5 km^2 and is meshed by a 18 x 14 grid with uniform spacing of 320

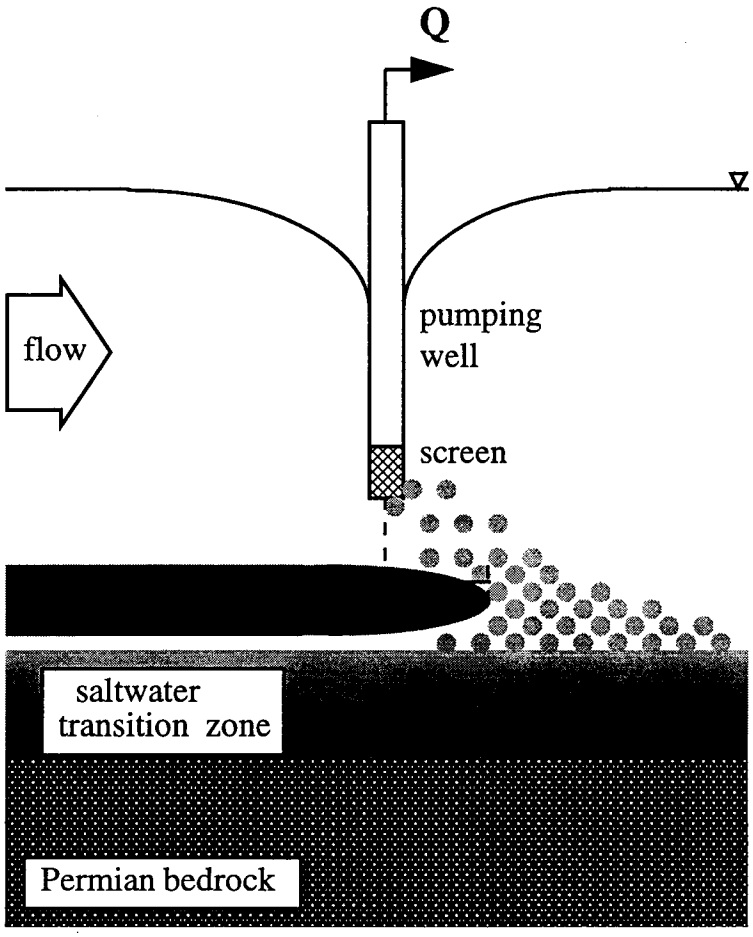

Figure 36. Hypothetical distribution of clay layers at the Siefkes site.

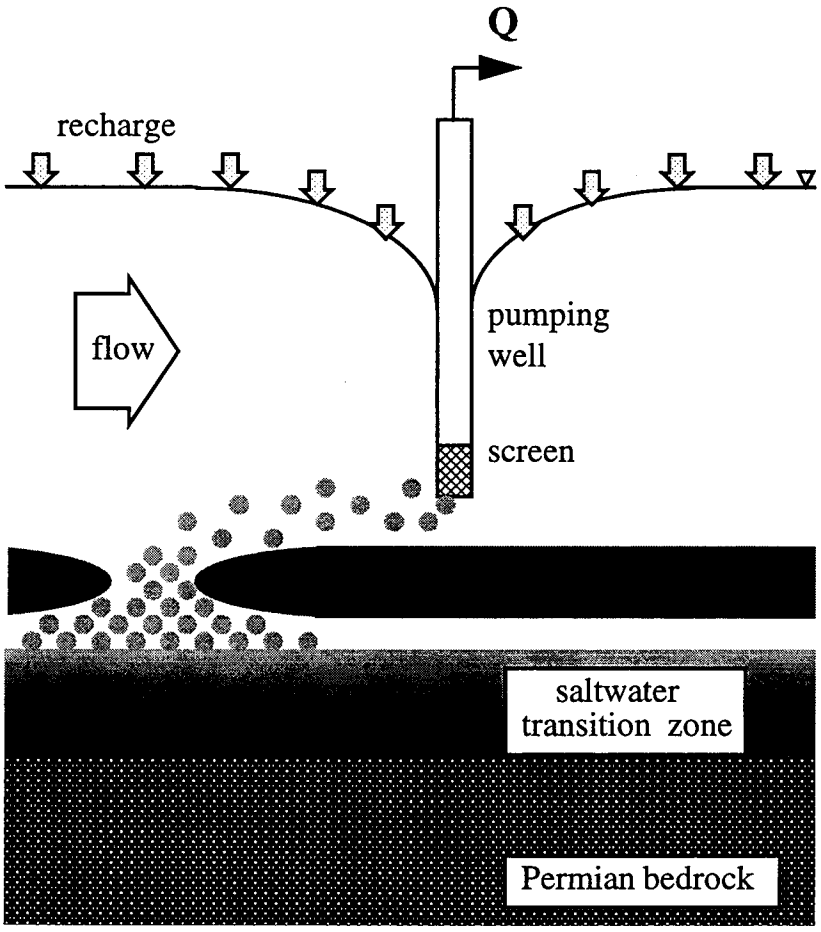

Figure 37. Hypothetical distribution of clay layers at the Siefkes site.
Source of salt from upstrem saline water.

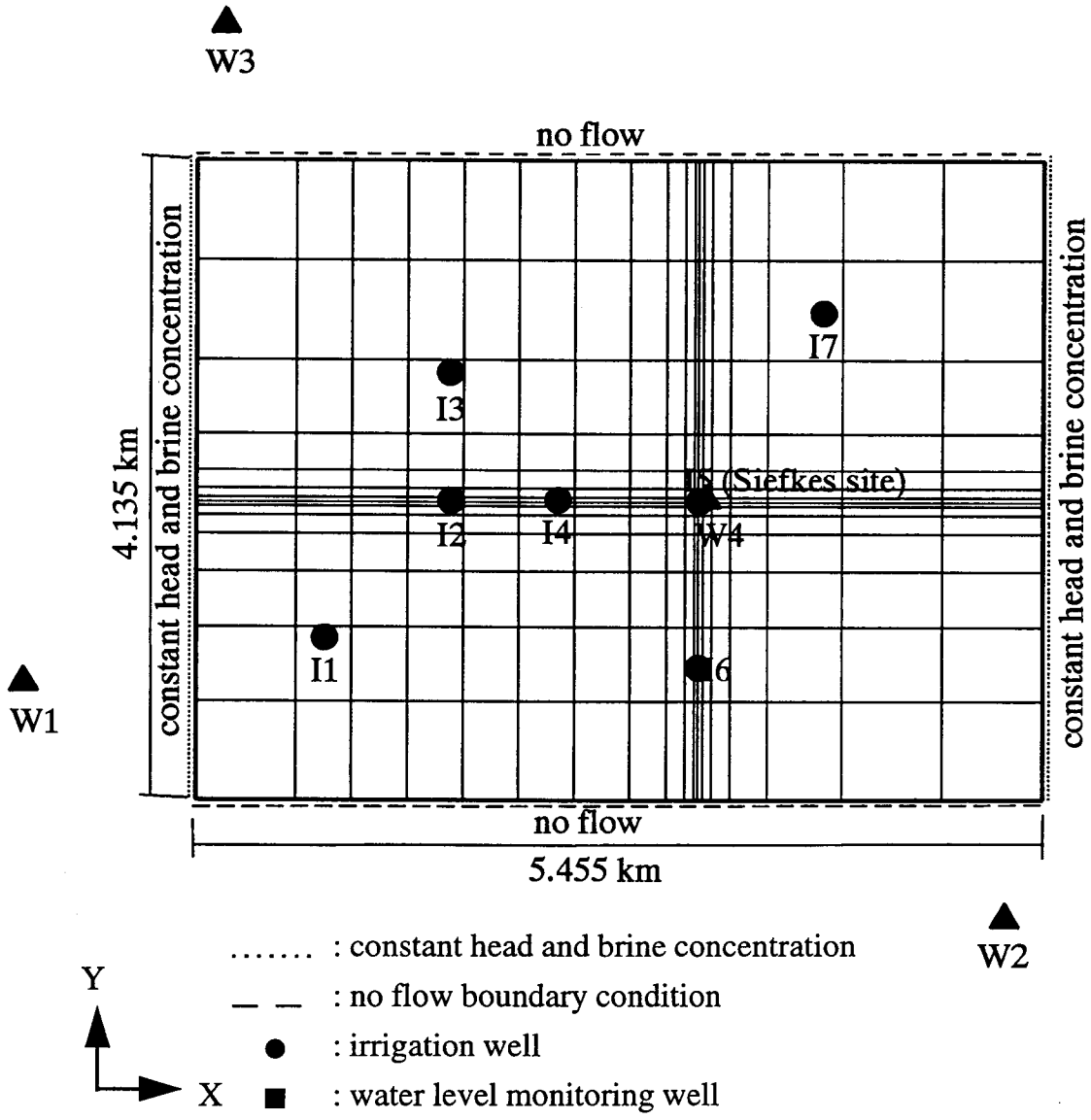

Figure 38. Mesh of the simulation area in X and Y directions and boundary conditions.

Table 9. Historical annual ground-water pumpages (m^3/year) for irrigation at seven sites (annual pumpages before 1994 are estimated values reported by water users). Site numbers refer to irrigation wells shown in Fig. 38.

Year	Site# 1	Site# 2	Site# 3	Site# 4	Site# 5	Site# 6	Site# 7
1975				187329			
1976				272550			
1977							
1978				252568	255294		222039
1979				189327	193324		103314
1980							193965
1981		161179	122460	190968	165706	83038	157528
1982		170911		182605	140642	111741	150633
1983		216168	161080	242749	259648	172613	188057
1984		224851	172613	215674	190425	214589	246203
1985		198221	118760	180791	153717	157528	181877
1986							
1987		106474	102046	175882	162622	83396	246141
1988		217858	128467	270910	212406	221496	270737
1989		217858	128467	188969	175882	130527	188784
1990	187070	194964	137731	202599	198048	190363	201008
1991	307149	151361	106116	251840	269800	177708	249792
1992	132772	102219	96014	101898	93745	103724	199984
1993	50548	132168	97001	129738	99036	60761	123348
1994	220423	208582	215336	220917	209199	119278	245463
1995	102627	191809	166399	175527	202664	74380	192426
Maximum	307149	224851	215336	272550	269800	221496	270737
Normal	166767	178174	134780	201837	186399	135805	197723
Minimum	50548	102219	96014	101898	93745	60761	103341

meters in both the X and Y directions. The mesh in the Z direction is the same as the previous model.

The initial 1994 water table, saltwater-freshwater interface, and topography of bedrock surface were obtained by using the geostatistical techniques discussed above. Equations 3, 4, 5, and 6 are the semivariogram models adopted to estimate the initial water table, topography of the bedrock, and the location of saltwater-freshwater interface, respectively. The kriged 1994 water table and saltwater-freshwater interface are used as the initial conditions in the numerical model. As can be seen in Fig. 39, the water table slopes from the west to the east with a gradient approximately equal to 0.0025. The saltwater-freshwater interface generally follows the topography of the bedrock with high elevation in the southeast corner and low elevation in the northeast.

The boundary conditions were based on some results of a previous study by Sophocleous and Perkins (1993), which suggested a no-flow boundary condition on the south and north boundaries of the modeled aquifer. Since relatively constant high-salinity and constant piezometric heads were observed at the Permian bedrock, it is reasonable to assume constant hydraulic head and constant salinity at the bottom boundary. Constant piezometric heads were also assumed on the east and west boundaries. Since these boundaries are more than 2 km away from the Siefkes site, neither was expected to have a significant effect on the results.

The measured water levels at the Siefkes site (Fig. 5A) show that the change of water level mainly depends on the frequency of pumping activity. The lowest water tables were observed in the middle-to-late irrigation season since the pumping activity was greatest during that period. The highest water tables were measured in the early irrigation season due to the recovery during the nonirrigation season. Variation in discharged chloride concentration (Fig. 5B) were caused by variations in pumping rates, distribution of clay layer, and recharge rates. The clay layer greatly retards the upward movement of the deep-aquifer saline water under pumping stress. Lower measured chloride

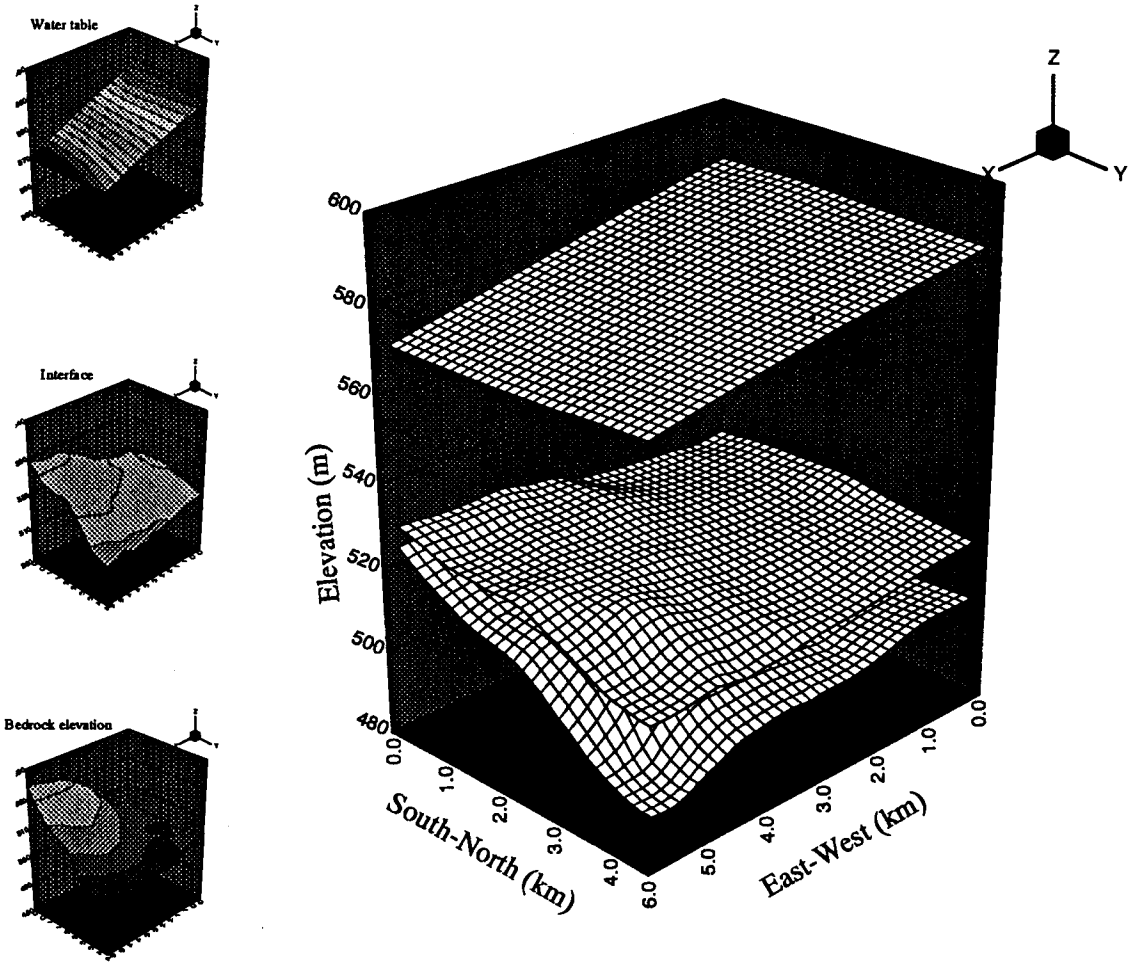

Figure 39. Three-dimensional plots of 1994 water table, saltwater-freshwater interface, and bedrock for the simulation area.

concentration in the early irrigation season results form the recharge during the nonpumping season.

Sources of freshwater recharge to the ground-water reservoir were return irrigation water, precipitation, and ground-water inflow. Recharge from precipitation is not expected to significantly relieve the saltwater-intrusion problem since it is only about 10% of annual precipitation (Sophocleous, 1993). The Great Bend Prairie aquifer has a relatively shallow water table, and therefore recharge from return irrigation water to the area where the irrigation water is applied is expected. However, the amount of return irrigation water has not been studied. Previous studies estimated 10% (Sophocleous, 1981) or 30 to 50% (Luckey et al, 1986) as irrigation return to ground water. Recharge from the movement of the ground water can be estimated by the following equation:

$$Q = K I A \tag{16}$$

where Q is the quantity of water (L^3/T), K is the hydraulic conductivity (L/T); I is the hydraulic gradient; and A is the cross-section area (L^2).

Calibration of the Simulation Model

The data available for calibration were the measured time series of discharged chloride concentration and drawdown from 1994-1995 at the Siefkes site; therefore, the model is only calibrated at the Siefkes site. Model calibration was performed by adjusting the distribution of clay layers (but still honoring observed drill logs) and the model parameters so that the measured time series data could be reproduced with reasonable accuracy. In addition, the annual pumpage had to be converted to daily values for the irrigation season to be used in the model. Since the daily pumping schedule was unknown, the total pumpage was disaggregated to obtain the daily values based on the

daily precipitation records at the Hudson weather station (Fig. 1) and the seasonal ground-water usage record. The values of the aquifer parameters used in the calibrated model for the clay layer distribution shown in Fig. 36 are summarized in Table 10. Comparisons of the simulated and measured values of chloride concentration, water drawdown, and the corresponding pumping rate are shown in Figure 40. The values of the aquifer parameters used in the calibrated model for the clay layer distribution shown in Fig. 37 are summarized in Table 11. The amount of return irrigation water depends on the weather conditions. Twenty percent of pumpage was assumed to return during the early and middle parts of the irrigation season, and this return was locally distributed to the irrigation area. Similarly, 15% percent of pumpage was assumed to return during the late irrigation season and winter nonpumping season. Comparisons of the simulated and measured values of chloride concentration, water drawdown, and the corresponding pumping rate are shown in Figure. 41.

From the results of both calibrated models, the computed chloride concentrations are in fair agreement with the measured values; however, the computed ground-water drawdowns are generally lower than the measurements. The discrepancies may be attributed mainly to the uncertainties in the model parameters and the distribution of clay layers in the aquifer. Despite the differences, the correspondences show a satisfactory match and both the numerical models are concluded to be calibrated.

Simulation for Long-Term Pumping Operation

Both calibrated models were used to simulate a 10-year pumping operation from January 1, 1996 through December 31, 2005 to estimate the temporal variation of the salinity of pumped water at three different annual pumpage values. The three values were obtained from the historical records of annual pumpage shown in Table 9. The maximum, normal, and minimum annual pumpages at each irrigation well were used to represent the dry, normal, and wet weather conditions, respectively. The annual pumpage was disaggregated into monthly values according to the following distribution (Kansas

Table 10. Values of parameters used in the calibrated model. The distribution of clay layers is shown in Fig. 36.

Aquifer Parameters

Horizontal hydraulic conductivity	K_X and K_Y = 43 m/d (140 ft/d)
Vertical hydraulic conductivity	K_Z = 6.9 m/d (22.6 ft/d)
Porosity	ϕ = 0.18
Bulk porous matrix compressibility	$\alpha = 2.58 \times 10^{-7}$[kg/(m s^2)]$^{-1}$
Longitudinal dispersivity	α_L = 1 m
Transverse dispersivity	α_T = 0.1 m

Properties of water and brine

Density of water	ρ_o = 1,000 kg/m^3
Density of brine	ρ = 1,036 kg/m^3
Coefficient of viscosity of water	$\mu = 1.0 \times 10^{-3}$ kg/(m s)
Solute molecular diffusivity	$D_m = 1.0 \times 10^{-10}$ m^2/s

Bedrock Properties

Horizontal hydraulic conductivity	K_X and K_Y = 0.043 m/d (0.14 ft/d)
Vertical hydraulic conductivity	K_Z = 0.0069 m/d (0.023 ft/d)
Porosity	ϕ = 0.09

Clay Layer Properties

Horizontal hydraulic conductivity	K_X and K_Y = 0.0344 m/d (0.011 ft/d)
Vertical hydraulic conductivity	K_Z = 0.004 m/d (0.001 ft/d)
Porosity	ϕ = 0.3

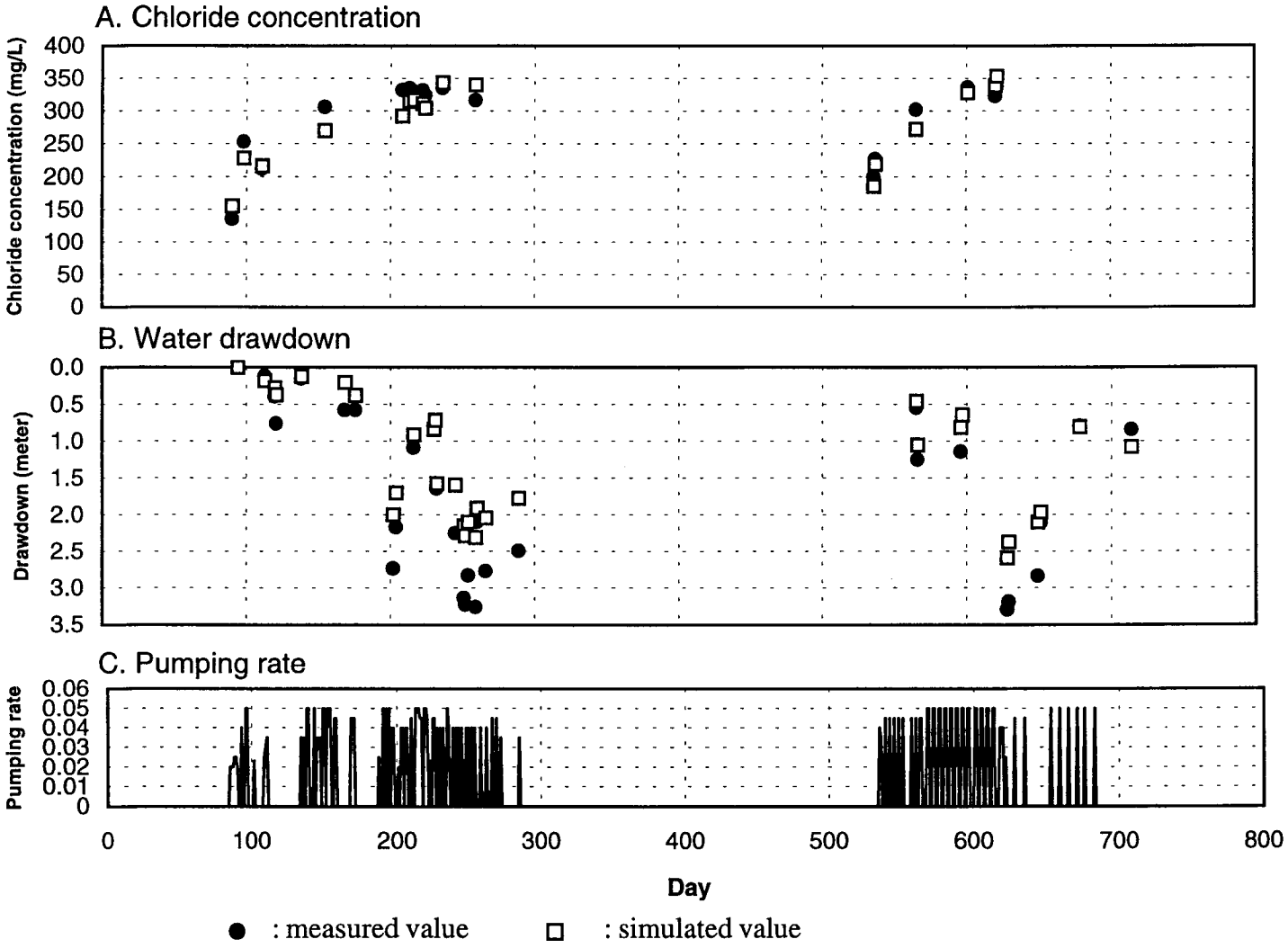

Figure 40. Comparison of simulated and measured values of A. discharged chloride concentration, B. water drawdown at the Siefkes site, and C. the corresponding pumping rate. (based on the distribution of clay layer shown in Fig. 36)

Table 11. Values of parameters used in the calibrated model. The distribution of clay layers is shown in Fig. 37.

Aquifer Parameters

Horizontal hydraulic conductivity	K_X and K_Y = 23 m/d (75 ft/d)
Vertical hydraulic conductivity	K_Z = 2.3 m/d (7.5 ft/d)
Porosity	ϕ = 0.2
Bulk porous matrix compressibility	$\alpha = 2.58 \times 10^{-7}[kg/(m\ s^2)]^{-1}$
Longitudinal dispersivity	α_L = 1 m
Transverse dispersivity	α_T = 0.1 m

Properties of water and brine

Density of water	$\rho_o = 1{,}000\ kg/m^3$
Density of brine	$\rho = 1{,}036\ kg/m^3$
Coefficient of viscosity of water	$\mu = 1.0 \times 10^{-3}\ kg/(m\ s)$
Solute molecular diffusivity	$D_m = 1.0 \times 10^{-10}\ m^2/s$

Bedrock Properties

Horizontal hydraulic conductivity	K_X and K_Y = 0.023 m/d (0.075 ft/d)
Vertical hydraulic conductivity	K_Z = 0.0023 m/d (0.0075 ft/d)
Porosity	ϕ = 0.05

Clay Layer Properties

Horizontal hydraulic conductivity	K_X and K_Y = 0.023 m/d (0.075 ft/d)
Vertical hydraulic conductivity	K_Z = 0.0023 m/d (0.0075 ft/d)
Porosity	ϕ = 0.3

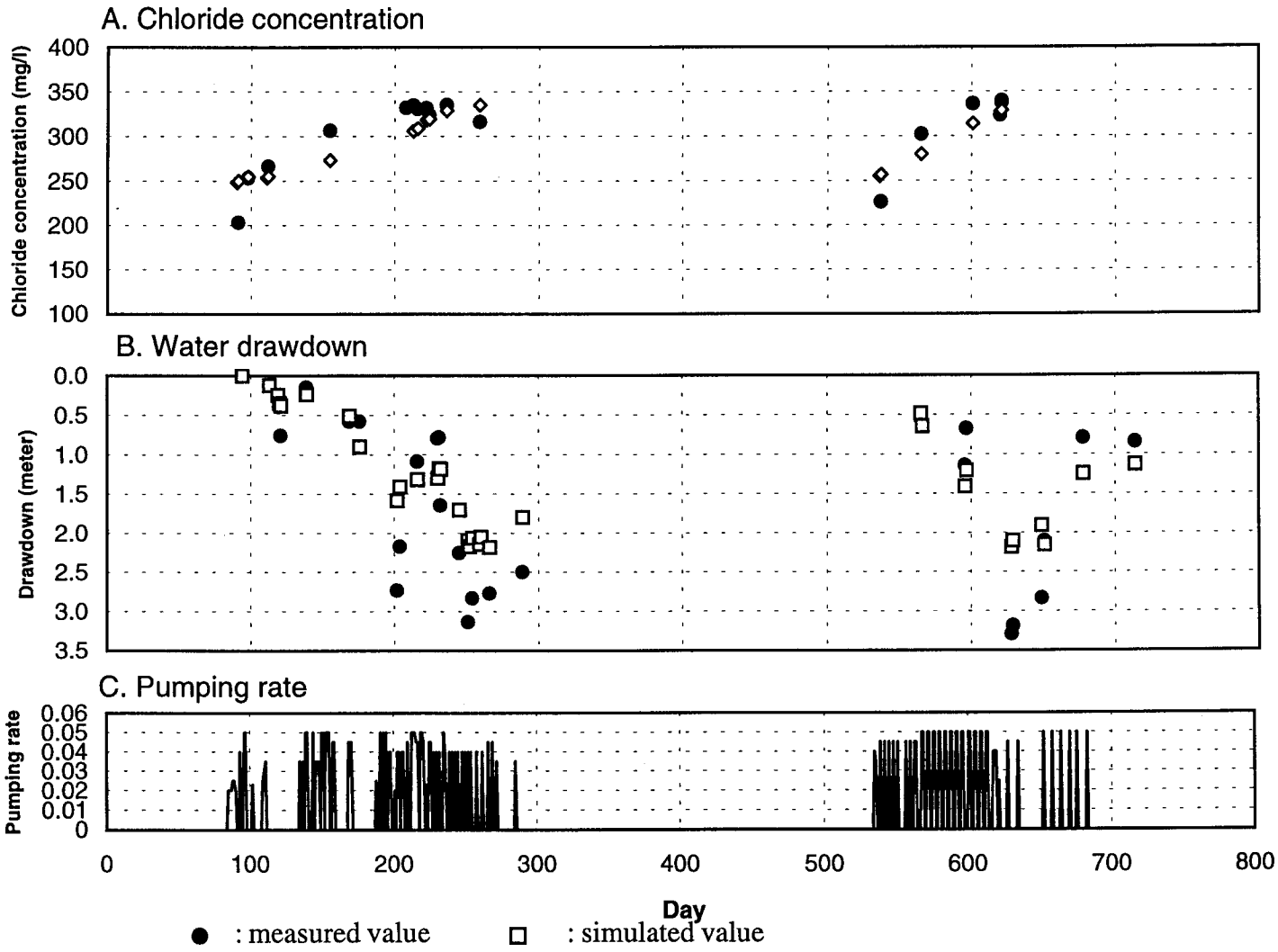

Figure 41. Comparison of simulated and measured values of A. discharged chloride concentration, B. water drawdown at the Siefkes site, and C. the corresponding pumping rate. (based on the distribution of clay layer shown in Fig. 37)

Irrigation Guide, 1977): 10% of irrigation requirements for May and October, 15% for June and September, and 25% for July and August. All irrigation wells were assumed to have the same pumping rate but with different pumping schedule. The monthly pumpage was determined by multiplying the number of days of pumping by the pumping rate. Pumping was activated from May through October during each year, and there was no pumping for the rest of the year. The ground-water recharge from the precipitation was assumed to be 10% of the annual precipitation. The target chloride concentration of pumped water was 500 mg/L, which is equal to 1.79% of the maximum salinity at the upper bedrock.

The computed time series of discharged ground-water salinity for the clay layer distribution shown in Fig. 36 are presented in Figs. 42 through 44 for the three scenarios of maximum, normal, and low annual pumpages. The results for the clay layer distribution shown in Fig. 37, including the return irrigation flow, are presented in Figs. 45 through 47. From the results of the simulation, it is seen that low pumpage can alleviate the problem of saltwater intrusion and keep the salinity of discharged water below the target value at the end of each of the ten years of operation (Figs. 42 and 45). For normal pumpage, the salinity of discharged water met the requirement most of the time but exceeds the target value in the years 2001 and 2002 (Fig. 43); however, the salinity of discharged water is still below the target value at the end of the ten years (Fig. 46) if the return irrigation flow is considered. For maximum pumpage, the salinity of pumped water from both models exceeded the target value of 500 mg/L. By the end of the tenth year the salinity was much larger than the targeted value. Based on these results, it is clear that the aquifer is vulnerable during consecutive dry years with maximum required pumpage. In practice, the required pumpage for irrigation depends on the available rainfall. It is likely that a combination of the three scenarios would occur for long-term operation. The weather factor through forecasting must be included in the model for real-time operation.

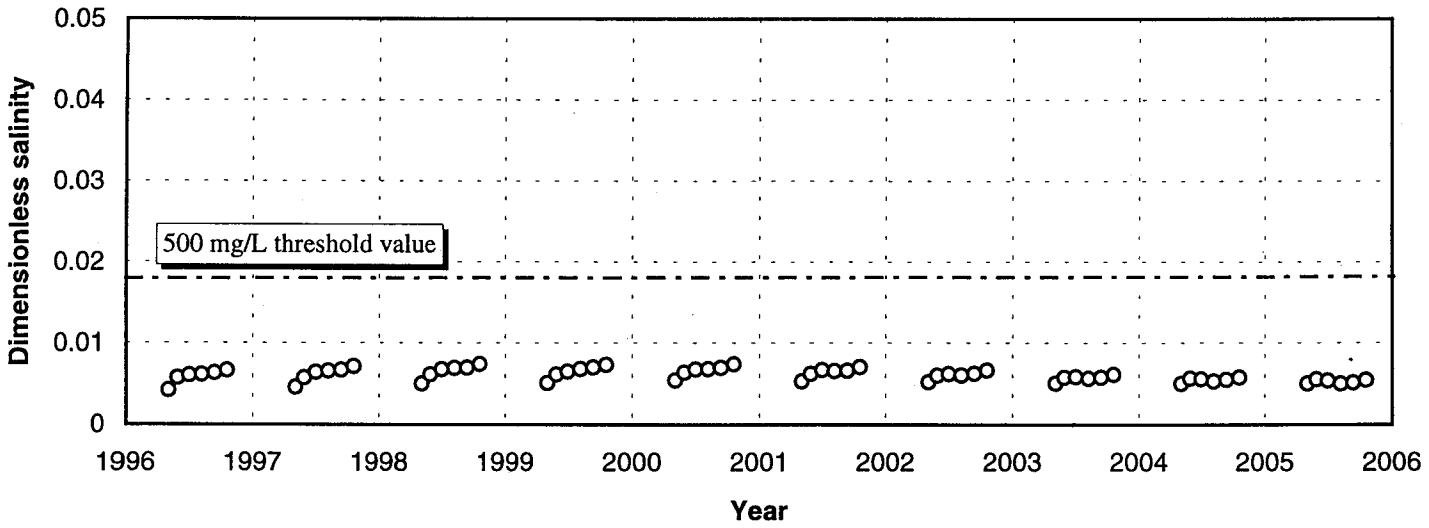

Figure 42. Chloride concentration of pumped water at the Siefkes site at low pumping rate (0.017 m^3/s) and relatively high surface recharge for simulated 10-year operation (based on the distribution of clay layers shown in Fig. 36)

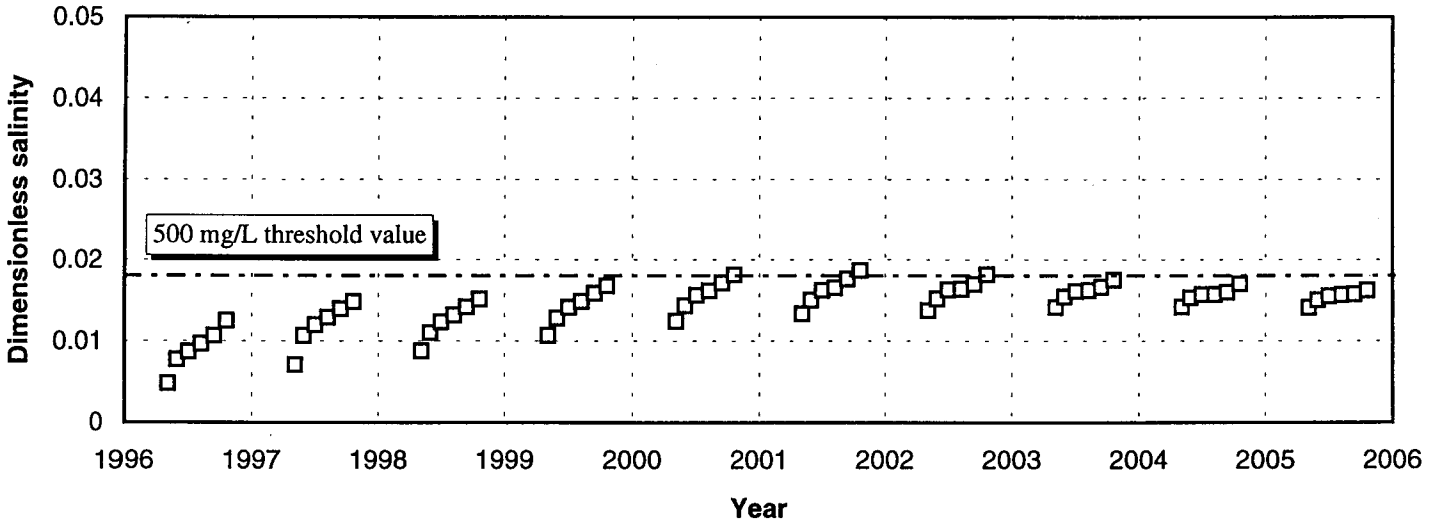

Figure 43. Chloride concentration of pumped water at the Siefkes site at average pumping rate (0.033 m^3/s) and normal surface recharge for simulated 10-year operation based on the distribution of clay layers shown in Fig. 36)

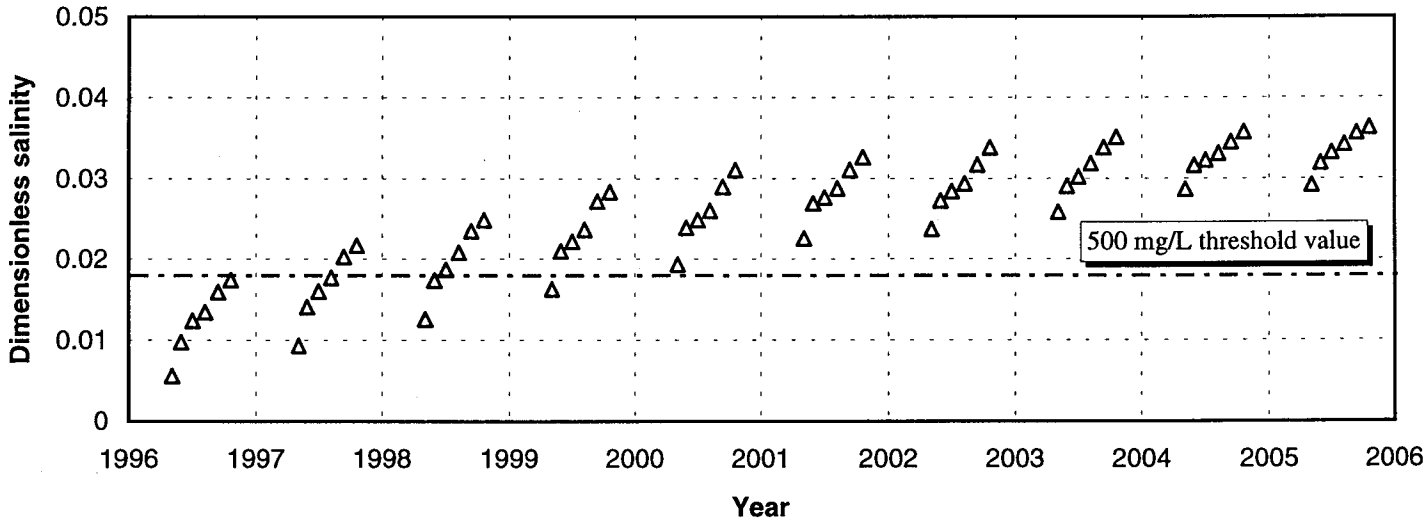

Figure 44. Chloride concentration of pumped water at the Siefkes site at high pumping rate (0.048 m^3/s) and relatively low surface recharge for simulated 10-year operation (based on the distribution of clay layers shown in Fig. 36)

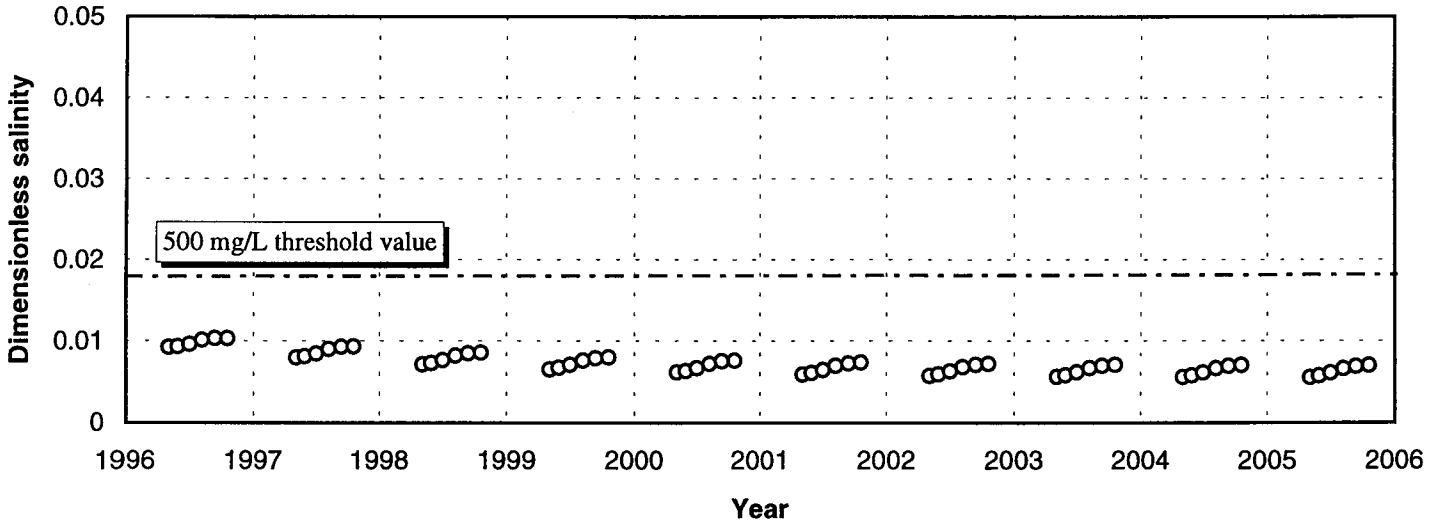

Figure 45. Chloride concentration of pumped water at the Siefkes site at low pumping rate (0.017 m^3/s) and relatively high surface recharge for simulated 10-year operation (based on the distribution of clay layers shown in Fig. 37)

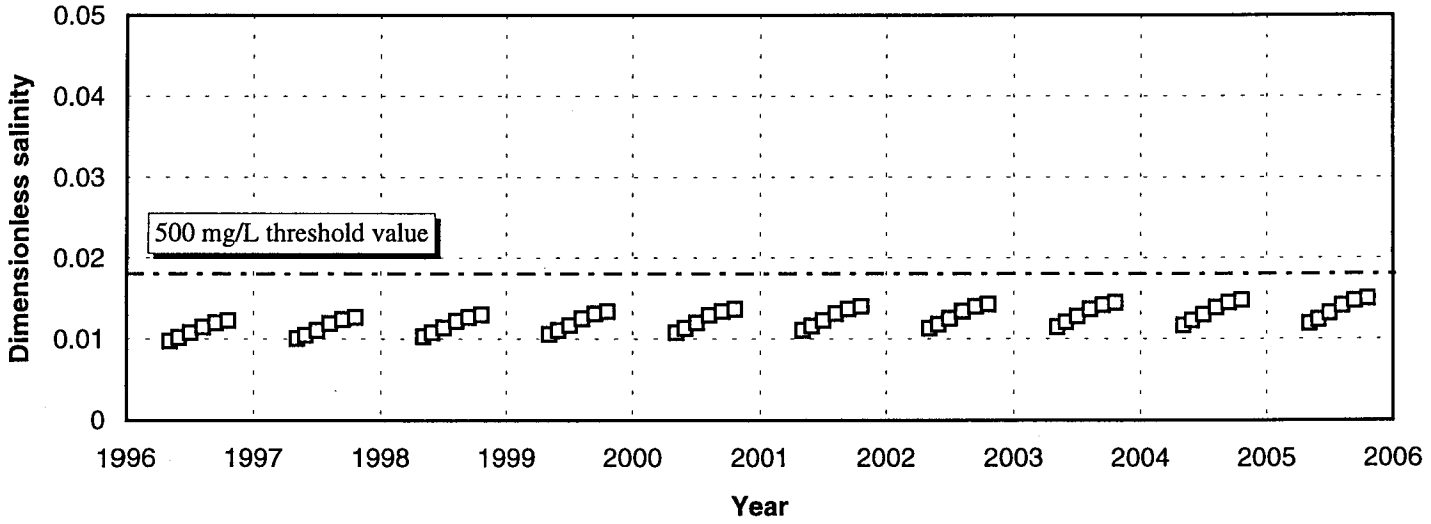

Figure 46. Chloride concentration of pumped water at the Siefkes site at average pumping rate (0.033 m^3/s) and normal surface recharge for simulated 10-year operation based on the distribution of clay layers shown in Fig. 37)

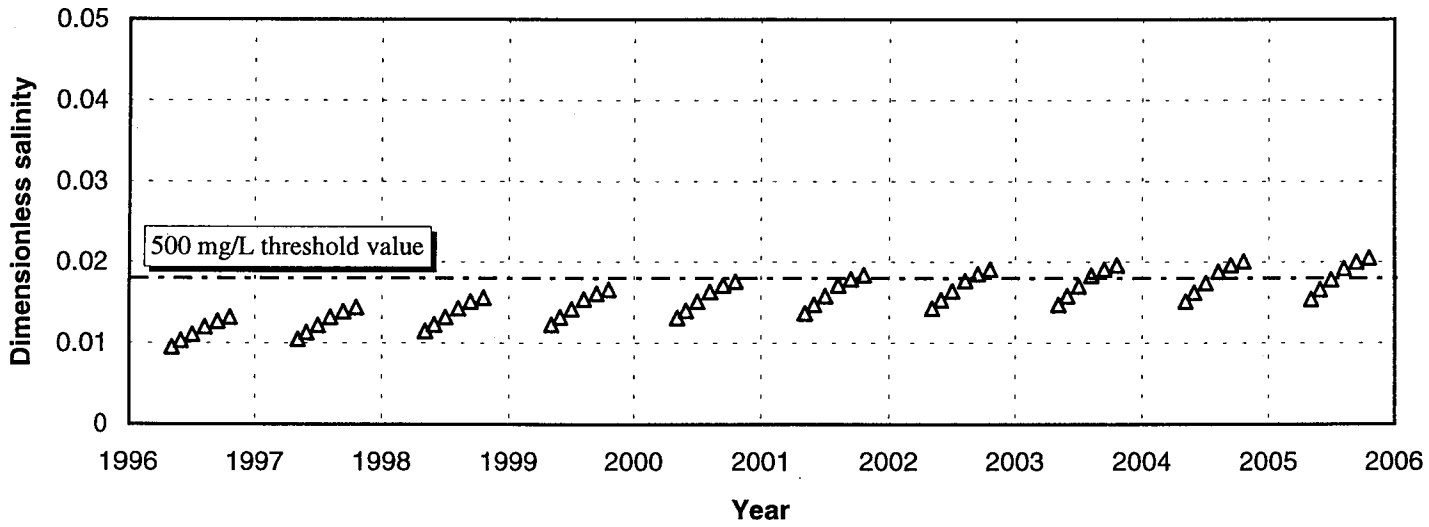

Figure 47. Chloride concentration of pumped water at the Siefkes site at high pumping rate (0.048 m^3/s) and relatively low surface recharge for simulated 10-year operation (based on the distribution of clay layers shown in Fig. 37)

GROUND-WATER SALINITY DECISION SUPPORT MANAGEMENT MODEL

Saltwater migration into vulnerable areas in the Great Bend Prairie aquifer is a major concern in managing the water resources of this area; however, uncertainties regarding the distribution of low-permeability clay lenses, salt, saltwater-bearing formations, and aquifer parameters make the prediction of saltwater contamination a difficult task. Mathematical formulations and model simulations of ground-water flow and contaminant transport were discussed in the previous chapter of this report, as well as in previous progress reports. Sensitivity analyses have provided an understanding of how the sources of salt, rates of salt discharge, aquifer parameters, and the surrounding (boundary) conditions interact to cause ground-water flow patterns and consequent brine movement in the ground-water system. To maintain a long-term ground-water supply that minimizes saltwater intrusion from underlying geologic formations, a relatively simple ground-water management decision support model is developed here, based on limited field data and extensive modeling analyses. The purpose of the model is to identify vulnerable areas and to provide a helpful tool for developing management policies to prevent saltwater intrusion.

The development of the ground-water management model in this study is similar to the approach used by Sophocleous (1992), who developed a model to estimate and regionalize ground-water recharge in the Great Bend Prairie. The results of sensitivity analyses of the saltwater intrusion process quantified the governing factors and provided insights into the dynamic relationships between saltwater and freshwater in the ground-water system. These preliminary conceptual simulations indicate that the spatial distribution and continuity of clay layers within the aquifer are the most important factors controlling flow patterns and salinity distribution. The pumping rate, hydraulic conductivity, local recharge, and location of the well screen relative to saline water are other important parameters governing the saltwater intrusion process. To quantify the significance of variables discussed in the sensitivity analysis to the saltwater upconing, a

linear multiple regression analysis was conducted to develop a relationship between discharged saltwater salinity and these variables. Finally, a simple ground-water management model based on the knowledge of the study area, the sensitivity analyses, and the results from a multiple regression analyses, will be developed to provide technical support for evaluation of proposed irrigation wells for future ground-water use.

Linear Multiple Regression Analysis

The sensitivity analysis shows that, saltwater intrusion is affected by numerous parameters. The existence of clay layer(s) above the saltwater-freshwater interface, the pumping rate (m^3/sec), the horizontal and vertical hydraulic conductivitives (m/d), the uniformly distributed and especially the localized recharge (cm/d), the distance between well screen and the saltwater-freshwater interface (m), the effective porosity, the location of salt source, and longitudinal and transverse dispersivities (cm) are considered as the independent variables to develop a linear multiple-regression salinity model. Therefore, the significance of each of the above parameters can be quantified. The dependent variable in this model is a dimensionless salinity measure, which is the ratio of the chloride concentration in alluvial aquifer water to that of the average Permian brine in the area (Cl_{avg} = 28,000 mg/L). The SPSS/PC+ backward regression analysis (Norusis, 1990) is adopted to determine the smallest number of independent variables. The probability of *F-to-remove* with the default value of 0.1 is adopted as the criterion to remove a variable at each step in this backward-elimination procedure. The results of this backward-elimination procedure are summarized in Table 12.

The coefficient of determination, R_{sq}, is the square of the multiple correlation coefficient, Mult*R*, which indicates how well the regression model explains the observed data. *Adj* R_{sq} is similar to R_{sq}; however, it takes into account the different number of degrees of freedom (Plane and Oppermann, 1977).

Tables 13 to 18 show the variables in the regression equation at each step. Because the variables in the multiple regression analysis are in different units, the

Table 12. Backward-selection regression equations and diagnostics.

	Clay	K_v	Q_p	*DTI*	*LREC*	K_h	ϕ	α_v	α_h	*WTG*	*UREC*	Constant
Step 1	-0.0182	4.85E-05	3.22E-09	-0.0022	-2.12E-06	-1.69E-06	0.17903	1.40E-04	4.03E-05	-2.43E-04	-0.2788	0.03973
Step 2	-0.0183	4.84E-05	3.21E-09	-0.0022	-2.13E-06	-1.70E-06	0.17848					0.04564
Step 3	-0.0187	4.80E-05	3.19E-09	-0.0022	-2.17E-06	-1.73E-06						0.08235
Step 4	-0.0171	4.96E-05	3.28E-09	-0.0022		-1.57E-06						0.07748
Step 5	-0.0181	4.86E-05	3.23E-09		-2.10E-06							0.05006
Step 6	-0.0166	5.01E-05	3.31E-09									0.04584

Step summary

STEP	MultR	R_{sq}	$AdjR_{sq}$	F(Eqn)	SigF	$R_{sq}CH$
1	0.8015	0.6424	0.4239	2.9396	0.0206	0.6424
2	0.7812	0.6103	0.4863	4.9219	0.0018	-0.0321
3	0.7648	0.5848	0.4765	5.4000	0.0013	-0.0255
4	0.7274	0.5292	0.4311	5.3943	0.0018	-0.0556
5	0.7428	0.5517	0.4800	1.4928	0.0003	0.0225
6	0.7068	0.4996	0.4418	2.9081	0.0004	-0.0521

Q_p : pumping rate (L/day)
ϕ : effective porosity (dim.)
K_v : vertical conductivity (m/day)
K_h : horizontal conductivity (m/day)
α_h : horizontal dispersivity (cm)
α_v : vertical dispersivity (cm)
Clay : distribution of clay layers (dim.)
WTG : water table gradient (dim.)
UREC : unifore recharge (cm/day)
LREC : localized recharge (cm/day)
DTI : depth of well screen to interface (m)

Table 13. Variables in the regression equation at step 1.

Variable	Beta	VIF	F	SigF
Clay	-0.261615	1.052	3.274	0.0871
DTI	-0.113588	1	0.649	0.4308
ϕ	0.160229	1.005	1.286	0.2717
α_v	0.050314	1.019	0.125	0.7277
α_h	0.144533	1.019	1.032	0.3232
K_v	0.399597	1.019	7.887	0.0116
K_h	-0.138914	1.019	0.953	0.3419
Q_p	0.497588	1.02	12.224	0.0026
WTG	-0.015005	1.036	0.011	0.9178
UREC	-0.08512	1.047	0.348	0.5624
LREC	-0.231743	1.048	2.579	0.1257
Constant			0.653	0.4294

Table 14. Variables in the regression equation at step 2.

Variable	Beta	VIF	F	SigF
Clay	-0.263314	1.019	3.842	0.0628
DTI	-0.113588	1	0.728	0.4026
ϕ	0.159735	1.002	1.437	0.2433
K_v	0.398618	1.008	8.899	0.0069
K_h	-0.139893	1.008	1.096	0.3065
Q_p	0.496597	1.008	13.809	0.0012
LREC	-0.233362	1.018	3.02	0.0962
Constant			1.023	0.3228

Table 15. Variables in the regression equation at step 3.

Variable	Beta	VIF	F	SigF
CLAY	-0.268158	1.018	3.914	0.06
DTI	-0.113588	1	0.715	0.4066
K_v	0.395826	1.008	8.614	0.0074
K_h	-0.142685	1.008	1.119	0.3011
Q_p	0.493769	1.008	13.402	0.0013
LREC	-0.23798	1.017	3.085	0.0923
Constant			6.06	0.0217

Table 16. Variables in the regression equation at step 4.

Variable	Beta	VIF	F	SigF
CLAY	-0.245045	1.008	3.035	0.0943
DTI	-0.113588	1	0.658	0.4254
K_v	0.409144	1.004	8.494	0.0076
K_h	-0.129367	1.004	0.849	0.3659
Q_p	0.50726	1.005	3.056	0.0014
Constant			4.969	0.0354

Table 17. Variables in the regression equation at step 5.

Variable	Beta	VIF	F	SigF
CLAY	-0.259703	1.014	3.708	0.0656
K_v	0.400698	1.006	8.897	0.0063
Q_p	0.498704	1.007	13.779	0.001
LREC	-0.229921	1.014	2.908	0.1005
Constant			26.292	0

Table 18. Variables in the regression equation at step 6.

Variable	Beta	VIF	F	SigF
CLAY	-0.238067	1.005	2.929	0.0989
K_v	0.413165	1.004	8.838	0.0063
Q_p	0.511333	1.004	13.536	0.0011
Constant			21.95	0.0001

coefficients derived do not indicate the actual weight for each variable (Table 12). To eliminate this problem, we used the β-coefficient concept, which adjusts the regression coefficients to eliminate the difference caused by the difference in units, and provides a standardized way (Z-scores) to compare the significance of the regression variables. To check the multicollinearity between independent variables, the variance inflation factor, VIF, is used as a principal diagnostic for multicollinearity. The value of VIF = 1 indicates that there is no redundant information in the other independent variables. The results of VIF shown in Tables 13 to 18 indicate that all the variables are independent of each other.

Ground-water Salinity Model

All regression equations derived from the backward-elimination procedure at each step (Table 12) were considered to develop the ground-water management model. Each independent variable is further classified into the same number of data classes and outlined in Table 19. Note that for the variables negatively related to salinity, the higher the variable values, the lower the class rank assigned. The reverse is true for the positively-related variables. For each step, the β coefficients are normalized to 1 and used to weigh the class ranking of each salinity-affecting variable. The higher the ranking, the greater the salinity hazard. Six selected ground-water salinity models that are derived to calculate salinity scores are listed below.

1. Salinity score = $(\text{nbeta}_1) \times (\text{Disc. clay class rank}) + (\text{nbeta}_2) \times (K_v \text{ class rank}) +$
$(\text{nbeta}_3) \times (Q_p \text{ class rank}) + (\text{nbeta}_4) \times (DTI \text{ class rank}) +$
$(\text{nbeta}_5) \times (LREC \text{ class rank}) + (\text{nbeta}_6) \times (K_h \text{ class rank}) +$
$(\text{nbeta}_7) \times (\phi \text{ class rank}) + (\text{nbeta}_8) \times (\alpha_v \text{ class rank}) +$
$(\text{nbeta}_9) \times (\alpha_h \text{ class rank}) + (\text{nbeta}_{10}) \times (WTG \text{ class rank}) +$
$(\text{nbeta}_{11}) \times (UREC \text{ class rank})$ (17)

2. Salinity score = $(\text{nbeta}_1) \times$ (Disc. clay class rank) + $(\text{nbeta}_2) \times (K_v$ class rank) + $(\text{nbeta}_3) \times (Q_p$ class rank) + $(\text{nbeta}_4) \times (DTI$ class rank) + $(\text{nbeta}_5) \times (LREC$ class rank) + $(\text{nbeta}_6) \times (K_h$ class rank) + $(\text{nbeta}_7) \times (\phi$ class rank) (18)

3. Salinity score = $(\text{nbeta}_1) \times$ (Disc. clay class rank) + $(\text{nbeta}_2) \times (K_v$ class rank) + $(\text{nbeta}_3) \times (Q_p$ class rank) + $(\text{nbeta}_4) \times (DTI$ class rank) + $(\text{nbeta}_5) \times (LREC$ class rank) + $(\text{nbeta}_6) \times (K_h$ class rank) (19)

4. Salinity score = $(\text{nbeta}_1) \times$ (Disc. clay class rank) + $(\text{nbeta}_2) \times (K_v$ class rank) + $(\text{nbeta}_3) \times (Q_p$ class rank) + $(\text{nbeta}_4) \times (DTI$ class rank) + $(\text{nbeta}_5) \times (K_h$ class rank) (20)

5. Salinity score = $(\text{nbeta}_1) \times$ (Disc. clay class rank) + $(\text{nbeta}_2) \times (K_v$ class rank) + $(\text{nbeta}_3) \times (Q_p$ class rank) + $(\text{nbeta}_4) \times (LREC$ class rank) (21)

6. Salinity score = $(\text{nbeta}_1) \times$ (Disc. clay class rank) + $(\text{nbeta}_2) \times (K_v$ class rank) + $(\text{nbeta}_3) \times (Q_p$ class rank) (22)

where $nbeta_i = \dfrac{beta_i}{\sum_{i=1}^{n} beta_i}$

The choice of the above six salinity models depends on the availability of data. If more field data are available, more reliable prediction can be given. Use of model 1 (Eq. 17) is expected to be more reliable than the use of model 6 (Eq. 22). However, the results from the ground-water salinity models can provide only general guidance for selecting a possible new irrigation well, for example, because of the large uncertainties involved in

Table 19. Ranges and rankings of the variables considered in the sensitivity and regression analyses.

Class rank	Q_p (gpm)	Disc. clay (meter)	K_v (m/day)	*DTI* (meter)	*LREC* (m/day)	K_h (m/day)	ϕ	α_h (meter)	α_v (meter)	*WTG*	*UREC* (cm/yr)
1	< 160	>160	<0.23	>20	>0.025	>230	>0.3	<0.1	<0.01	0	>22.9
2	160~480	120~160	0.23~1.15	16~20	0.02~0.025	115~230	0.25~0.3	0.1~0.5	0.01~0.05	0~0.001	17.8~22.9
3	480~800	80~120	1.15~2.3	12~16	0.15~0.02	23~115	0.2~0.25	0.5~1	0.05~0.1	0.001~0.002	12.7~17.8
4	800~1120	40~80	2.~11.5	8~12	0.01~0.015	11.5~23	0.15~0.2	1~5	0.1~0.5	0.002~0.003	7.6~12.7
5	1120~1440	10~40	11.5~23	4~8	0.005~0.01	2.3~11.5	0.1~0.15	5~10	0.5~1	0.003~0.004	2.5~7.6
6	>1440	0~10	>23	0~4	0~0.005	<2.3	<0.1	>10	>1	>0.005	0~2.5

Q_p : pumping rate
ϕ : effective porosity
K_v : vertical conductivity
K_h : horizontal conductivity
α_h : horizontal dispersivity
α_v : vertical dispersivity
Disc. clay : distance of discontinuous clay layer to pumping well
WTG : water table gradient
UREC : uniform recharge
LREC : localized recharge
DTI : depth of well screen to interface

the ground-water system. The models are applicable within the vulnerable eastern portion of the GMD5.

Example

An example is provided here to demonstrate the use of the ground-water salinity model. The field conditions at the Siefkes site are considered in this example. The aquifer thickness at the Siefkes site from the ground level to the Permian bedrock is approximately 60 m. The transition zone of saltwater-freshwater interface is defined as the zone in which chloride concentration exceeds 500 mg/L, which is approximately 40 meters below the ground level, with a clay lens above it. A layer of dark clay exists around 42 m from the ground surface; however, the lateral extent of the clay layer is not certain. An irrigation well exists at the Siefkes site with the pumping rate of 50 x 10^{-3} m^3/s (800 gpm), and the well is screened from 18 to 24 meters and 27 to 37 meters below ground level. A series of slug tests was conducted by Butler et al. (1993) at two GMD5 network monitoring wells near the Siefkes site to determine the hydraulic conductivity of the alluvial aquifer. The test values are 9.63 and 17.3 m/day, respectively. Annual recharge is about 5 cm, and the amount of return irrigation water is not certain.

Because the field data are very limited, some assumptions are made as follows: (1) the vertical hydraulic conductivity, K_v, is about 1/5 of the horizontal hydraulic conductivity, K_h; (2) a discontinuous clay layer is located within approximately 30 meters of the irrigation well; and (3) the return of irrigation water to the aquifer is about 10% of the total pumpage. Based on the field data and assumptions, models 3 to 6 (Eq. 19 to 22) can be used to determine the salinity vulnerability of the Siefkes site.

Only model 3 (Eq. 19) is considered in this example. The rank of each variable is as follows.

variable	Disc. clay	K_v	Q_p	*DTI*	K_h	*LREC*
	30 m	2.7 (m/d)	800 gpm	3 m	13.5 (m/d)	0.005 (m/d)
rank	5	4	3	6	4	6
$nbeta_i$	0.16	0.24	0.30	0.07	0.09	0.14
score	0.8	0.96	0.9	0.42	0.36	0.84

The total score is 4.28 /6.0 (6.0 is the maximum score for model 3). This means that the Siefkes site has about 70% chance to experience saltwater intrusion. Because the irrigation well has two screen areas, less-saline water will be discharged from the upper-screen area than from the lower-screen area. Additionally, the extent of clay layers is not known; therefore, the result from the above model may be underestimated.

CONCLUSIONS AND RECOMMENDATIONS

This study focuses on saltwater intrusion into the Great Bend aquifer near the Siefkes site in south-central Kansas. Geostatistical analysis of available field data provided needed initial and boundary conditions for establishing a mathematical model for the saltwater intrusion phenomenon. The use of the SWIFT-II three-dimensional model to simulate saltwater upconing beneath pumping wells provided a great deal of detail about the influence of aquifer parameters, the distribution of clay layers, and saltwater upconing interactions from nearby pumping activities. Because of uncertainties about aquifer parameters and the distribution of clay layers in the entire GMD5 area, simulation of a large-scale model was not practical. The smaller-scale conceptual model adopted in this study was based on limited actual observations at the Siefkes site and typical parameter values. The most important factors affecting the salinity of discharged water are the location and configuration of clay layers in the aquifer, the pumping rate, and the hydraulic conductivities of the medium. The effects of dispersivity on saltwater intrusion are significant but not substantial. The effect of recharge from precipitation in the study area on the salinity of discharged water is relatively insignificant.

The detail and quantification from the numerical model of the saltwater intrusion under various conditions provided by this simulation work can be used by local water management officials to minimize saltwater upconing. Some conclusions and practical management recommendations drawn from this study are listed below:

1. Geostatistical analysis of the field data for water level, saltwater-freshwater interface, and the bedrock elevation suggests that the saltwater-freshwater interface and the bedrock elevation are closely correlated and that the interface generally follows the topography of the bedrock.

2. Clay layers or clay lenses are extensively dispersed in the Great Bend aquifer. Their spatial distribution is uncertain but is a critical factor in predicting the saltwater upconing due to pumping. Experimenting with the numerical model for different clay

layer configurations provides some valuable understanding of the effect of clay layer on the temporal variation of the salinity of pumped water.

3. The modeling results show that the most important factors affecting the salinity of discharged water are the pumping rate, the location and configuration of clay layers in the aquifer, and the hydraulic conductivities of the medium. The effects of uncertainties in aquifer porosity and dispersivity on predicting ground-water salinity are not substantial, and the effect of recharge from precipitation in the study is insignificant.

4. The calibrated model used for the simulated 10-year pumping operation produces time distributions of the salinity of discharged ground water under high, medium, and low annual pumpages for irrigation. The results provide a guide for ground-water management under the constraint of the allowable target salinity of pumped water for irrigation.

5. The ground-water management model discussed in this study can only provide general guide for the selection of a possible irrigation well. The final decision still depends on the knowledge of the investigated area.

6. Use low pumping rates over extended periods instead of high pumping rates for short periods.

7. Locate the well screen above a clay layer of low permeability, if such a clay layer can be identified.

8. Preferably install shallow pumping wells.

9. If high pumping rates need to be used, use safe separation distances to minimize the interaction from nearby pumping activities.

10. If freshwater is available in saltwater-affected areas, artificial recharge, preferably by injection wells, may alleviate a significant portion of the saltwater problem.

11. Mapping the location of the saltwater-freshwater interface and of the clay layers above it needs to be systematically pursued in a saltwater management area.

12. As the salinity of discharged water for irrigation increases with time, the residual chloride concentration in the soil would also increase, which would eventually

affect the crop production. Field measurements of the residual chloride concentration in the soil are recommended for further research.

REFERENCES

Akaike, H., "A Bayesian Extension of the Minimum AIC Procedure of Auto-regressive Model Fitting," Biometrika, Vol. 66, No. 2, August 1979, p. 237-242.

Bear, J., "On the Tensor Form of Dispersion," Journal of Geophysical Research, Vol. 66, No. 4, 1961, p. 1185-1197.

Buddemeier, R. W., Garneau, G., Healey, J. M., Ma, T. S., Sophocleous, M. A., Whittemore, D. O., Young, D., and Zehr, D., "The Mineral Intrusion Project: Report of Progress During Fiscal Year," 1993, 157 p.

Buddemeier, R. W., Young, D. P., Garneau, G. W., "Aquifer Characteristics and Hydrogeology," Kansas Geological Survey, Open-file Report 94-28d, 1994. 19 p.

Butler, J. J. Jr., Liu, W., and Young, D. P., "Analysis of October 1993 Slug Tests in Stafford, Pratt, and Reno Counties," Kansas Geological Survey, Open-File Report 93-52, 1993, 70 p.

Cobb, P. M., "The Distribution and Mechanisms of Salt Water Intrusion in the Fresh Water Aquifer and in rattlesnake Creek, Stafford County, Kansas." MS thesis, Department of Civil Engineering, University of Kansas, Lawrence, 1980, 176 p.

Cobb, P. M., Colarullo, S. J., and Heidari, M., "A Groundwater Flow Model for the Great Bend Aquifer, South-Central Kansas," Kansas Geological Survey, Open-file Report 83-3, 1982, 12 p.

Davis, B. M., "Uses and Abuses of Cross-Validation in Geostatistics," Mathematical Geology, Vol. 19, No. 3, 1987, p. 241-248.

Deutsch, C., and Journel, A., "GSLIB: Geostatistical Software Library and User's Guide," Oxford University Press, New York, 1992.

Fader, S. W., and Stullken, L. E., "Geohydrology of the Great Bend Prairie, South-Central Kansas," Irrigation Series 4, Kansas Geological Survey, 1978, 19 p.

Frind, E. O., "The Principal Direction Technique: A New Approach to Groundwater Contaminant Transport Modeling. In: Finite Elements in Water Resources," Proceedings of the 4th International Conference, Hannover, Springer-Verlag, Berlin, 1982, p. 13/25-13/42.

Garneau, G., W., "Detection and Characterization of the Distribution of Mineral Intrusion in the Great Bend Prairie Aquifer, South-Central Kansas," Kansas Geological Survey, Open-file Report 95-35, June, 1995, 102 p.

Gillespie, J. B. and Hargadine, G. D., "Geohydrology and Saline Ground-Water Discharge to the South Fork Ninnescah River in Pratt and Kingman Counties, South-Central Kansas," U.S. Geological Survey, Water Resources Investigations Report 93-4177, Lawrence, Kansas, 1994, 51 p.

Jacobs, H. S. and Whitney, D. A., "Determining water quality for irrigation," Cooperative Extension Service, Kansas State University, Manhattan, Kansas. 1975, 8 p.

Jian, X., Olea, R. A., and Yu, Y. S., "Semivariogram Modeling by Weighted Least Squares," Computers and Geosciences, 1996, in press.

Kansas Irrigation Guide and Irrigation Planners Handbook, U.S. Department of Agriculture, Soil Conservation Service, 1977.

Latta, B. F., "Geology and Ground-Water Resources of Barton and Stafford counties," Kansas Geological Survey Bulletin 88, Lawrence, KS, 1950.

Layton, D. W., and Berry, D. W., "Geology and Ground-Water Resources of Pratt County, South-Central Kansas," Kansas Geological Survey, Bulletin 205, 1973, 33 p.

Luckey, R. R., Gutentag, E. D., Heimes, F. J., and Weeks, J. B., "Digital Simulation of Ground-Water Flow in the High Plains Aquifer in parts of Colorado, Kansas, Nebraska, New Mexico, Oklahoma, South Dakota, Texas, and Wyoming," U. S. Geological Survey Professional Paper 1400-D, 1986, 57 p.

Ma, T. S. and Sophocleous, M. A., "Simulations of Saltwater Upconing in the Great Bend Prairie Unconfined Aquifer," Kansas Geological Survey Open-File Report 94-28f, 1994.

Matheron, G., "Principles of Geostatistics," Economic Geology, Vol. 58, 1963, p. 1246-1266.

Mitchell, J. E., Woods, J., McClain, T. J., and Buddemeier, R. W., "January 1992 Kansas Water Levels and Data Related to Water-Level Changes," Technical Series 3, Kansas Geological Survey, 1993, 130 p.

Norusis, M., SPSS/PC+ Statistics 4.0. SPSS Inc., Chicago, Illinois, 1990, 382 p.

Olea, Ricardo A., "CORRELATOR - an Interactive Computer System for Lithostratigraphic Correlation of Wireline Logs," Petrophysical Series 4, Kansas Geological Survey, 1988, 85 p.

Plane, D. R. and Oppermann, E. B., "Statistics for Management Decisions," Business Publications, Inc., Dallas, Texas, 1977, 527 p.

Price, H. S., Varga, R. S., and Warren, J. E., "Application of Oscillation Matrices to Diffusion-Convection Equations," Journal of Mathematics and Physics, Vol. 45, No. 3, 1966, p. 301-311.

Reeves, M., Ward, D. S., Johns, N. D., and Cranwell, R. M., "Theory and Implementation for SWIFT II, the Sandia Water-Isolation Flow and Transport Model for Fractured Media," Rep. NUREG/CR-3328 and SAND83-1159, Sandia National Laboratory, Albuquerque, New Mexico, 1986.

Rosner, M. Lanita, "The Stratigraphy of the Quaternary Alluvium in the Great Bend Prairie, Kansas," M.S. thesis, University of Kansas, Lawrence, 1988, 183 p.

Scheidegger, A. E., "General Theory of Dispersion in Porous Media," Journal of Geophysical Research, Vol. 66, No. 10, 1961, p. 153-162.

Sophocleous, M. A., "The Declining Ground-Water Resources of Alluvial Valleys — A Case Study," Ground Water, Vol. 19, No. 2, 1981, p. 214-226.

Sophocleous, M. A., Arnold, B., and McClain, T., "Great Bend Prairie of Kansas: Pre-Cenozoic Bedrock and Predevelopment Water-table Maps and Data Bases," Open-file Report 90-15, Kansas Geological Survey, 1990.

Sophocleous, M. A., "Groundwater Recharge Estimation and Regionalization: Rhe Great Bend Prairie of Central Kansas and Its Recharge Statistics," Journal of Hydrology, vol. 137, 1992, p. 113-140.

Sophocleous, M. A., "Comparative Review and Synthesis of Ground Water Recharge Estimate for the Great Bend Prairie Aquifer of Kansas," Kansas Geological Survey Bulletin 235, 1993, pp 41-54.

Sophocleous, M. A., Perkins, S. P., and Pourtakdoust, S., "Stream-Aquifer Numerical Modeling of the Kinsley to Great Bend Reach of the Arkansas River in Central Kansas," Kansas Geological Survey, Open-file Report 93-21, 1993, 106 p.

Sophocleous, M. A. and Perkins, S. P., "Stream-Aquifer Modeling and Preliminary Mineral Intrusion Analysis of the Lower Rattlesnake Creek Basin with Emphasis on the Quivira National Wildlife Refuge, Kansas," Kansas Geological Survey, Open-file Report 93-7, 1993, 194 p.

Sophocleous, M. A., Townsend, M. A., Vogler, L. D., McClain, T. J., Marks, E. T., and Coble, G. R., "Stream-Aquifer Testing of the Arkansas River Alluvial Aquifer Near Great Bend, Central Kansas," Kansas Geological Survey, Open-file Report 87-2, 1987, 90 p.

Varga, R. S., "Matrix Iterative Analysis," Prentice-Hall, Inc., Englewood Cliffs, New Jersey, 1962, 322 p.

Whittemore, D. O., "Ground-Water Geochemistry in the Mineral Intrusion Area of Groundwater Management District No. 5, South-Central Kansas," Kansas Geological Survey, Open-file Report 93-2, 1993, 36+ p.

Woods, J. J., Mitchell, J. E., and Buddemeier, R. W., "January 1994 Kansas Water Levels and Data Related to Water-Level Changes," Kansas Geological Survey, Technical Series 5, 1994, 106 p.

Young, David P., "Mineral Intrusion: Geohydrology of Permian Bedrock Underlying the Great Bend Prairie Aquifer in South-Central Kansas," Kansas Geological Survey, Open-file Report 92-44, 1992, 47 p.

Young, D. P., "Effects of Groundwater Pumpage on Freshwater-Saltwater Transition Zone Characteristics, Water Quality and Water Levels at the Siefkes Intensive Study Site," Kansas Geological Survey, Open-file Report 95-45c, 1995.

Appendix A. Relative locations of the Siefkes site, four GMD5 monitoring wells and four local existing shallow wells, and their corresponding gamma-ray and EM logs (Buddemeier et al., 1993).

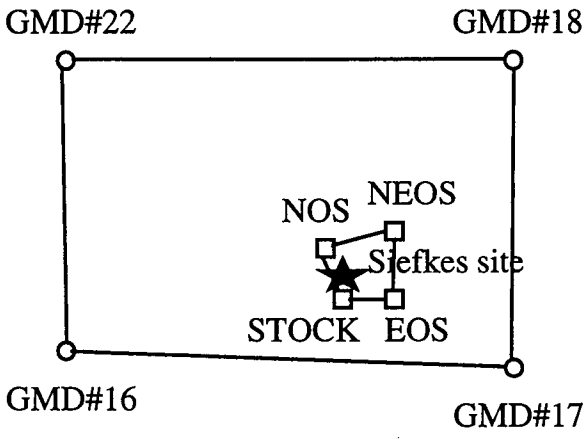

★ : Siefkes site

□ : local existing shallow well

o : GMD5 monitoring well

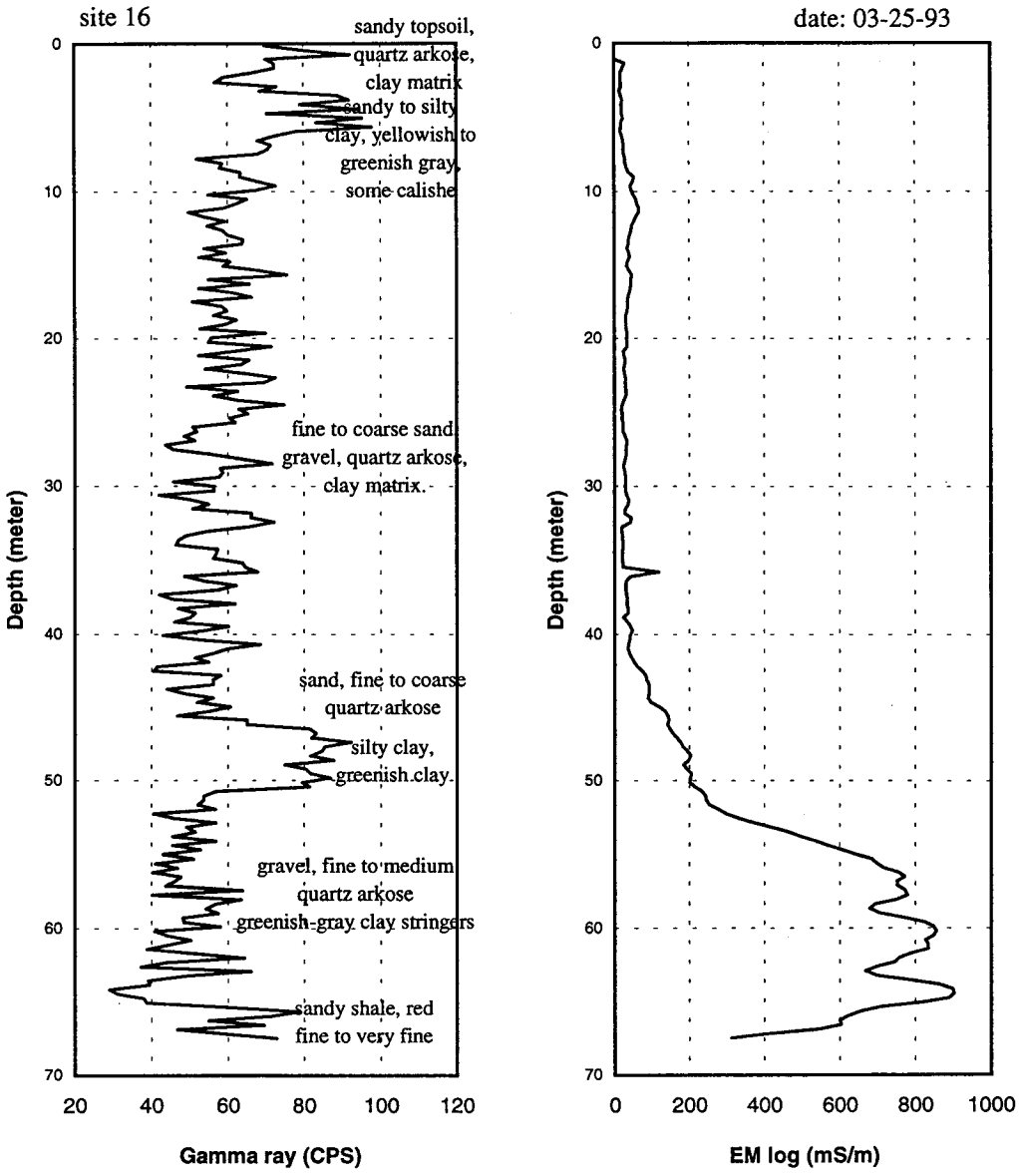

Gamma-ray and EM logs of GMD5 monitoring well # 16.

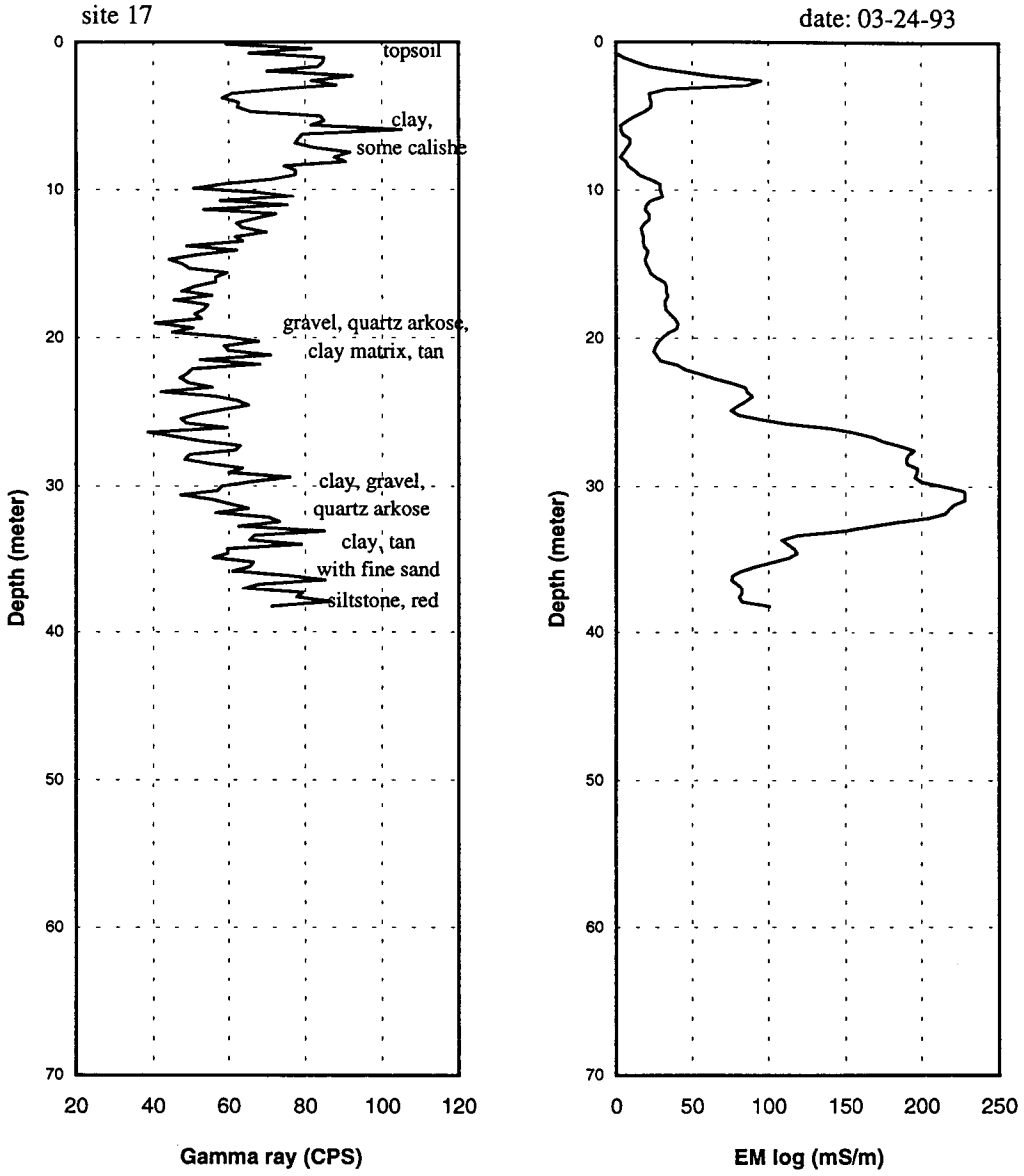

Gamma-ray and EM logs of GMD5 monitoring well # 17.

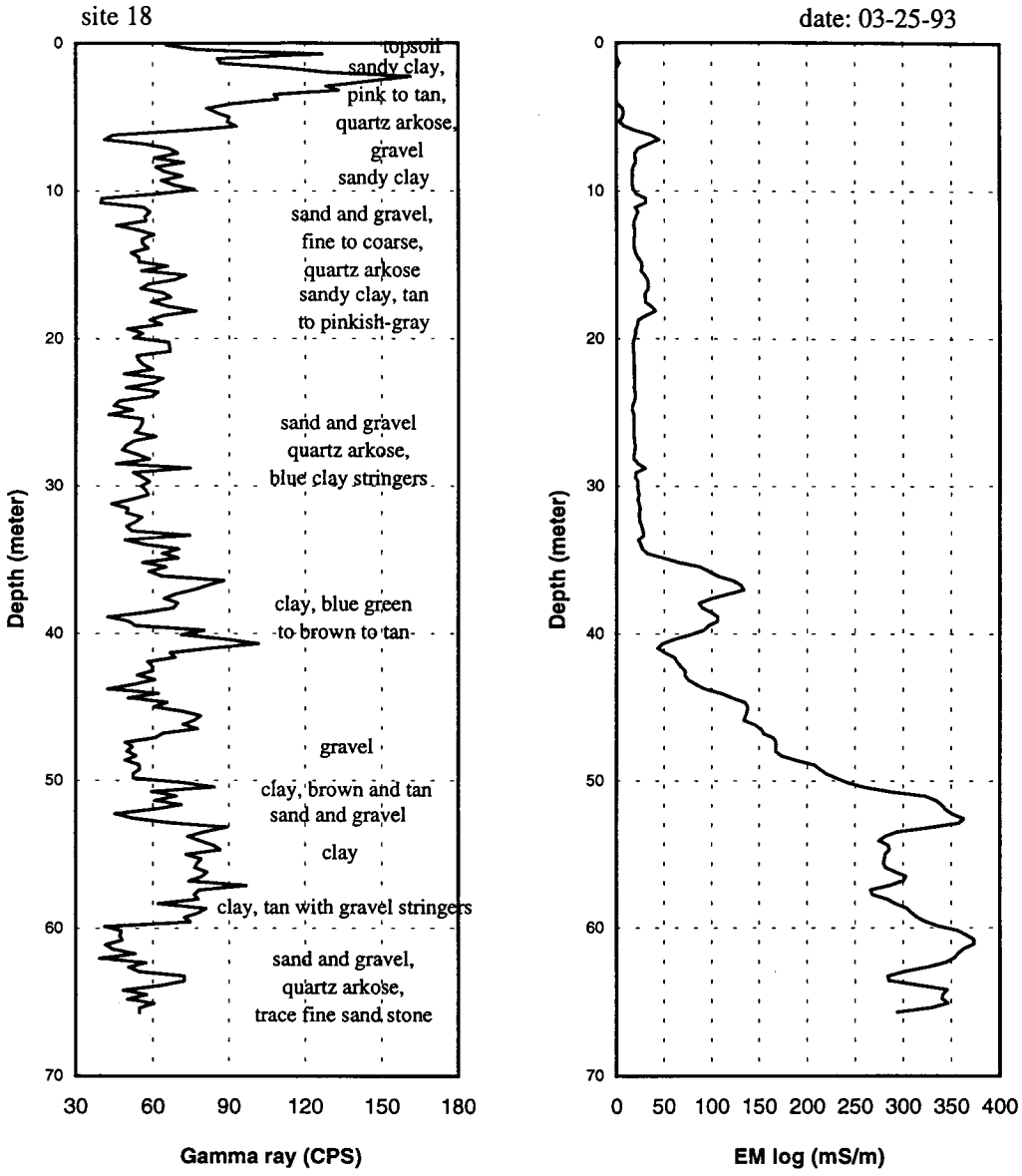

Gamma-ray and EM logs of GMD5 monitoring well # 18.

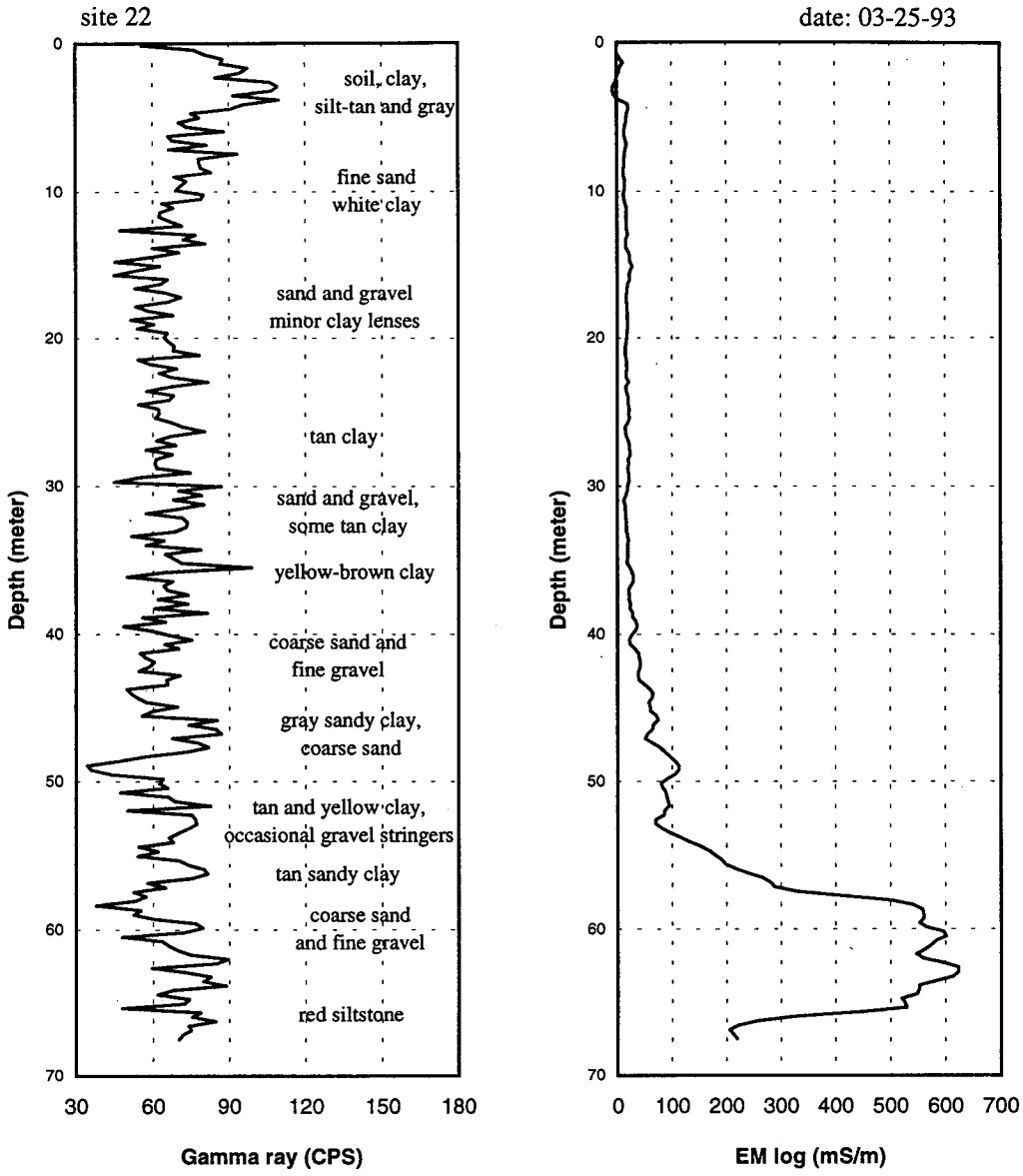

Gamma-ray and EM logs of GMD5 monitoring well # 22.

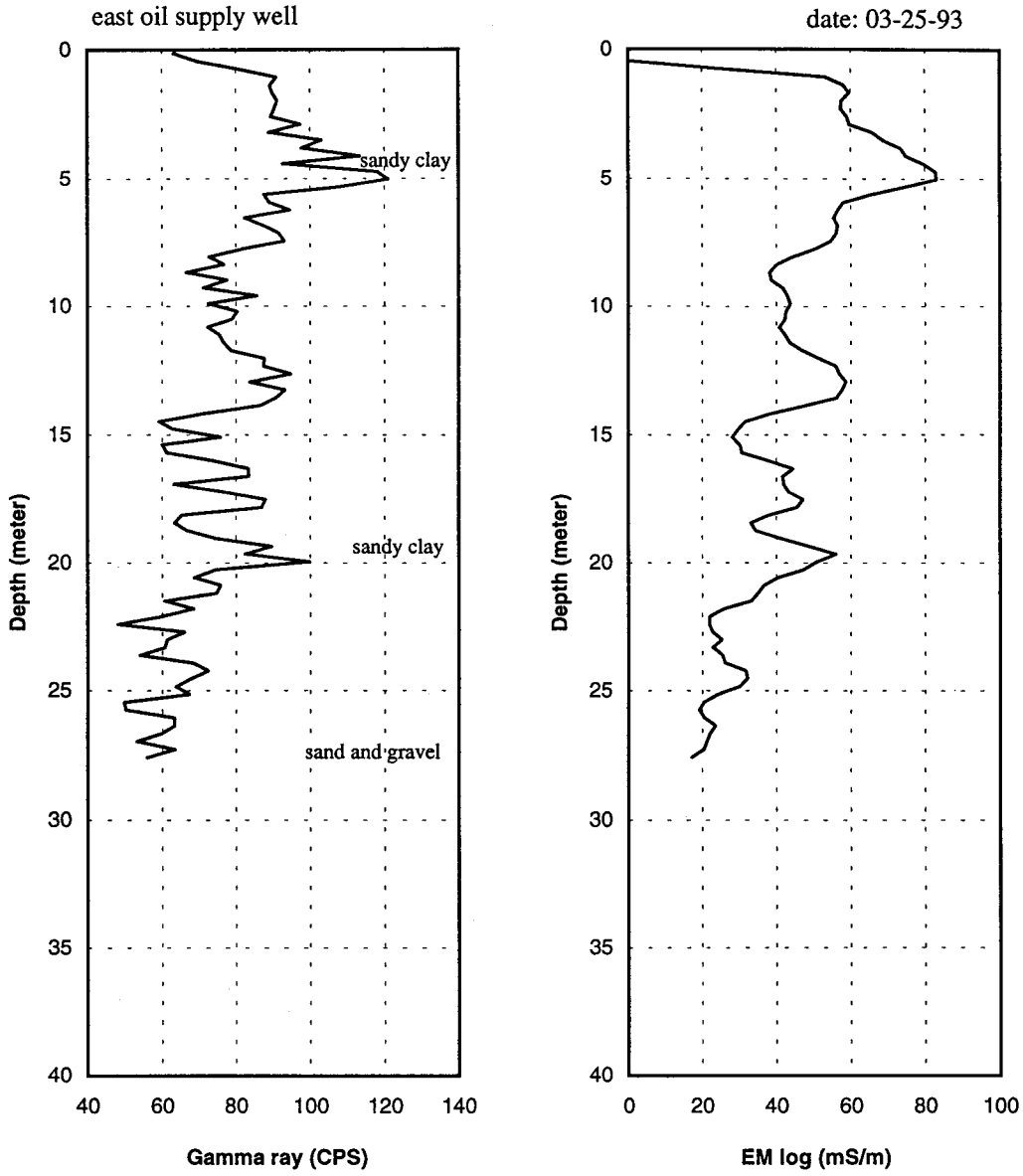

Gamma-ray and EM logs of east oil supply well (EOS).

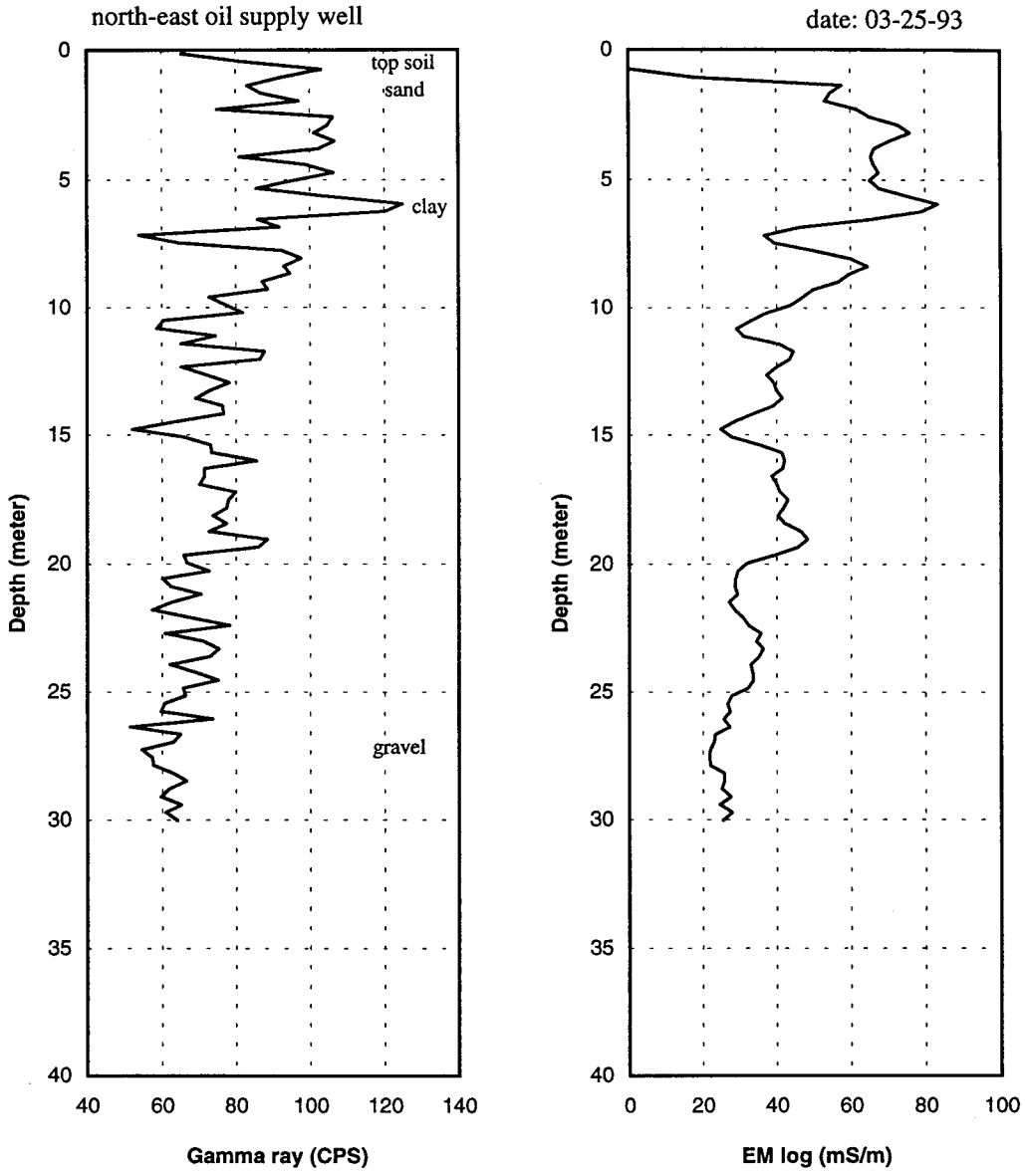

Gamma-ray and EM logs of north-east oil supply well (NEOS).

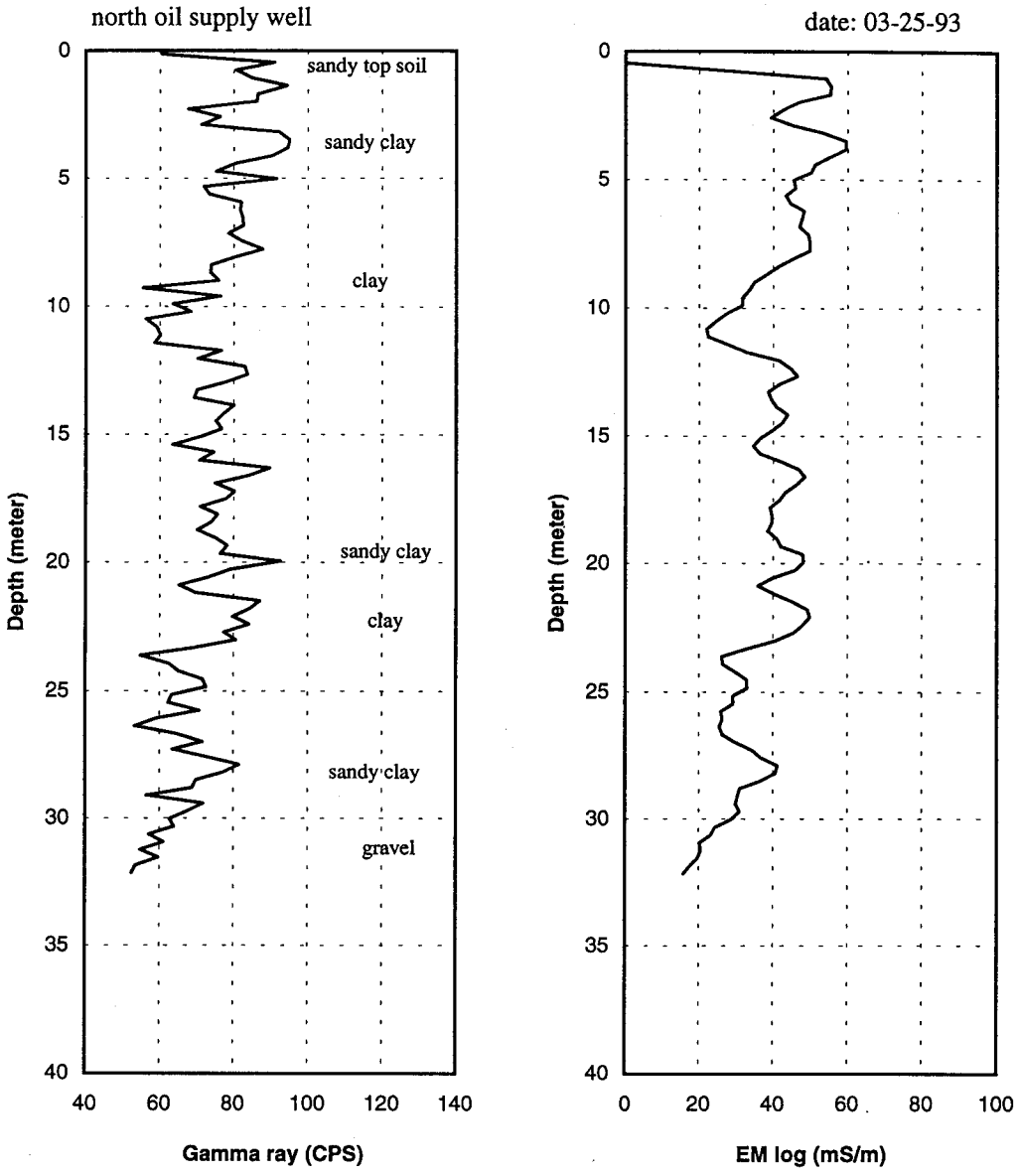

Gamma-ray and EM logs of north oil supply well (NOS).

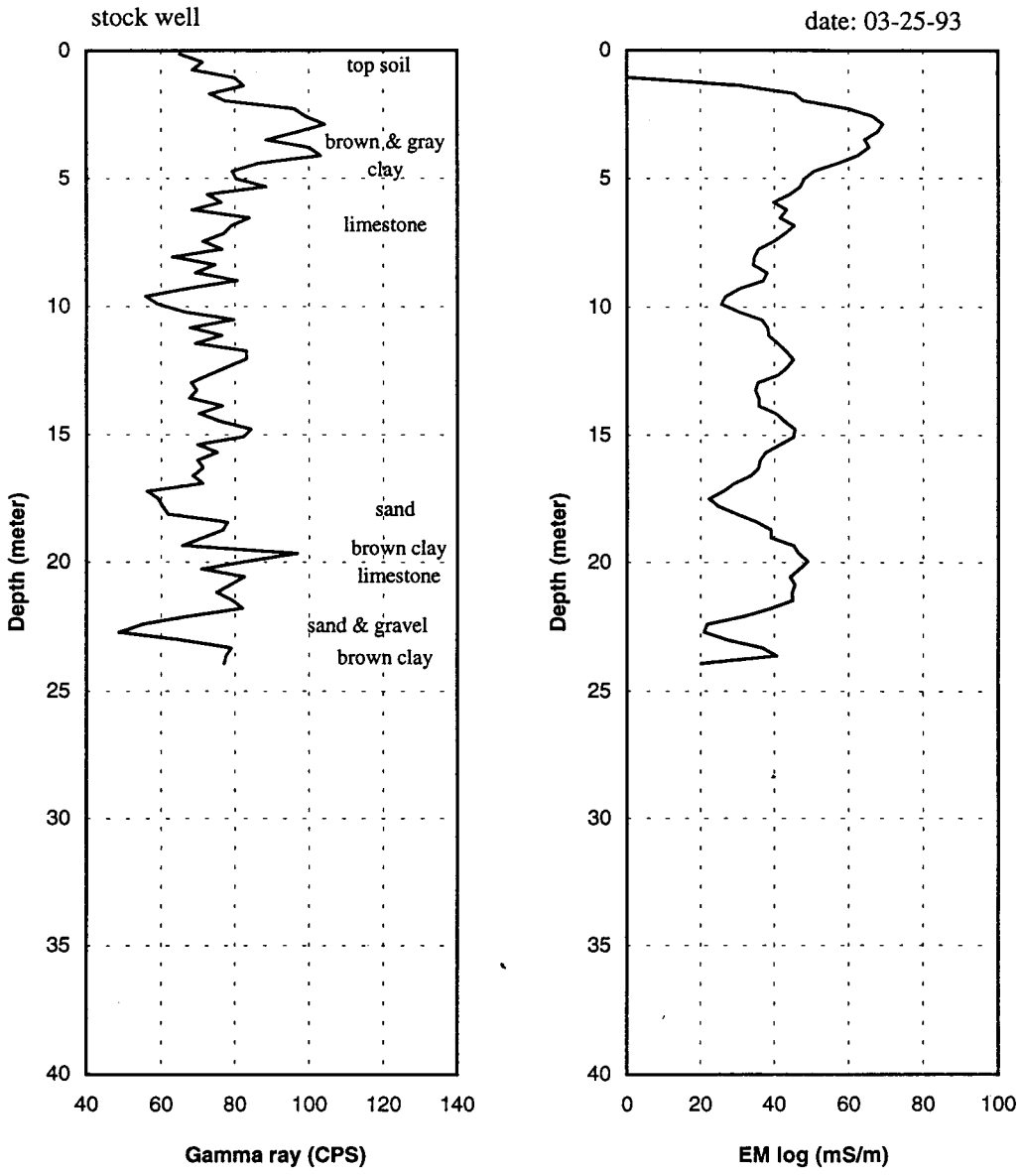

Gamma-ray and EM logs of north stock well (STOCK).